

# **The Carbon Pump of the Northwest-European Shelf - Variability due to Phytoplankton Dynamics and Climate Change**

**Dissertation zur Erlangung  
des Doktorgrades der  
Naturwissenschaften an  
der Fakultät für Mathematik,  
Informatik und Naturwissenschaften  
im Fachbereich Geowissenschaften  
der Universität Hamburg**

vorgelegt von  
Ina Lorkowski  
aus Lüdenscheid

Hamburg, 2012



---

1. Gutachter:  
Prof. Dr. Carsten Eden  
Institut für Meereskunde  
Universität Hamburg

2. Gutachter:  
Dr. Johannes Pätsch  
Institut für Meereskunde  
Universität Hamburg

Die Disputation fand am 18.1.2013 statt.



## 0.1 Summary

The presented work examines in detail the carbon cycle of the North Sea and the main drivers of the interannual variability of the carbon fluxes by using the ecosystem model ECOHAM. This study consists of three main parts:

In the first part, several long-term simulations with different scenarios conducted with ECOHAM were analysed. The main goal of these simulations was to examine the driving mechanisms of the interannual variability of the carbon shelf pump and especially of the air-sea flux of CO<sub>2</sub> between ocean and atmosphere. It was found that the export of carbon into the North Atlantic via shelf pumping was mainly correlated with the amount of water that was exported into the North Atlantic. During the whole simulation period from 1970 to 2006, the North Sea was found to be a sink for atmospheric CO<sub>2</sub> and absorbed in the mean about 1.31 mol C m<sup>-2</sup> yr<sup>-1</sup>. The northern North Sea was responsible for most of the uptake, whereas the southern North Sea oscillated between being a sink or a source. During the last ten years of the simulation period, the uptake of atmospheric CO<sub>2</sub> declined visibly. This trend in the simulation was mainly due to the increasing surface temperature of the North Sea and a decline in pH. During a long-term simulation without biological processes the North Sea was an increasing source for atmospheric CO<sub>2</sub> due to river input of inorganic carbon, indicating that biology is the most important factor for the North Sea being a sink for atmospheric CO<sub>2</sub>. Within the simulation period, the North Sea was subject to a strong phosphate eutrophication. During this eutrophication, the primary production in the model increased, while the net ecosystem production, thus the primary production minus respiration, did not react. A biologically induced air-sea flux was calculated and it was shown that the biological influence of the air-sea flux can be attributed to the net ecosystem production. This explained, why the eutrophication phase had no visible impact on the air-sea flux. Furthermore, it was found that the biological and physical effects on the air-sea flux counteracted in some years, e.g. in 1996, resulting in an intermediate net effect for the air-sea flux: In 1996, low surface temperatures favoured the dissolution of CO<sub>2</sub>, whereas the low temperatures and low river loads of nitrogen induced a low net ecosystem production. In the sum, both extreme values were balanced against each other. All in all, this part of the study gives insight into the most important processes driving the variability of the carbon fluxes of the North Sea.

In the second part, the method to differentiate between the physical and biological impact on the air-sea flux, which was already used in the first study, was compared with another method to find the most appropriate approach to calculate the influence of biology on the air-sea flux. For the first method, the assumption was made that biological and physical effects on the air-sea flux add up. Therefore, long-term simulations with and without biology were conducted and the difference between the two simulated pCO<sub>2</sub> values was taken as the biologically influenced pCO<sub>2</sub>. The second method was introduced by Takahashi *et al.* (1993), who linearised the temperature effect on pCO<sub>2</sub> by using experiments and statistical analysis and thus calculated a linearisation coefficient to estimate the changes in pCO<sub>2</sub> that are not due to temperature. The methods were compared by applying them at two stations in the North Sea, one in the northern and one in the southern area. The weak points in the superposition assumption were due to the fact that changes in temperature induce different changes in pCO<sub>2</sub> at different pCO<sub>2</sub> levels, while the Takahashi-approach does not account for external sinks or sources, as e.g. river inputs, in the area where the calculation is made. To account for different regional properties, horizontally different linearisation factors were calculated

---

and displayed. Despite their respective weaknesses, results of both methods agree quite well.

In the third part, a special aspect of the marine carbon cycle was implemented in the model and its impact on the carbon fluxes was analysed. The concept of the carbonate counterpump describes the release of  $\text{CO}_2$  into the water column due to biogenic calcification. The released  $\text{CO}_2$  may affect the air-sea flux and the carbon shelf pump. The reaction of calcification due to climate change and ocean acidification is currently under debate. In the North Sea, the calcification mainly occurs in the northern part and is attributed to coccolithophores. The coccolithophores were implemented in ECOHAM together with a prognostic representation of calcification and Total Alkalinity. The simulation results were compared with data from a ship expedition. The main goal of this study was to analyse the impact of the coccolithophores on the carbon cycle of the North Sea and the carbon shelf pump. It was found that the calcification reduced the uptake of atmospheric  $\text{CO}_2$  by the North Sea. But this reduction was lower than would be expected when regarding the amount of calcification because of the increased export of particulate inorganic carbon, which was stored in the deep water and in the sediment. In some scenario simulations with doubled atmospheric  $\text{pCO}_2$ , a reduced calcification and a reduced export of particulate inorganic carbon was found. The decrease in calcification is a negative feedback on rising atmospheric  $\text{pCO}_2$ , while the decrease in export is a positive feedback on rising atmospheric  $\text{pCO}_2$ . In connection to the sinking of coccoliths, the ballast hypothesis was developed, which assumes that the sinking of organic matter is enhanced by coagulation of ballast minerals and organic material. The influence of this ballasting material on zooplankton fecal pellets was found to be very small in a sensitivity simulation. The export of carbon into the North Atlantic decreased by 10 % in a simulation with coccolithophores in comparison to a simulation without coccolithophores. In summary the model results point into the direction of a decreased efficiency of the carbon shelf pump due to the presence of coccolithophores.

After these three chapters, some additional questions were discussed, for which there was no space in the three manuscripts. The influence of salinity on the gas exchange was investigated and the results of a long-term simulation with constant temperature and a long-term simulation with constant atmospheric  $\text{pCO}_2$  were discussed to further investigate the different impact factors on the air-sea flux. It was shown that the influence of the variability in salinity does play a minor role for the interannual variability of the air-sea flux. Further, it was found that at constant atmospheric  $\text{pCO}_2$ , the decreasing trend in the air-sea flux remains, but the magnitude of the air-sea flux was lower. The temperature thus determined the trend, whereas the atmospheric  $\text{pCO}_2$  determined the strength of the air-sea flux.

In summary, it was found that the most important factors for the variability of the air-sea flux were temperature, pH and net ecosystem production. The export into the North Atlantic was determined by the export of water. The biological contribution to the air-sea flux could be calculated by either assuming a superposition or by a linearisation of the temperature effect, depending on the local characteristics. Further, it was found that the carbonate counterpump slightly weakened the carbon shelf pump.

## 0.2 Zusammenfassung

Die vorliegende Arbeit untersucht den Kohlenstoffkreislauf der Nordsee mit der Kohlenstoffschelfpumpe, die interannuellen Variabilitäten der einzelnen Kohlenstoffflüsse und das Zusammenspiel der für die Variabilität entscheidenden Faktoren mit Hilfe des Ökosystemmodells ECOHAM. Die Arbeit gliedert sich in drei Teile:

Im ersten Abschnitt werden anhand von Langzeitsimulationen mit und ohne Biologie, sowie einigen Sensitivitätsstudien die treibenden Mechanismen der interannuellen Variabilität der Kohlenstoffpumpe, vor allem des Gasaustausches von  $\text{CO}_2$  zwischen Ozean und Atmosphäre, untersucht. Die Nordsee war über den gesamten Simulationszeitraum von 1970 bis 2006 eine Senke für atmosphärisches  $\text{CO}_2$  und nahm im Mittel  $1.31 \text{ mol C m}^{-2} \text{ yr}^{-1}$  auf. Die nördliche Nordsee war hierbei für den Großteil der Aufnahme verantwortlich, während die südliche Nordsee zwischen Quelle und Senke schwankte. Die Aufnahme von  $\text{CO}_2$  nahm vor allem in den letzten zehn Simulationsjahren deutlich ab. Eine Langzeitsimulation ohne biologische Prozesse zeigte, dass diese Abnahme hauptsächlich von der zunehmenden Oberflächentemperatur der Nordsee und dem abnehmenden pH-Wert induziert wurde. Innerhalb des Simulationszeitraumes, etwa von Ende der siebziger bis Anfang der neunziger Jahre war die Nordsee einer starken Phosphateutrophierung ausgesetzt. Diese Eutrophierungsphase weist im Modell eine erhöhte Primärproduktion auf, die Netto-Ökosystem-Produktion, also die Primärproduktion minus der Respiration, war jedoch nicht erhöht. Nach Berechnung eines nur durch die Biologie verursachten Gasaustausches zeigte sich, dass der biologische Einfluss auf den Gasaustausch durch die Netto-Produktion bestimmt wurde, so dass diese Eutrophierungsphase der Nordsee keinen Einfluss auf die Netto- $\text{CO}_2$ -Aufnahme der Nordsee hatte. Ohne biologische Produktion war die Nordsee über den gesamten Simulationszeitraum eine Quelle für atmosphärisches  $\text{CO}_2$ , da durch die Flüsse ständig anorganischer gelöster Kohlenstoff in die Nordsee eingebracht wurde. Des weiteren zeigte sich, dass in einigen Jahren, zum Beispiel in 1996, die physikalischen und biologischen Treiber in unterschiedliche Richtungen arbeiteten, so dass der Nettoeffekt für den Gasaustausch ein anderer war, als man bei einzelner Betrachtung der beiden Faktoren erwartet hätte. 1996 zeichnete sich durch eine niedrige Oberflächentemperatur aus, die die Lösung von  $\text{CO}_2$  in Seewasser begünstigt, während die Netto-Produktion in diesem Jahr auf Grund der niedrigen Temperatur und niedriger Stickstoffeinträge durch Flüsse nur geringe Werte aufwies und somit durch die Biologie eine nur geringe Aufnahme von  $\text{CO}_2$  stattfand. In der Summe ergab sich dann ein mittlerer Wert für den Gasaustausch, die beiden Extrema wurden gegeneinander ausgeglichen. Für den Transport des Kohlenstoffs von der Nordsee in den Nordatlantik und somit für die Effizienz der Kohlenstoffpumpe war die Menge an Wasser, die die Nordsee über den norwegischen Küstenstrom verließ, ausschlaggebend. Insgesamt bietet dieser Teil der Arbeit einen grundlegenden Einblick in die wichtigsten Prozesse des Kohlenstoffkreislaufs der Nordsee.

Im zweiten Abschnitt wurde die Methode zur Unterscheidung zwischen physikalischen und biologischen Einflussfaktoren auf den Gasaustausch, die auch im ersten Teil verwendet wurde, mit einer anderen Methode verglichen. Ziel war es, den bestmöglichen Ansatz zur Berechnung des Einflusses der Biologie auf den Gasaustausch zu finden. Bei der ersten Methode wird angenommen, dass sich physikalische und biologische Effekte addieren. Es wurde je ein Langzeitlauf mit und ohne Biologie durchgeführt. Der Lauf ohne Biologie simuliert den rein physikalisch/chemisch beeinflussten  $\text{pCO}_2$ , während die Differenz zwischen dem  $\text{pCO}_2$  aus dem physikalischen Lauf und dem

---

pCO<sub>2</sub> aus dem Standardlauf als biologisch induzierter pCO<sub>2</sub> angesehen wird. Im Vergleich dazu wird die Methode nach Takahashi *et al.* (1993) herangezogen. In der Studie wurde mit Laborexperimenten und statistischen Analysen ein Koeffizient berechnet, der den Temperatureffekt auf den Gasaustausch linearisiert. Dadurch kann die Änderung im Gasaustausch berechnet werden, die nicht durch Änderungen der Temperatur hervorgerufen wird. Die Methoden wurden für zwei Stationen in der Nordsee, einer nördlich gelegenen und einer südlich gelegenen Station, angewendet und die Ergebnisse miteinander verglichen. Es zeigte sich, dass die Schwachstellen bei der Additionsannahme darin liegen, dass die Auswirkungen einer Temperaturänderung unterschiedlich stark bei unterschiedlichen pCO<sub>2</sub>-Werten ausfallen. Dies bringt einen kleinen Fehler in die Berechnung des biologisch induzierten Gasaustausches, während der Ansatz von Takahashi *et al.* (1993) externe Quellen und Senken, wie z.B. Flusseinträge, die im Einzugsgebiet vorhanden sind, nicht berücksichtigt. Um unterschiedliche physikalischen Gegebenheiten in der Linearisierung zu berücksichtigen, wurden horizontal unterschiedliche Linearisierungsfaktoren berechnet. Trotz der jeweiligen Schwachstellen weisen beide Methoden eine gute Übereinstimmung auf.

Im dritten Abschnitt wurde ein weiterer Aspekt des Kohlenstoffkreislaufs in das Modell implementiert und dessen Einfluss auf die Kohlenstoffflüsse analysiert. Die sogenannte Karbonat-Gegenpumpe entsteht dadurch, dass bei der Bildung von biogenem Kalzit nicht nur partikulärer anorganischer Kohlenstoff entsteht, sondern auch CO<sub>2</sub> freigesetzt wird. Das freigesetzte CO<sub>2</sub> kann den Gasaustausch und die Kohlenstoffpumpe beeinflussen. Die Entwicklung der Kalkbildung wird insbesondere im Zusammenhang mit dem globalen Klimawandel und der Ansäuerung der Meere diskutiert. In der Nordsee findet die Kalkbildung hauptsächlich im nördlichen Teil statt. Das Kalziumkarbonat wird dort von den Coccolithophoriden gebildet. Diese wurden in ECOHAM zusammen mit einer prognostischen Kalkbildung und einer prognostischen Alkalinität implementiert und die Ergebnisse wurde mit Daten aus einer Schiffsexpedition verglichen. Ziel der Studie war es, den Einfluss der Coccolithophoriden auf den Kohlenstoffkreislauf der Nordsee und die Schelfpumpe zu bestimmen. Es zeigte sich, dass die Kalkbildung die Aufnahme von atmosphärischem CO<sub>2</sub> durch die Nordsee verringert. Diese Reduzierung der CO<sub>2</sub>-Aufnahme fällt aber kleiner aus, als man es auf Grund der Größenordnung der Kalkbildung erwarten würde. Das liegt an dem erhöhten Export von partikulärem anorganischem Kohlenstoff, der im tiefen Wasser oder im Sediment gespeichert wird. In den durchgeführten Szenarienrechnungen mit verdoppeltem atmosphärischen CO<sub>2</sub> wurde eine Verringerung der Kalkbildung und eine Verringerung des vertikalen Exports an partikulärem anorganischen Kohlenstoff festgestellt. Die Verringerung der Kalkbildung stellt eine negative Rückkopplung zu den steigenden atmosphärischen CO<sub>2</sub> - Konzentrationen dar, während die Verringerung des Exports eine positive Rückkopplung darstellt. Im Zusammenhang mit dem Absinken der Kalkschalen hat sich die Ballast-Hypothese entwickelt, bei der angenommen wird, dass durch Verklebung von Ballastmineralien und organischem Material ein erhöhter vertikaler Export stattfindet. Der Einfluß dieses anorganischen Ballasts auf Zooplanktonkot wurde in einer Sensitivitätsstudie als sehr gering befunden. Der Export von Kohlenstoff in den Nordatlantik verringert sich in der Simulation mit Coccolithophoriden im Vergleich zu einer Simulation ohne Coccolithophoriden um etwa 10 %. Insgesamt deuten die Modellergebnisse darauf hin, dass die Kohlenstoffpumpe durch die Anwesenheit der kalkbildenden Algen abgeschwächt wird.

Am Ende der Arbeit werden noch einige ergänzende Fragestellungen aufgezeigt und diskutiert, die in den einzelnen Manuskripten keinen Platz fanden. Der Einfluß des

Salzgehaltes auf den Gasaustausch wurde untersucht, sowie eine Langzeitsimulation mit konstanter Temperatur und eine Langzeitsimulation mit konstantem atmosphärischen  $p\text{CO}_2$  durchgeführt, um den Einfluß der einzelnen Faktoren auf den Gasaustausch noch genauer zu bestimmen. Es zeigte sich, dass der Einfluß der Schwankungen im Salzgehalt auf die interannuelle Variabilität des Gasaustausches eine untergeordnete Rolle spielt. Außerdem stellte sich heraus, dass bei konstantem atmosphärischen  $\text{CO}_2$  der abnehmende Trend im Gasaustausch erhalten blieb, aber der Gasaustausch selbst deutlich geringer ausfiel als in dem Standardlauf. Die Temperatur bestimmte also den Trend, während der atmosphärische  $p\text{CO}_2$  die Stärke des Gasaustausches bestimmte.

Zusammenfassend stellte sich heraus, dass die wichtigsten Faktoren für die Variabilität des Gasaustausches die Temperatur, der pH und die Netto-Ökosystem-Produktion sind. Der Export in den Nordatlantik wird durch die exportierte Wassermenge bestimmt. Der biologische Anteil am Gasaustausch kann je nach örtlichen Gegebenheiten durch Subtrahieren des physikalischen Anteils oder durch Linearisierung berechnet werden. Desweiteren zeigten die Simulationen, dass die Karbonat-Gegenpumpe die Kohlenstoffschelfpumpe abschwächt.



# Contents

0.1	Summary . . . . .	5
0.2	Zusammenfassung . . . . .	7
	Table of Contents . . . . .	10
<b>1</b>	<b>Introduction</b>	<b>15</b>
1.1	My contributions to the manuscripts . . . . .	22
<b>2</b>	<b>Interannual variability of carbon fluxes in the North Sea from 1970 to 2006</b>	<b>23</b>
2.1	Abstract . . . . .	23
2.2	Introduction . . . . .	23
2.3	Material and Methods - The Model . . . . .	25
2.3.1	Model setup . . . . .	25
2.3.2	External data . . . . .	27
	Meteorological forcing data . . . . .	27
	Deposition data . . . . .	27
	Boundary conditions . . . . .	28
	River data . . . . .	29
2.4	Results . . . . .	30
2.4.1	Hydrodynamic results . . . . .	30
	Temperature analysis . . . . .	30
	Thermocline . . . . .	30
	Water exchange . . . . .	31
2.4.2	Biogeochemical results . . . . .	32
	The standard run . . . . .	32
	The “no-biology”- run . . . . .	37
	Biologically induced air-sea flux . . . . .	37
2.5	Discussion . . . . .	37
2.5.1	Carbon budget . . . . .	37
2.5.2	Physical and biological drivers of the air-sea flux . . . . .	41
2.5.3	pCO <sub>2</sub> and DIC . . . . .	43
2.5.4	River loads and eutrophication . . . . .	45
2.5.5	Uncertainties and sensitivities . . . . .	47
2.6	Conclusion . . . . .	48
<b>3</b>	<b>Two techniques to separate physically and biologically mediated pCO<sub>2</sub> in seawater</b>	<b>49</b>
3.1	Abstract . . . . .	49
3.2	Introduction . . . . .	49
3.3	Materials and Procedures . . . . .	50
3.4	Assessment . . . . .	52
3.4.1	Comparison of the two methods . . . . .	52
	FLEX . . . . .	52
	GLOBEC . . . . .	55

3.4.2	Determination of constants for the North Sea . . . . .	56
3.5	Discussion . . . . .	61
3.6	Comments and recommendations . . . . .	63
<b>4</b>	<b>The impact of coccolithophores on the carbon budget of the North Sea</b>	<b>65</b>
4.1	Abstract . . . . .	65
4.2	Introduction . . . . .	65
4.3	The model . . . . .	66
4.3.1	Forcing, boundary conditions and river input . . . . .	67
4.3.2	Prognostic Alkalinity, calcite saturation and dissolution of calcite . . . . .	67
4.3.3	Implementation of coccolithophores . . . . .	67
4.3.4	Sinking and mineral ballast . . . . .	70
4.3.5	Climate change scenarios . . . . .	70
4.4	Results . . . . .	70
4.4.1	Validation/Calibration . . . . .	70
4.4.2	Carbon fluxes . . . . .	74
Climate change scenarios . . . . .	80	
4.4.3	Calcite saturation and pH . . . . .	83
4.5	Discussion . . . . .	83
4.5.1	Carbon fluxes . . . . .	83
4.5.2	Uncertainties and Sensitivities . . . . .	89
4.6	Conclusion . . . . .	90
<b>5</b>	<b>Interannual variability of the air-sea flux -Some additional aspects</b>	<b>91</b>
<b>6</b>	<b>Final Discussion</b>	<b>95</b>
6.1	The role of the North Sea in the global carbon cycle . . . . .	95
6.2	What is influencing the export of carbon from the North Sea into the North Atlantic? . . . . .	95
6.3	The driving mechanisms for the interannual variability of the air-sea flux in the North Sea and their interaction . . . . .	95
6.4	How can the impact of biology on the air-sea flux of CO <sub>2</sub> be identified? . . . . .	96
6.5	The influence of the coccolithophores on the carbon fluxes . . . . .	96
6.6	Does the explicit modelling of coccolithophores lead to improved model results? . . . . .	97
6.7	What changes in the carbon fluxes can be expected due to climate change and ocean acidification? . . . . .	97
<b>7</b>	<b>Conclusion</b>	<b>99</b>
<b>8</b>	<b>A0: The carbon cycle as implemented in ECOHAM</b>	<b>101</b>
<b>9</b>	<b>A1: The model equations</b>	<b>105</b>
<b>10</b>	<b>A2: Processes and their parameterisation</b>	<b>109</b>
<b>11</b>	<b>A3: Special functions used for process parameterisations</b>	<b>121</b>
<b>12</b>	<b>A4: Parameters of the biogeochemical model</b>	<b>125</b>
<b>13</b>	<b>A5: Equations for the implementation of coccolithophores</b>	<b>129</b>

<b>14 A6: Sinking and mineral ballast</b>	<b>133</b>
<b>15 A7: List of resulting publications</b>	<b>135</b>
<b>Bibliography</b>	<b>137</b>



# 1 Introduction

Since the industrial revolution humans emit a significant amount of CO<sub>2</sub> from fossil fuels into the atmosphere and change the equilibrium between the carbon pools of the earth. CO<sub>2</sub> acts as a greenhouse gas and its additional release might lead to drastic changes in the heat budget and thus in the climate system of the earth. An increase in annual mean temperature has already been observed (Mann *et al.*, 1998). Therefore it is of great importance to understand the driving mechanisms and the most sensitive features of the global carbon cycle. Fig. 1.1 shows a diagram from the 2001 IPCC report (IPCC, 2001).

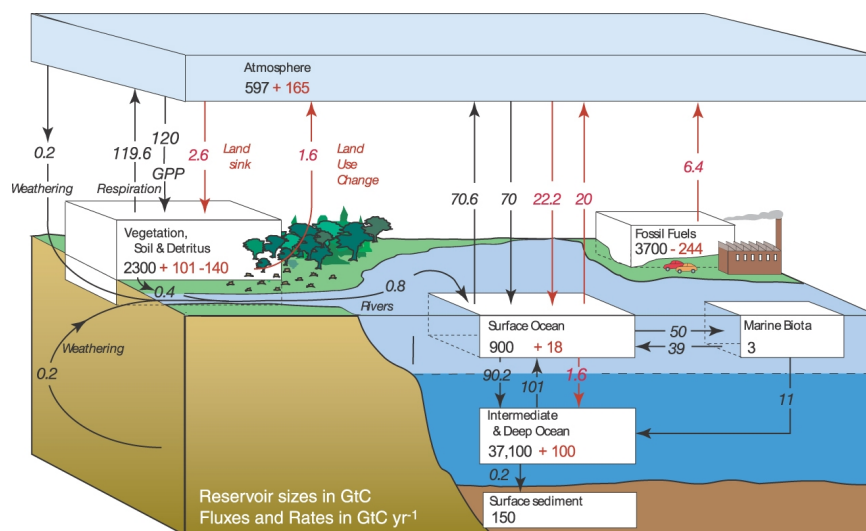


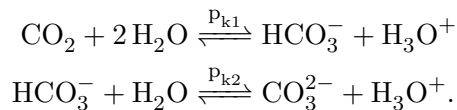
Figure 1.1: The global carbon cycle from IPCC (AR4, WG1 their Fig. 7.3). The red numbers indicate the additional anthropogenic fluxes and changes in the reservoirs.

The ocean in the mean is taking up about 2.2 GtC yr<sup>-1</sup> of the additionally emitted anthropogenic carbon and most of it is stored in the deep ocean, where it might take about 1000 years until the CO<sub>2</sub> gets in contact with the atmosphere again via upwelling. Nevertheless the carbon fluxes for different regions might deviate significantly from the mean values. Most of the carbon is taken up by the Atlantic Ocean (34-41 % depending on the calculation method) and the Southern Ocean (20-34 %)(Feely *et al.*, 2001). The high uptake of the Atlantic is mainly attributed to the north, where high primary production and low surface pCO<sub>2</sub> come together (Feely *et al.*, 2001). The Pacific takes up only about 12-25 % net, because the uptake in the north is compensated by the high release of CO<sub>2</sub> close to the equator (Feely *et al.*, 2001). The Indian Ocean takes up about 16-19 %, mostly due to the cooling of tropical water (Feely *et al.*, 2001). The role of marginal seas, coastal oceans and estuaries is currently under debate (Borges, 2005).

CO<sub>2</sub> dissolves in seawater when the partial pressure in the atmosphere is higher than the partial pressure in seawater. The partial pressure in seawater is determined by several factors, as temperature, salinity and pH and it can be reduced by biological drawdown

and increased by respiration. Advection of carbon-rich or carbon-poor water influences the local  $p\text{CO}_2$  as well. There have been attempts to analyse the physical, chemical and biological contributions to the seawater  $p\text{CO}_2$  development. While Takahashi *et al.* (2002) used laboratory experiments and statistical methods, Previdi *et al.* (2009) used model results and a Taylor series to separate the different contributors to air-sea flux variability. Previdi *et al.* (2009) found, as the most prominent drivers of interannual variability, changes in sea surface temperature (SST) and new production.

When the atmospheric  $p\text{CO}_2$  rises, the additionally dissolved  $\text{CO}_2$  changes the equilibrium of the carbonate system into the direction of lower pH following the chemical equilibrium:



The equilibrium constants  $p_{k1}$  and  $p_{k2}$  depend on temperature, pressure and salinity. The consequences of this ongoing acidification of seawater are up to now not well known, but several laboratory studies report on severe impacts of ocean acidification on marine organisms (Fabry *et al.*, 2008; Kroeker *et al.*, 2010). Especially calcifying organisms, such as corals or planktonic calcifying algae as the coccolithophores are expected to be affected (Kleypas *et al.*, 2006). An additional effect of ocean acidification was found by Ilyina *et al.* (2010) who observed that the ability of seawater to absorb sound decreases with decreasing pH values. This might influence the communication of marine mammals and the propagation of noise in the ocean.

A special role in the marine carbon cycle is attributed to the shelf seas. They represent only 7.6% of the area of the global oceans, but they are highly productive, extensively used by humans and are representing the interface between the anthropogenically influenced coastal area and the global ocean. Though they are easily accessible for measurement campaigns, it is still not completely clear whether the shelf areas as a whole are sinks or sources for atmospheric  $\text{CO}_2$ . Several studies exist which try to define the importance of shelf and marginal seas for the global carbon budget. Borges (2005) collected data sets of the air-sea flux of  $\text{CO}_2$  from different types of coastal areas, as e.g. estuaries, mangroves, salt marshes and open shelf seas. By upscaling the corresponding air-sea fluxes for the global domain, several very different values for the global air-sea flux resulted, indicating the large variability and uncertainty with regard to the contribution of different coastal environments to the global carbon budget. In their synthesis Cai *et al.* (2006) classified different shelf seas by considering their physical and geological properties as well as their nutrient status and their geographical position. They analysed different data sets for the different shelf types and stated that mid-high latitude shelves are sinks for atmospheric  $\text{CO}_2$ , whereas low latitude shelves are sources for atmospheric  $\text{CO}_2$ . Laruelle *et al.* (2001) used a scaling approach to identify the amount of absorbed atmospheric  $\text{CO}_2$  by different shelf types. They found that the shelves in the tropics are sources for atmospheric  $\text{CO}_2$ , while continental shelves in the temperate regions and high latitudes are sinks for atmospheric  $\text{CO}_2$ . The North Sea was classified as a temperate open shelf with a sink for atmospheric  $\text{CO}_2$  of  $1.0 \pm 1.0 \text{ mol C m}^{-2} \text{ yr}^{-1}$ . While these scaling approaches are useful for global estimates of carbon uptake, they lack the ability to identify interannual changes and variability due to specific regional forcing.

Tsunogai *et al.* (1999) were the first to introduce the concept of the continental shelf pump mechanism. They conducted a study in which they determined the fugacity of

---

CO<sub>2</sub> for the East China Sea and found that it absorbs much more atmospheric CO<sub>2</sub> as could be expected by regarding the biological production and respiration processes, as well as the amount of carbon that is finally stored in the sediment. They suggested that the carbon dioxide that has been taken up from the atmosphere is transported into deeper waters of the adjacent ocean via mixing and lateral advection. This process is mainly triggered by the chemical dissolution of CO<sub>2</sub> in seawater and not primarily by the biological production (Tsunogai *et al.*, 1999). Thus, the shelf pump mechanism combines the biological carbon pump, the solubility pump and the lateral advection of carbon from the shelf into the adjacent deep ocean.

The biological pump describes the fixation of inorganic carbon via photosynthesis by marine phytoplankton. This organic material then sinks into deeper water and partly gets remineralised. When the carbon has reached a certain depth below the mixed layer, where it is not in contact with the atmosphere anymore, it may be stored in the deeper water and the sediment for a longer time period. Thus, atmospheric CO<sub>2</sub> would be effectively exported from the atmosphere into the ocean.

The dissolution of atmospheric CO<sub>2</sub> in seawater, and the transport of this carbon-enriched water into the deep via the thermohaline circulation is termed solubility pump.

Bates (2006) found an active carbon shelf pump in the Chukchi Sea as responsible for the region being a sink for atmospheric CO<sub>2</sub>, while Yool & Fasham (2001) extrapolated the shelf pump mechanism for the whole global domain and found a significant effect on the distribution of deep water carbon due to shelf pumping.

The here presented study focusses on one specific shelf sea, the North Sea - located on the Northwest European Continental Shelf (NECS). The model area is ranging from 47° 41' to 63° 53' N and from 15° 5' W to 13° 55' E. Several hydrographic and hydrodynamic features of the North Sea are of importance for the behaviour of the ecosystem. The general circulation pattern is shown in Fig. 1.2. The inflow into the North Sea is dominated by water from the North Atlantic, which enters via the north-western boundary, and to a much lesser extent by water entering via the English Channel and an inflow from the Baltic Sea. Almost all water, which is then a mixture of freshwater from rivers and the Baltic Sea and oceanic water (Otto *et al.*, 1990) leaves the North Sea via the Norwegian coastal current. The turnover time of the North Sea water is about one year (Otto *et al.*, 1990). Additionally, the North Sea is strongly influenced by tides, dominated by the M2 tide, which results in a dryfall of the shallow Wadden Sea area twice a day. This strong tidal forcing enhances the mixing (Otto *et al.*, 1990) and thus the nutrient supply for marine production. This tidal influence is stronger in the shallow southern North Sea, which as a result is almost always well mixed (Otto *et al.*, 1990), while the deeper northern North Sea is partly stratified during summer. Regarding the vertical exchange and structure a bit further, due to the high turbulence in the southern North Sea, the vertical heat exchange is enhanced and further promotes a mostly homogeneous water column (Otto *et al.*, 1990), while the deep northern North Sea shows lower turbulence and lower vertical heat exchange (Otto *et al.*, 1990), leading to the stratification in summer. The North Sea exhibits a clearly defined annual cycle with sea surface temperatures (SST) ranging in the mean from 6 °C in winter to 20 °C in summer (OSPAR, 2000). The regional temperature distribution is affected by inflow from the North Atlantic, heat exchange with the atmosphere and water depth (OSPAR, 2000). The temperature variability is higher in the shallow southern North Sea with an amplitude of 8 °C, while the northern regions exhibit amplitudes of 2 °C (OSPAR, 2000). The salinity varies between 32 and 34.5 psu in the open North Sea, while the

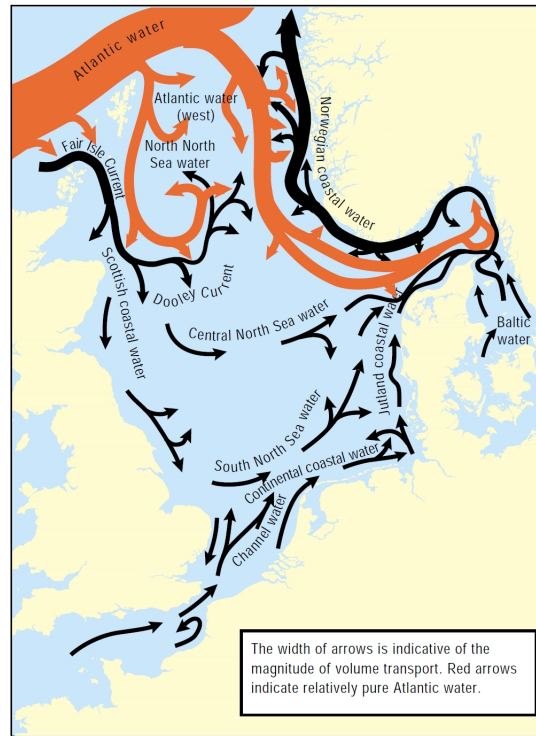


Figure 1.2: The general circulation pattern of the North Sea, after Turrell (1992) and OSPAR (2000)

spatial pattern is also dependent on the inflow of water from the North Atlantic, the freshwater via rivers and the Baltic Sea (OSPAR, 2000). Especially close to rivermouths and the outflow from the Baltic Sea, salinity may decrease to 10 psu (OSPAR, 2000). The seasonal variability in salinity for the open North Sea is small, while locally salinity may vary due to changes in freshwater supply (OSPAR, 2000).

The North Sea is affected by anthropogenic activities in the coastal regions and via input from rivers from the North European continent and Great Britain. It is extensively used by humans as a food source, for energy production via oil platforms and via offshore windparks and as a touristic venue. Several countries have economic interests in this area. Especially the food and tourism related activities rely on a healthy ecosystem. The North Sea is also subject to several external forcings that might change the equilibrium of the ecosystem itself. Eutrophication due to high nutrient loads by rivers might change the biodiversity as well as global shipping, ocean acidification and rising water temperatures.

Thomas *et al.* (2004) described the shelf pump mechanism for the North Sea (Fig. 1.3). The displayed section from south to north shows the well mixed southern North Sea and the seasonally stratified northern North Sea.  $\text{CO}_2$  is fixed by phytoplankton via photosynthesis. The phytoplankton is then grazed by zooplankton and enters the heterotrophic foodweb. In the northern North Sea, particulate organic carbon (POC) sinks below the mixed layer depth and gets remineralised in the deeper water without contact to the atmosphere. It can then be advected into the North Atlantic and may be stored there in the deep water for a longer time period. The northern North Sea is considered to be a sink for atmospheric  $\text{CO}_2$ . In the southern North Sea, the remineralisation and respiration releases  $\text{CO}_2$  into the well-mixed water column and the

released carbon dioxide might escape into the atmosphere. The heterotrophic southern North Sea is thought to be a small source for atmospheric CO<sub>2</sub> in the Thomas *et al.* (2004) study, whereas Gypens *et al.* (2004) and Gypens *et al.* (2011) have shown that the interannual variability is quite high leading the southern North Sea to oscillate between being a sink or a source for atmospheric CO<sub>2</sub>.

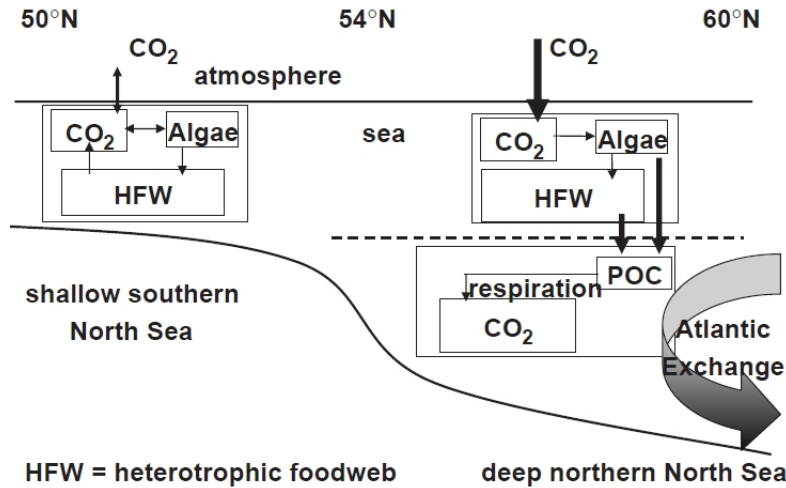


Figure 1.3: The carbon shelf pump concept for the North Sea. Figure taken from (Thomas *et al.*, 2004), their Fig. 4.

Bozec *et al.* (2005) conducted a study in 2001 to verify the shelf pump mechanism in the North Sea. Their data set supports the hypothesis, that the North Sea takes up atmospheric CO<sub>2</sub>, which is then exported into the North Atlantic. They found that the shallow southern North Sea is always well mixed and net heterotrophic, and thus is a source for atmospheric CO<sub>2</sub>, while the mixed layer of the northern North Sea was autotrophic and a sink for atmospheric CO<sub>2</sub>.

The concept of Thomas *et al.* (2004) did not explicitly include the effect of calcifying organisms such as coccolithophores. They contribute to the so-called carbonate counter pump (Fig. 1.4). During the formation of calcium carbonate by marine organisms, CO<sub>2</sub> is released into the water column according to the reaction:



Therefore calcification decreases total alkalinity (TA) by 2 mol and dissolved inorganic carbon (DIC) by 1 mol, while pCO<sub>2</sub> rises. This additional release of CO<sub>2</sub> into the water column might affect the air-sea flux in the direction of a lower uptake capacity for atmospheric CO<sub>2</sub>.

Coccolithophores are the most important marine calcifiers and are responsible for about 80 % of marine calcification (Müller *et al.*, 2008). They are distributed almost over the whole globe and are able to form large blooms in the North Sea, especially in the northern part (e.g. Holligan *et al.* (1989, 1993a); Burkill *et al.* (2002); van der Wal *et al.* (1995); Archer *et al.* (2001); Rees *et al.* (2002); Widdicombe *et al.* (2002); Wilson *et al.* (2002)). Thus, their blooms might affect the air-sea flux especially in the northern North Sea and the efficiency of the carbon shelf pump. The impact of coccolithophores on different ecosystems and the carbon cycle has already been studied by several authors. Joassin *et al.* (2011) investigated a mesocosm study and successfully

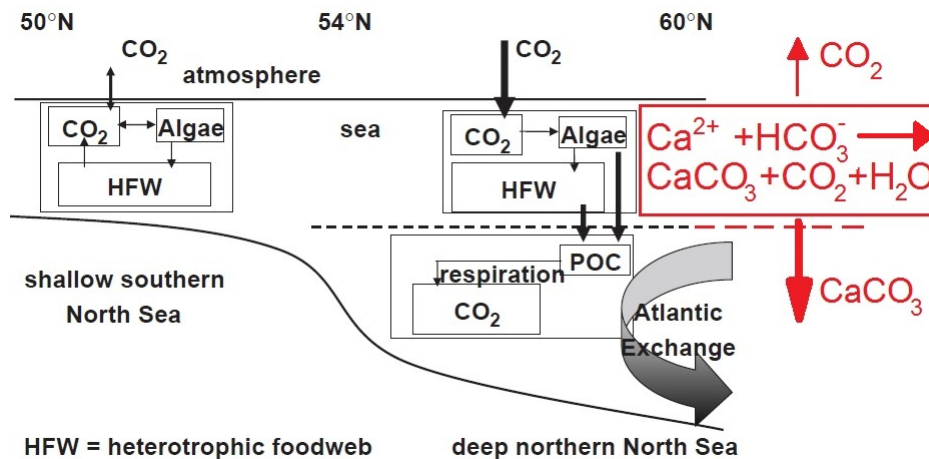


Figure 1.4: The carbon shelf pump concept for the North Sea with the inclusion of the carbonate counter pump. Figure modified from (Thomas *et al.*, 2004), their Fig. 4.

modelled the carbon and nitrogen fluxes during a bloom of coccolithophores. In the Bay of Biscay, Suykens *et al.* (2010) found a small change in the uptake of atmospheric CO<sub>2</sub> due to blooms of coccolithophores within a data set ranging from 2006 to 2008 and Harlay *et al.* (2010) found a small increase in seawater pCO<sub>2</sub> during a coccolithophore bloom in the northern Bay of Biscay in 2004. Murata (2006) found an increased seawater pCO<sub>2</sub> in the Bering Sea within a period from 1998 to 2002, which could be attributed to coccolithophore blooms. In the northeast Atlantic an increase in dissolved CO<sub>2</sub> was observed in summer 1991 attributed to calcification by coccolithophores (Robertson *et al.*, 1994).

Another often discussed effect is the ballasting of organic material by calcite (Francois *et al.*, 2002; Klaas & Archer, 2002; Armstrong *et al.*, 2002). Ingested coccoliths may ballast zooplankton faecal pellets and thus increase the sinking velocity of inorganic and organic carbon (Honjo, 1976; Buitenhuis *et al.*, 2001). Additionally, coccolithophores form transparent exopolymer particles (TEP), which can coagulate with organic and inorganic material (Harlay *et al.*, 2009). These aggregates sink rapidly to the seafloor and enhance the vertical export of carbon. These ballasting effects might weaken the effect of calcification on the partial pressure of CO<sub>2</sub> because the organic material is exported below the mixed layer before it gets remineralised and thus the released CO<sub>2</sub> does not increase the surface pCO<sub>2</sub> (Buitenhuis *et al.*, 1996).

In times of rising atmospheric CO<sub>2</sub> concentrations and ocean acidification, it is still under debate, how calcification might be affected. Most experiments point into the direction of decreasing calcification in a high CO<sub>2</sub> world (e.g. Riebesell *et al.* (2000); Delille *et al.* (2005); Engel *et al.* (2005); Zondervan *et al.* (2001)), while on a species basis the response might be more complex (Langer *et al.*, 2006). Some experiments even point into the opposite direction (Iglesias-Rodriguez *et al.*, 2008). Less calcification would mean a negative feedback on rising atmospheric CO<sub>2</sub> concentrations, while less ballast export might lead to a positive feedback on rising atmospheric CO<sub>2</sub>. It is still under debate which of the two processes are the most dominant, or if they cancel each other out.

This work is aiming at answering the following questions related to the marine carbon cycle and the special attributes of the North Sea described above:

- 
- What is the role of the North Sea in the global carbon cycle?
  - What is influencing the export of carbon from the North Sea into the North Atlantic?
  - What are the driving mechanisms for the interannual variability of the air-sea flux in the North Sea and how do they interact?
  - How can the impact of biology on the air-sea flux of CO<sub>2</sub> be identified?
  - What is the influence of the coccolithophores on the carbon fluxes and the continental shelf pump?
  - Does the explicit modelling of coccolithophores lead to improved model results?
  - What changes in the carbon fluxes can be expected due to climate change and ocean acidification?

To answer these questions, the biogeochemical ecosystem model ECOHAM (ECOlogical model HAMBurg) (e.g. Kühn *et al.* (2010); Pätsch & Kühn (2008); Moll & Radach (2003)) is used in this study. A short introduction of the carbon cycle in ECOHAM and a flux diagram is given in the appendix A0.

The three following chapters are prepared as manuscripts for publication and are therefore stand-alone studies as well as aspects of one single study. The first article deals with the carbon budget of the North Sea, the continental shelf pump mechanism and especially the air-sea flux. It tries to unravel the drivers for the interannual variability of the air-sea flux in the North Sea and the export into the North Atlantic by regarding a long-term simulation. The implementation of the model and the needed data sets are described. The main focus of the analysis of the results lies on the interplay between biological, physical and chemical drivers of the air-sea flux. During the work on the first manuscript, the question arose, how to correctly calculate the biological contribution to the air-sea flux. The so-called superposition method was already applied in the first manuscript and in the second manuscript the method is analysed further and compared to the method of Takahashi *et al.* (1993). This study clarifies how to analyse the influence of biology on the air-sea flux. The aim of the third study was to investigate the impact of coccolithophores and their calcification on the carbon budget. The implementation of the coccolithophores is described and the results are validated. Scenario runs are made to investigate the carbon fluxes and especially the calcification during warmer temperatures and higher CO<sub>2</sub> concentrations. In chapter 5 results of three additional simulations are presented and discussed, for which there was no time or space in the previous manuscripts. The influence of salinity, constant temperature and constant atmospheric pCO<sub>2</sub> on the air-sea flux are clarified. A final discussion and conclusions follow after chapter 5.

## 1.1 My contributions to the manuscripts

### Chapter 2

I prepared the set-up for the simulation, conducted the long-term simulations and prepared most of the figures and wrote most of the text. The chapter is already published as Lorkowski, I., Pätsch, J., Moll, A. & Kühn, W. 2012. *Interannual variability of carbon fluxes in the North Sea (1970-2006) - Abiotic and biotic drivers of the gas-exchange of CO<sub>2</sub>*. *Estuarine Coastal and Shelf Science*, 100, 38-57.

### Chapter 3

I conducted the simulation for this study and the text was written in close collaboration by Johannes Pätsch and me. It has been submitted as Pätsch, J. & Lorkowski, I. *Comparison of two techniques to separate physical and biological mediated pCO<sub>2</sub> in seawater*. *Limnol. Oceanogr. Methods* and has obtained a conditional accept up to now (Oct 2012) with minor revisions to be done.

### Chapter 4

I developed the coccolithophore implementation, prepared the model set-up and conducted the simulations, did the data analysis, prepared all the figures and wrote the text, except for the first paragraph about the implementation of the prognostic alkalinity (section 4.3.2). This manuscript will be submitted as Lorkowski, I., Pätsch, J. & Schwichtenberg, F. *The impact of coccolithophores on the carbon budget of the North Sea*.

## 2 Interannual variability of carbon fluxes in the North Sea from 1970 to 2006 - Competing effects of abiotic and biotic drivers on the gas exchange of CO<sub>2</sub>

### 2.1 Abstract

The three-dimensional biogeochemical model ECOHAM was applied to the Northwest European Continental Shelf (NECS) (47° 41' - 63° 53' N, 15° 5' W - 13° 55' E) for the years 1970-2006. The development of annual carbon fluxes was analysed for the North Sea as the inner shelf region. We divided the North Sea into several regions, the northern North Sea, the southern North Sea, the German Bight and the Southern Bight for a more detailed analysis. To separate the effect of physical and biological processes a second simulation without biology was performed. The results of our method for calculating the biological pCO<sub>2</sub> were in good agreement with the biological pCO<sub>2</sub> calculated after the method of Takahashi *et al.* (2002). While in the standard run the North Sea acted as sink for atmospheric CO<sub>2</sub>, in the run without biology the North Sea was a continuous source for atmospheric CO<sub>2</sub>. The main drivers of the air-sea flux variability were identified as being temperature, net ecosystem production and pH. The eutrophication due to high riverine nutrient inputs during the 1980s had no significant effect on the air-sea flux of CO<sub>2</sub> because in contrast to net primary production, net ecosystem production did not respond to the period of higher phosphate input. The increase of sea surface temperature of 0.027 °C yr<sup>-1</sup> over the simulation period and the pH decline of 0.002 yr<sup>-1</sup> led to a decline of the uptake of atmospheric CO<sub>2</sub> by the North Sea of about 30 % in the last decade of the simulation period. A special feature occurred in the year 1996, where a cold sea surface temperature anomaly led to an additional (physical) uptake of atmospheric CO<sub>2</sub> and corresponded with a low primary and net ecosystem production, which on the other hand led to less biologically induced uptake of CO<sub>2</sub>. Our results indicate an ongoing decline of the uptake capacity for atmospheric carbon dioxide of the North Sea for future scenarios.

### 2.2 Introduction

The detailed understanding of the global carbon cycle is of great importance in times of rising atmospheric CO<sub>2</sub> concentrations (IPCC, 2001). There has been increasing interest in understanding and quantifying the carbon fluxes in continental shelf seas and coastal areas (Borges & Gypens, 2010; Kühn *et al.* , 2010; Liu *et al.* , 2010; Omar *et al.* , 2010) and their contribution to the oceanic uptake of atmospheric carbon dioxide. The effects of anthropogenic activities and the reaction of the marine ecosystem are more pronounced in shelf seas than in the open sea. Additionally, systematic observation-surveys (Thomas *et al.* , 2004) and the establishment of long time series of measurements (Shadwick *et al.* , 2011) are logistically easier in nearshore regions.

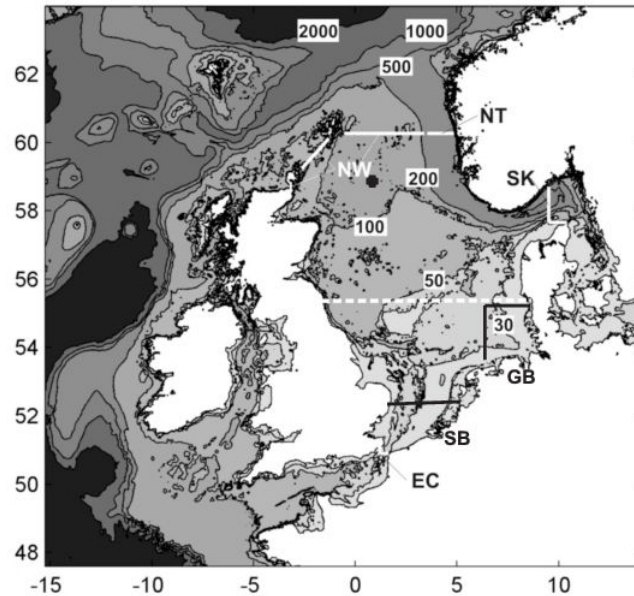


Figure 2.1: Model area with bottom topography and boundaries of the North Sea which we used for budgeting (bold line). EC: English Chanel, SK: Skagerrak, NT: Norwegian Trench, NW: North Western boundary. The boundary between southern and northern North Sea is indicated by the dashed line. The black lines indicate the subregions of the southern North Sea; GB: German Bight, SB: Southern Bight. The FLEX position is indicated by the black dot.

Such efforts become globally relevant because one component of the carbon budgets is the  $\text{CO}_2$  air-sea flux which may potentially result in the uptake of atmospheric  $\text{CO}_2$  in shelf seas (Omar *et al.*, 2010). The physically induced uptake, the biological fixation of inorganic carbon and the effective export of carbon into the adjacent deep ocean is called "continental shelf pump", a term firstly introduced by Tsunogai *et al.* (1999). The continental shelf pump mechanism has been applied to the South China Sea (Tsunogai *et al.*, 1999) and the North Sea (Bozec *et al.*, 2005; Thomas *et al.*, 2004). Furthermore global estimates of the magnitude of the continental shelf pump have been carried out (Thomas *et al.*, 2004; Yool & Fasham, 2001).

Our area of interest is the North Sea (NS) ( $511724 \text{ km}^2$ ) (Fig. 2.1), as part of the Northwest European Continental Shelf sea, constrained by the coastlines of Germany, the Netherlands and Belgium in the south, the United Kingdom in the west, and Norway and Denmark in the east. It is connected to the North Atlantic via the open north-western boundary and the English Channel and to the Baltic Sea via the Skagerrak. The North Sea can be divided into two parts, the permanently mixed shallow southern North Sea (SNS) ( $190760 \text{ km}^2$ ) which is strongly influenced by the coast and the adjacent river systems, and the deeper - seasonally stratified - northern North Sea (NNS) ( $320960 \text{ km}^2$ ), which is more strongly influenced by the North Atlantic Ocean. For this study, in the southern North Sea two subregions have been additionally separated: the German Bight (GB) ( $12563 \text{ km}^2$ ) and the Southern Bight (SB) ( $28099 \text{ km}^2$ ).

For the North Sea Thomas *et al.* (2005a) established a complete observation-based carbon budget resolving the seasonal cycle of the year 2001/02. The variability of DIC

and the partial pressure of CO<sub>2</sub> was discussed (Thomas *et al.*, 2005b). Using a model approach Kühn *et al.* (2010) investigated the seasonal and interannual variability of the North Sea-wide carbon fluxes for the years 1995 and 1996. Though the techniques differed, all these studies focussed on distinguishing biologically and physically driven carbon fluxes. The main goal of these efforts was to understand the impact of the variability of different drivers on the carbon fluxes and their possible feedbacks.

Within this study we deepen the investigations of Kühn *et al.* (2010) and widen the temporal range of simulations to the period 1970-2006. The years from 1977 to 1989 were characterised by a strong eutrophication of the southern North Sea (Peeters & Peperzak, 1990; van der Zee & Chou, 2005) mainly induced by high riverine phosphate loads. The nutrient-enrichment of the southern North Sea had a significant impact on the marine ecosystem (Vermaat *et al.*, 2008), particularly on the primary production (Skogen & Moll, 2005). The hydrodynamic properties of the northern North Sea are mainly governed by the influence of the North Atlantic. We investigate the interplay between the overall (climate-induced) trend of increasing SST (Wiltshire, 2008; Wiltshire *et al.*, 2010; Wiltshire & Manly, 2004) and acidification due to ongoing uptake of anthropogenic atmospheric CO<sub>2</sub> (Blackford *et al.*, 2008) in the shelf pump mechanism. For the continuous simulation from 1970-2006 the ecosystem model ECOHAM4 together with the hydrodynamic model HAMSOM (Backhaus, 1985; Pohlmann, 2006) were used.

Thomas *et al.* (2005b), and later also Omar *et al.* (2010) have shown that biology and temperature effects are responsible for most of the variations in pCO<sub>2</sub> in the North Sea on an interannual and seasonal scale. We therefore conducted two simulations, one with biology and one without biology to identify the main drivers of air-sea flux variability in the North Sea.

In the present work we analyse the different components of the organic and inorganic carbon budgets and subsequently identify the main drivers of their variability.

## 2.3 Material and Methods - The Model

### 2.3.1 Model setup

The three-dimensional model ECOHAM4 (ECOLOGICAL model, HAMBURG, version 4) consists of two components: first, the hydrodynamic module HAMSOM (Hamburg Shelf Ocean Model) (Backhaus, 1985), which simulates the three-dimensional advective flow field, the turbulent mixing, temperature and salinity. See Backhaus & Hainbucher (1987) and Pohlmann (1996) for a detailed description of the model. The second part is the biogeochemical module (Kühn *et al.*, 2010) which was used to calculate nitrogen and carbon budgets for the North Sea. The newer version of ECOHAM used for this study has an advanced phytoplankton module. The model includes 4 nutrients (nitrate, ammonium, phosphate, silicate), two phytoplankton groups (diatoms and flagellates), two zooplankton groups (micro- and mesozooplankton), bacteria, two fractions of detritus (fast and slowly sinking), labile dissolved organic matter, semi-labile organic carbon, oxygen, calcite, dissolved inorganic carbon, total alkalinity and the benthic state variables calcite and particulate organic matter (C, N, P, Si). The C:N:P ratio is fixed for both phytoplankton groups (C:N<sub>p</sub>=6.625, N:P<sub>p</sub>=20) (Quigg *et al.*, 2003), both zooplankton compartments (C:N<sub>z</sub>=5.5; N:P<sub>z</sub>=20) and bacteria (C:N<sub>b</sub>=4.0; N:P<sub>b</sub>=10); for diatoms a C:Si ratio of 5.76 has been applied. In order to maintain the prescribed molar C:N:P ratios within the zooplankton and bacteria compartments additional carbon, nitrogen and phosphorus fluxes were introduced (see Appendix A2).

The two detritus fractions and dissolved organic matter have freely varying elemental ratios. Calcite and 'large' detritus have a sinking velocity of 10 m d<sup>-1</sup>, 'small' detritus sinks with a velocity of 0.4 m d<sup>-1</sup>. Phytoplankton and zooplankton mortality (including mortality due to grazing by higher predators) and fecal pellet production are the sources for the two detritus fractions; 85 % of the detritus produced is directed into the slowly sinking detritus pool, 15 % feeds the faster sinking fraction. Together with the corresponding decay rates (see Appendix A4) the sinking velocities mainly determine the ratio between pelagic and benthic remineralisation.

A special feature of the model is that it allows for 'excess' or 'overflow' (Fogg, 1983) production (NPP<sub>exc</sub>) or 'carbon overconsumption' as specified by Toggweiler (1993). Carbon overconsumption is defined as carbon fixation by photosynthesis when the surface layers are depleted in bioavailable nutrients (Thomas *et al.*, 1999; Toggweiler, 1993). This fixed excess carbon is released in the form of dissolved or colloidal extracellular carbohydrates which tend to coagulate forming transparent exopolymer particles (TEP) (Engel, 2002; Schartau *et al.*, 2007). In the model the excess carbon is immediately channelled into the pool of slowly degradable semi-labile dissolved organic carbon, which is eventually metabolized by the bacteria (on a time scale of 9 months). Thus, the model differentiates between 'normal' exudation by phytoplankton, the result of which is labile dissolved organic matter with Redfield composition (Fogg, 1983), and an excess exudation of semi-labile organic carbon.

The model also simulates the production of calcium carbonate (CaCO<sub>3</sub>), but in a very simplified way: the flagellates produce calcite together with organic matter (OM), the corresponding molar production ratio is CaCO<sub>3</sub>-C:OM-C = 1:70, according to an estimate of the ratio between carbonate production and primary production in the ocean (Chung *et al.*, 2003; Langer, 2008). This approach obviously neglects the specific seasonality and the regional differences in the CaCO<sub>3</sub> production by coccolithophorids, but supplies a carbonate production on the Northwest European Continental Shelf which is in the range of global estimates. The carbonate shells become part of the fast-sinking detritus and are dissolved while sinking through the water column and in the sediment layer. The dissolution rate is a function of the carbonate oversaturation (see Appendix A2).

The air-sea flux of CO<sub>2</sub> is calculated according to:

$$F(\text{CO}_2) = k \cdot (\text{pCO}_2^{\text{air}} - \text{pCO}_2^{\text{wat}}), \quad (2.1)$$

where pCO<sub>2</sub><sup>air</sup> denotes the prescribed partial pressure of CO<sub>2</sub> in the atmosphere, pCO<sub>2</sub><sup>wat</sup> the partial pressure of CO<sub>2</sub> in the near-surface water and k the wind-dependent gas transfer or piston velocity. We use the empiric expression derived by Wanninkhof (1992) for the gas transfer velocity in case of steady wind speed (their equation 8). The annual time series for the partial pressure of atmospheric CO<sub>2</sub> is calculated based on the Mauna Loa data set taking into account an annual increase of 1.32 μatm yr<sup>-1</sup> for the years before 1995, and 2.0 μatm yr<sup>-1</sup> for the years after 1995 (Doney *et al.*, 2009). The pCO<sub>2</sub><sup>wat</sup> is calculated from the water temperature, salinity, DIC and TA (Total Alkalinity) by applying the equilibrium equations of the carbonate system using the carbonic acid constants according to Mehrbach *et al.* (1973) as refit by Dickson & Millero (1987). The surface pCO<sub>2</sub> is calculated in the upper layer of the model (0 - 10 m depth) (Weiss, 1974). A negative F(CO<sub>2</sub>) indicates an outgassing of carbon dioxide from the sea. TA is calculated prognostically but is restored to prescribed values derived from the CANOBA data set with a relaxation time of two weeks (Kühn *et al.*, 2010).

Oxygen dynamics, involved in the primary production, in the remineralisation processes and in nitrification/denitrification, are formulated according to Neumann (2000) and Fennel *et al.* (2006). The full set of biogeochemical equations is given in the Appendix A1.

The horizontal resolution of the model area is  $0.2^\circ$  in latitude and  $1/3^\circ$  in longitude, i.e. about 20 km for both directions. The model is set up with 24 vertical layers with increasing thickness towards the bottom; the surface layer has a time-varying thickness (mean  $z = 10$  m) due to surface elevation. The underlying layers (10 - 50 m) are resolved by 5 m steps. Below 50 m the thickness of the layers increases successively. After some validation exercises for the different state variables at different stations in the North Sea, the model was run from 1970 to 2006 continuously after a 2-year spin up in 1970.

### 2.3.2 External data

#### Meteorological forcing data

The meteorological forcing is provided by NCEP Reanalysis (Kalnay *et al.*, 1996) and consists of six-hourly fields of air temperature, relative humidity, cloud coverage, wind speed, atmospheric pressure and wind stress in 2 dimensions for every year. We calculated 2-hourly and daily mean short wave radiation from astronomic insolation and cloudiness after Budyko's model including the effect of surface albedo (Berliand, 1960; Budyko, 1974). Moll & Radach (1991) checked simulated versus observed data at Helgoland for the applicability of such a method in the North Sea. The annual mean air temperature in the NECS region increased during our simulation period. A linear regression reveals an increase of  $0.02^\circ\text{C}$  per year. The relative humidity and cloud cover exhibit low seasonal and interannual variations. The wind speed fluctuated weakly on interannual timescales, while the seasonal variability is quite high; the annual standard deviation ranges up to about 50 % of the annual mean values.

#### Deposition data

The atmospheric deposition of nitrogen is considerable in the North Sea region (Schlünzen & Meyer, 2007) and is included in our model. It is ranging from 280 to 440 ktN yr<sup>-1</sup> (Tab. 2.1). This is in the same order of magnitude as the overall input of nitrogen by rivers into the North Sea (Radach & Pätsch, 2007). For this study we adapted the data for dry and wet deposition of oxidised and reduced nitrogen given by EMEP (Cooperative program for monitoring and evaluation of the long-range transmissions of air pollutants in Europe) and interpolated them on the Northwest European Continental Shelf area (see also Pätsch & Kühn (2008)). These data are available in steps of five years from 1980 to 2000 and afterwards on a yearly basis. We linearly interpolated the deposition values for the gaps and extrapolated the data for the period from 1970 to 1980 with an increase adapted from Pätsch & Radach (1997). In that study the deposition in 1970 was estimated to be 87.5 % of the deposition of 1980. The values for the total North Sea region are given in Tab. 2.1.

In the last 6 years, the values are showing a decreasing trend. The available data suggest, that the amount of oxidised nitrogen decreased stronger than the amount of reduced nitrogen (not shown). The horizontal offshore gradient of annual nitrogen input is showing a decrease in atmospheric nitrogen deposition towards the North Atlantic. Increased atmospheric deposition occurs along the continental coast, in the English Channel and in the Skagerrak and Kattegat. Atmospheric inputs of silicon and

Year	N deposition [k tons yr <sup>-1</sup> ]
1980	422.4
1985	436.6
1990	379.7
1995	335.0
2000	401.2
2001	350.1
2002	347.1
2003	310.3
2004	317.6
2005	300.1
2006	276.3

Table 2.1: Annual atmospheric oxidised and reduced dry and wet deposition of total inorganic nitrogen for the North Sea region.

phosphorus are rather minor sources (Jickells, 2005) compared to riverine sources and are therefore neglected.

### Boundary conditions

The hydrodynamic boundary conditions are defined as described in Pohlmann (2006) and are repeated for every year. For the biogeochemical module, we prescribed depth-dependent monthly mean values for all state variables at the open boundaries of the shelf region (Fig. 2.1). All values but the DIC concentrations are identical for every year with a seasonal variability. Boundary conditions of nitrate, phosphate and silicate were derived from the World Ocean Atlas 2001 (Conkright *et al.*, 2002).

Concentrations of DIC [mmol C m<sup>-3</sup>] and TA [mmol m<sup>-3</sup>] at the open boundaries were supplied by the Max-Planck-Institute for Meteorology, Hamburg for 1995. These model data are described in Kühn *et al.* (2010). Since DIC is continuously rising due to anthropogenic CO<sub>2</sub> emissions we calculated monthly time-dependent boundary conditions using the given data for 1995:

$$\text{DIC}(\text{year}) = \text{DIC}(1995) + \text{offDIC} \quad (2.2)$$

$$\text{offDIC} = (\text{year} - 1995) \cdot 2.0 \cdot 0.65 \quad \text{for year} = 1996 \text{ to } 2006 \quad (2.3)$$

$$\text{offDIC} = (\text{year} - 1995) \cdot 1.32 \cdot 0.65 \quad \text{for year} = 1970 \text{ to } 1994 \quad (2.4)$$

$$(2.5)$$

This was applied to DIC in the whole water column. The increase of atmospheric CO<sub>2</sub> from 1970 up to 1994 was about 1.32 ppm yr<sup>-1</sup>, while it was 2.0 ppm yr<sup>-1</sup> for the period from 1996 to 2006. The factor 0.65 mmol C m<sup>-3</sup> ppm<sup>-1</sup> transfers the pCO<sub>2</sub> increase to DIC increase (Thomas *et al.*, 2001). This factor is dependent on several other variables, e.g. temperature, alkalinity, DIC and the pCO<sub>2</sub> value itself. Thus it is not constant in natural environments, but the value of 0.65 represents most of the changes quite well.

The seasonal variability ranging from 362 ppm in April down to 347 ppm in August/September in 1995 includes the mean value 359 ppm of the Mauna Loa observations (Doney *et al.*, 2009) for 1995.

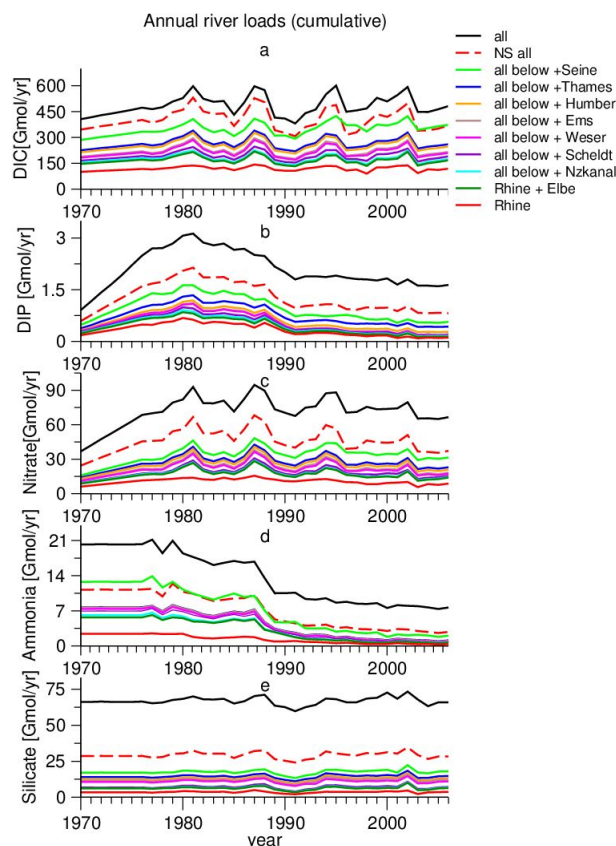


Figure 2.2: Cumulative annual loads of the most important rivers, for the North Sea region (dashed line) and the NECS region. (a) DIC, (b) phosphate, (c) nitrate, (d) ammonia, (e) silicate.

### River data

Coastal seas like the North Sea are strongly affected by river inputs (deYoung *et al.*, 2004). To determine the effect of nutrient input via the river systems in the model area (Fig. 2.1), daily river loads were affiliated to the model as forcing/boundary conditions. In Fig. 2.2 the time series of annual loads of the most important rivers are shown.

We prescribed the following variables: dissolved inorganic carbon (DIC), inorganic nutrients (phosphate, nitrate + nitrite, ammonia, and silicate), alkalinity and total organic carbon (TOC), nitrogen (TON), phosphorus (TOP) and organic silicate (opal). The main river systems entering the Northwest European Continental Shelf system were determined according to their discharge volumes. We used several different sources to collect and complete the needed data sets, but some gaps still remained in the data (see below). The river load data for the German, Dutch and Belgian coast are described in Pätsch & Lenhart (2008) and for the time interval 1977-2000 in Radach & Pätsch (2007). The data for the Norwegian coast are from OSPAR (2005) and the data for the UK rivers are from Heath *et al.* (2002).

Observed river concentrations from Pätsch & Lenhart (2008) (ZMK data) are only available from 1977 to 2006. To obtain values for the whole simulation period the data were extrapolated from 1976 to 1970. Thereto the river loads for 1977-1979 were averaged and then used to calculate the values for the years 1970-1976. For ammonium

and silicate, the averaged values were used as constant for every year, while nitrate, nitrite and particulate organic nitrogen are linearly decreasing from 1977 to 1970, with the value of 1970 being only half of the value in 1977. For phosphate and particulate organic phosphorus, the river loads are linearly decreasing up to one third of the averaged value in 1970. The total alkalinity, dissolved inorganic carbon as well as particulate organic carbon correspond to the river loads of 1977.

The Scandinavian and British river loads were derived from Heath *et al.* (2002) representing the year 1990; in most cases only annual estimates were available. These values were used for each of our simulation years 1977-2006. For the years 1970-1976 the extrapolation rules described above were applied.

The data provided by OSPAR were only available as monthly values from 1984 to 2004. The monthly means were interpolated to daily values. To fill the period between 1984 and 1970 the same method as for the ZMK data was used. To extrapolate the data from 2005 to 2006, the mean values of the years 2002-2004 were used. Gaps in data sets were filled by taking the mean value of the two preceding and the two following years. The carbonate species were calculated with the end-member method (Kaul & Froelicher, 1984). This method accounts for the correlation between salinity and tracer concentrations. Therefore, the end-member values were multiplied by the freshwater discharge of the specific river. The end-member values were not directly available for the Ijssel, Weser and Nordzeekanal, so the end-members of rivers nearby and with similar characteristics were applied (Pätsch & Lenhart, 2008).

We assumed a ratio of about 10 % of the original river load of total organic carbon to be bioavailable and added it to the slowly sinking detritus pool of the model (compare Kühn *et al.* (2010)).

## 2.4 Results

### 2.4.1 Hydrodynamic results

#### Temperature analysis

The annual mean SST for the North Sea region (Fig. 2.1) is shown in Fig. 2.3. Monitoring observations for the North Sea temperature (Loewe *et al.*, 2009) were compared with the simulation. The simulated SST is always a bit higher than the observed SST. This may be due to the fact, that we only warm up the upper layer of the water column with the incoming radiation (Pohlmann, 2006). The modelled SST time series exhibits pronounced interannual and decadal variations. The series bears an overall increasing trend of 0.027 °C yr<sup>-1</sup> and 0.08 °C yr<sup>-1</sup> over the last decade.

#### Thermocline

The thermocline is defined by the existence of a local vertical temperature gradient:

$$\frac{\delta T}{\delta z} \geq 0.1 \quad \left[ \frac{\text{K}}{\text{m}} \right] \quad (2.6)$$

where T [K] represents the temperature and z [m] the depth. While the mean thermocline depth exhibits low interannual variability and varies always around 16 m, the maximum thermocline depth shows clear variations with values from 15.6 m (1982) to 23.6 m (1971). Our simulated mean thermocline depth is a bit shallower than found in other studies (Nielsen & St John, 2001; van Haren & Howarth, 2004; Warrach, 1998).

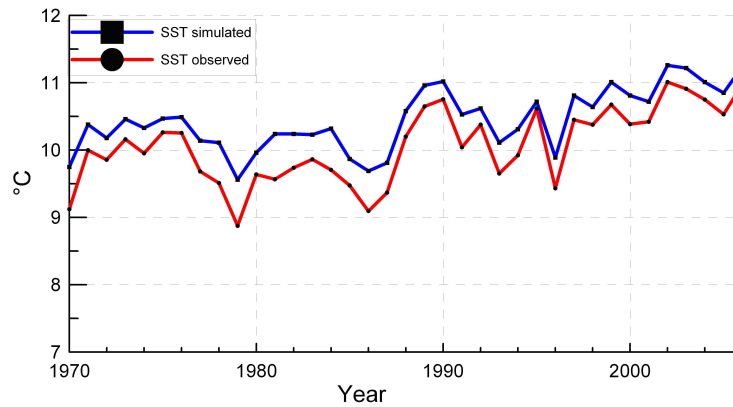


Figure 2.3: Development of annual mean SST for the North Sea region. Comparison of ECOHAM4 simulation and observations (Loewe *et al.*, 2009)

### Water exchange

To obtain a reasonable description of the shelf pump, it is important that the general flow pattern and the water budget are well reproduced. The water budget of the North Sea is characterised by an inflow of North Atlantic water via the north-western boundary (Shetland Current (SC), Fair Isle Current (FC), Pentland Firth (PF)) and via the English Channel (EC), an inflow of Baltic seawater via the Skagerrak (SK) and an outflow of North Sea water via the Norwegian Trench (NT) (see Fig. 2.1). The largest volume of water is brought into the North Sea via the north-western boundary, the main contributors being the Shetland and the Fair Isle Current. The mean water transport via the different sections is given in Tab. 2.2.

The variability of the annual North Atlantic inflow can be partly explained by the variability of the North Atlantic Oscillation Index ( $r = 0.51$ ). The outflow via the Norwegian Trench is mainly controlled by the magnitude of the North Atlantic inflow.

The volume of water that is transported into the North Atlantic via the Norwegian Trench and its carbon concentrations are important contributors to the strength of the shelf pump. Estimates for the Norwegian outflow ranged from 1.34 Sv to 1.8 Sv (Otto *et al.*, 1990) (and references therein), while the mean transport of our simulations is lower with an outflow of 1.31 Sv. Another modelling study calculated the outflow along the Norwegian coast as being about 1.29 Sv (Huthnance *et al.*, 2009). OSPAR (2000) gave a value of 1.5 Sv. Our simulated mean value of the North Atlantic inflow is lower than the transport given by OSPAR and ICES (Tab. 2.2), while it is about two times higher than the estimate by Huthnance *et al.* (2009). The simulated mean value of water import via the English Channel is slightly lower than the estimated range provided by Otto *et al.* (1990) (Tab. 2.2). The inflow from the Baltic Sea was estimated by the ICES study (Haarich *et al.*, 1992; ICES, 1983) to be about 0.02 Sv, which is considerably lower than our mean inflow (Tab. 2.2).

The differences between our results and the estimates of other studies are within an acceptable range, considering a) that the water transport is dependent on the position where the section for its calculation is placed b) that the other studies also rely mostly on model estimates.

	Model results water import [Sv]	Other calculations/refernces water import [Sv]
via English Channel	0.08	0.1-0.17 (Otto <i>et al.</i> , 1990)
via north-western boundary	1.11	0.59 (Huthnance <i>et al.</i> , 2009) 1.4 (OSPAR, 2000) 1.6 (ICES, 1983)
via Skagerrak	0.11	0.02 (Haarich <i>et al.</i> , 1992), (ICES, 1983)
via Norwegian Trench	-1.31	-1.8-(-1.34) (Otto <i>et al.</i> , 1990) -1.29 (Huthnance <i>et al.</i> , 2009) -1.5 (OSPAR, 2000)

Table 2.2: Comparison of the mean modelled water transport with different data sets.

## 2.4.2 Biogeochemical results

### The standard run

We used our simulation results to calculate carbon budgets for every year for the whole North Sea. Annual total carbon budgets, containing organic and inorganic, particulate and dissolved carbon species, for the years 1985, 1995 and 2005 are given in Fig. 2.4. The exchange with the atmosphere (air), the river input (river), the import via the north-western boundary, the English Channel and the Skagerrak and the export via the Norwegian Trench are considered.

The  $\Delta C$  in the budget stands for the difference of carbon content between 1 January and 31 December, due to surface elevation or concentration changes in the pelagic and sediment. This value can be positive or negative, depending on the biogeochemical and hydrodynamic conditions of the year in question. It can be seen from Fig. 2.4 that the fluxes of carbon from the atmosphere and from river input are of the same order of magnitude. This is also the case for all other years.

The simulated annual air-sea fluxes for the total, the northern and the southern North Sea, the German Bight and the Southern Bight are given in Fig. 2.5.

While the total North Sea (Fig. 2.5a) acted as a sink of atmospheric  $\text{CO}_2$ , a feature which was dominated by the northern North Sea (Fig. 2.5b), the southern North Sea (Fig.2.5c) oscillated between being a source and a sink for atmospheric  $\text{CO}_2$ . The two subregions of the southern North Sea, the German Bight and the Southern Bight (Fig. 2.5d,e), are sources for atmospheric  $\text{CO}_2$  during the whole period. Schiettecatte *et al.* (2007) found the SB in the years 2003-2004 to be a sink for atmospheric  $\text{CO}_2$  and Thomas *et al.* (2004) found the SB to be a source in 2001-2002, while our model shows that the SB is a stronger source in 2001-2002 than in 2003-2004. Gypens *et al.* (2011) analysed the air-sea flux in the Southern Bight as well. They found an increase of the  $\text{CO}_2$  source between 2000 and 2002 with a maximum in 2001, which is in correspondence with our results. The mean uptake of  $\text{CO}_2$  by the northern North Sea was about  $2.12 \text{ mol C m}^{-2} \text{ yr}^{-1}$ , while it was  $-0.05 \text{ mol C m}^{-2} \text{ yr}^{-1}$  for the southern North Sea and  $1.31 \text{ mol C m}^{-2} \text{ yr}^{-1}$  for the total North Sea. The last number corresponds quite well with the estimate by Thomas *et al.* (2004) of  $1.38 \text{ mol C m}^{-2} \text{ yr}^{-1}$  for the uptake of atmospheric  $\text{CO}_2$  by the North Sea in the years 2001 and 2002. The uptake of atmospheric  $\text{CO}_2$  by the North Sea for the whole simulation period showed minima in the years 1997 and 2006, as well as a decline of the  $\text{CO}_2$  uptake over the last decade, induced by the northern North Sea.

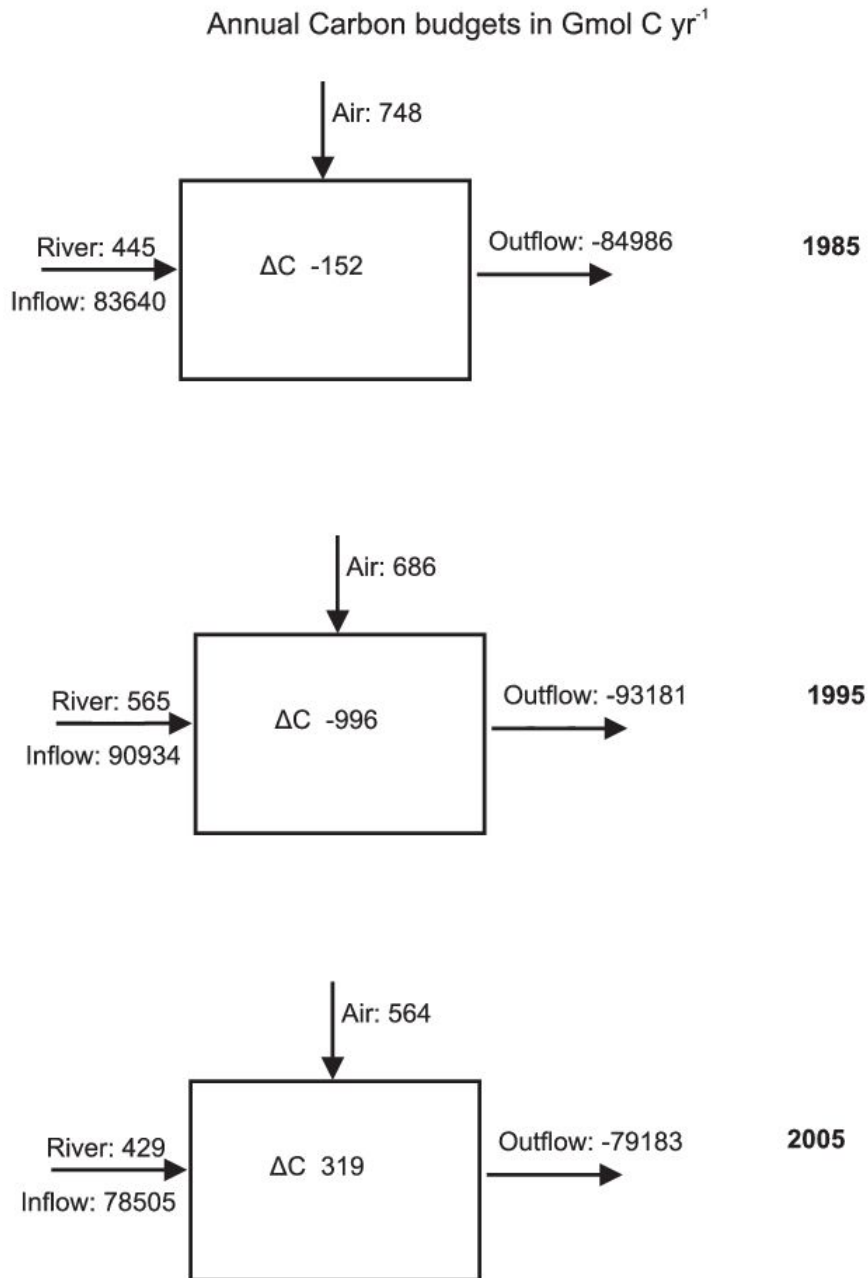


Figure 2.4: Carbon budget for the North Sea 1985, 1995 and 2005, fluxes in Gmol C yr<sup>-1</sup>. **Inflow:** import of carbon into the North Sea; **River:** import of carbon via rivers; **Air:** air-sea flux of CO<sub>2</sub>;  $\Delta C$ : storage; **Outflow:** Export of carbon from the North Sea.

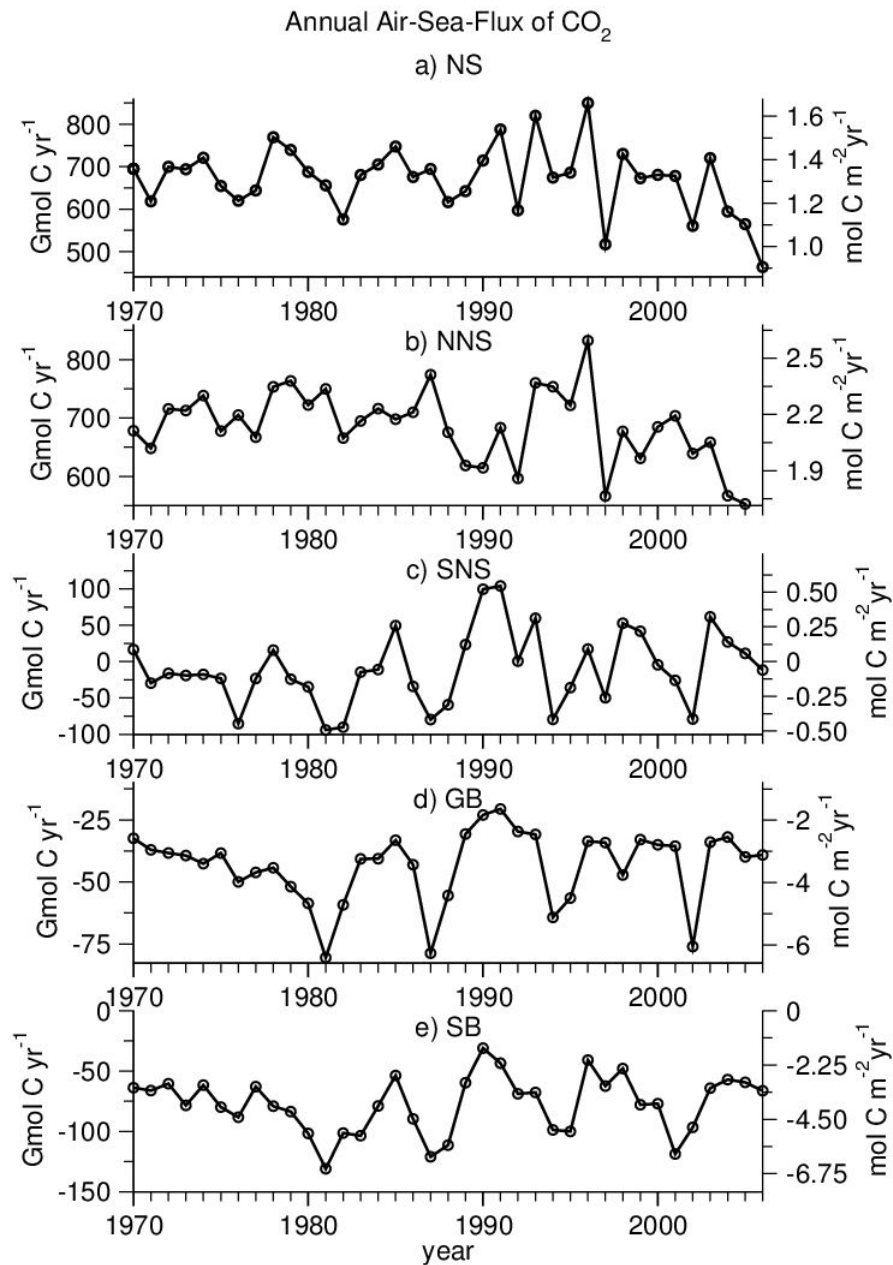


Figure 2.5: Annual air-sea flux of CO<sub>2</sub> for the (a) total, (b) northern and (c) southern North Sea, (d) German Bight, (e) Southern Bight.

The mean total carbon concentration, comprising organic and inorganic, particulate and dissolved carbon species, in the water entering the North Sea is about  $2.17 \text{ mol C m}^{-3}$ , while the mean concentration in the water leaving the North Sea via the Norwegian Trench is about  $2.2 \text{ mol C m}^{-3}$  resulting in an enrichment of  $0.03 \text{ mol C m}^{-3}$ . Thomas *et al.* (2004) estimated, that the increase in DIC concentration of the water leaving the North Sea was  $0.024 \text{ mol C m}^{-3}$ . Since we include all carbon pools, not only DIC in our calculations, our mean model result is in good agreement with their result for the years 2001/2002. About 85 % of the water and 85 % of the carbon is leaving the North Sea below a mean thermocline depth of 25 m, resulting in an effective export of organic and inorganic carbon into the adjacent North Atlantic Ocean.

The sedimentation and long-term deposition of particulate organic material in the North Sea accounts for less than 1 % of primary production (de Haas *et al.*, 2002; Luff & Moll, 2004; Radach & Lenhart, 1995; Thomas *et al.*, 2005a). ECOHAM4 uses a simple benthic layer model (Moll, 1998; Pätsch & Kühn, 2008). After one year almost all of the sedimented organic carbon is remineralised again, so that there is no real long-term storage of carbon in the sediments. Therefore, since we are examining mainly annual budgets, the sedimentation flux does not play an important role.

The simulated pH declined by  $0.002 \text{ yr}^{-1}$  in the northern North Sea during the simulated time period, which corresponds well with values from Olafsson *et al.* (2009) for the Iceland Sea. The mean decline differs depending on the region. We averaged the regional pH of the years 1970 - 1980 and the years 1996 - 2006 respectively and calculated the mean decline as the difference between these averages divided by 26 years (2001-1975). This procedure was applied to smooth annual fluctuations. We found that in the southern North Sea the pH declines by about  $0.0015 \text{ yr}^{-1}$ , while it declines by about  $0.002 \text{ yr}^{-1}$  in the northern North Sea.

When we examine the sum of the net primary production (NPP) of the two phytoplankton groups (Fig. 2.6a) it can be seen that the NPP responds to the high-phosphate induced eutrophication during the eighties with elevated values (Fig. 2.2b). During 1996, a year with negative SST anomalies (Fig. 2.10) and low nutrient input by rivers (Fig. 2.2), phytoplankton is reacting with a lower NPP.

If the two phytoplankton groups were examined separately (Fig. 2.6b+c), it can be seen that diatoms increase their NPP more in spring and autumn due to the eutrophication signal, while the non-diatoms react more in the summer months. The mean value of total annual NPP is about  $7898 \text{ Gmol C yr}^{-1}$ , with a contribution by diatoms of about  $3016 \text{ Gmol C yr}^{-1}$  and of non-diatoms about  $4882 \text{ Gmol C yr}^{-1}$ . In the German Bight, non-diatoms (Fig. 2.6d) are responding very strongly to the elevated DIP inputs by Elbe and Weser (Fig. 2.2), while diatoms (Fig. 2.6e) are reacting more on the peaks of DIN input around 1981, 1987, 1994 and 2002 by the two entering rivers (Fig. 2.2). In the Southern Bight, the non-diatoms (Fig. 2.6f) do not react strongly on the elevated DIP inputs of mainly the river Rhine (Fig.2.2), while diatoms (Fig. 2.6g) show elevated NPP in years with elevated DIN levels.

The annual NEP (Net Ecosystem Production;  $\text{NEP} = \text{NPP} - \text{heterotrophic respiration}$ ) does not respond to the eutrophication but shows a minimum value in the low SST year 1996 (Fig. 2.7). The mean NEP for the North Sea is about  $335 \text{ Gmol C yr}^{-1}$ . In the northern part of the North Sea the NEP can become slightly negative in some years. The annual NEP in the southern North Sea is always positive and higher than in the northern North Sea. In the German Bight, the NEP switches between autotrophy and heterotrophy and shows slightly elevated levels after 1987. The Southern Bight is mostly heterotrophic. Both regions do not show a significant effect of eutrophication.

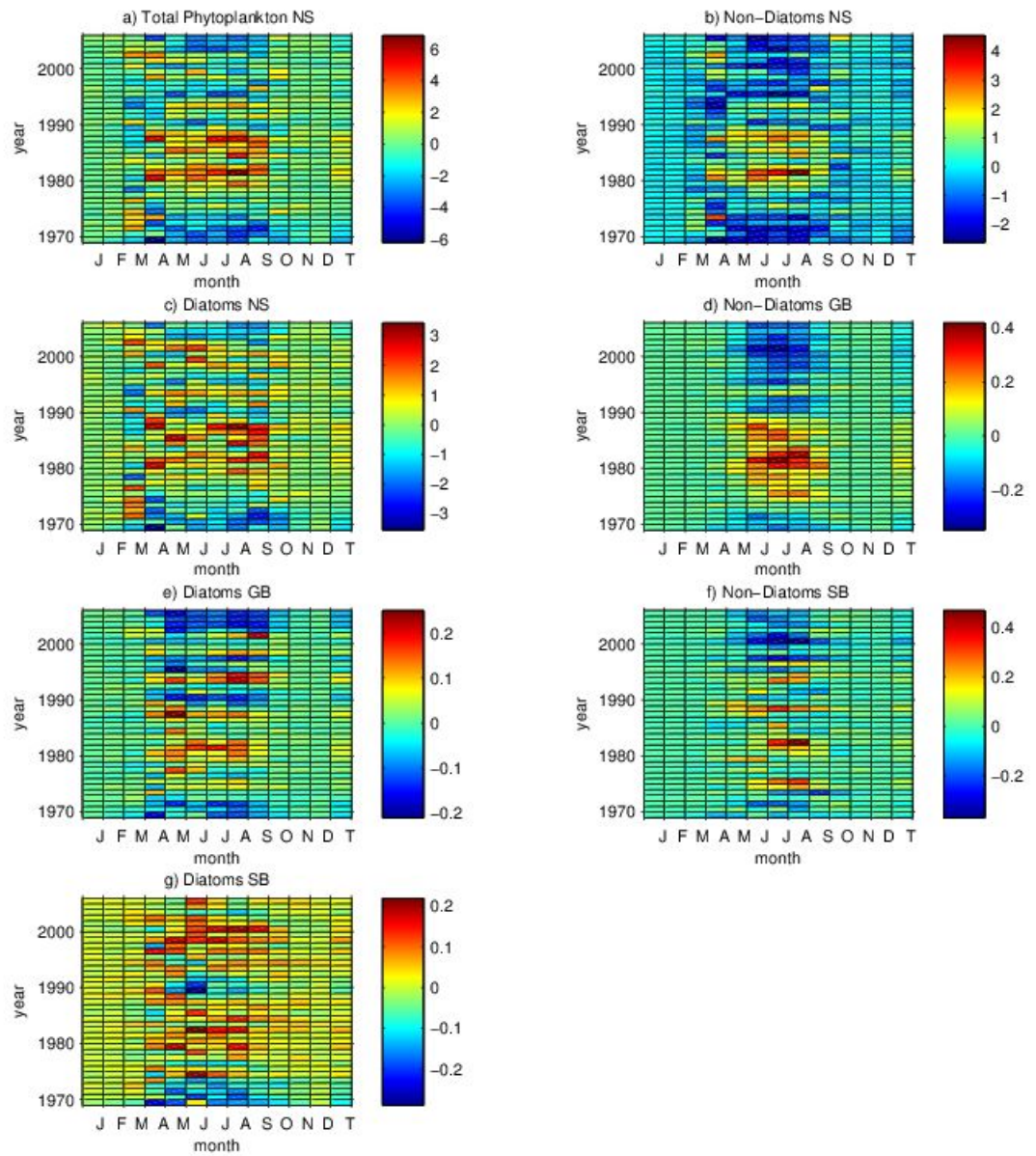


Figure 2.6: Anomalies of primary production [ $\text{Gmol C d}^{-1}$ ] for every month and the year (called: T). (a) Total phytoplankton North Sea, (b) non-diatoms North Sea, (c) diatoms North Sea, (d) non-diatoms German Bight, (e) diatoms German Bight, (f) non-diatoms Southern Bight, (g) diatoms Southern Bight.

This is in contrast to findings of Gypens *et al.* (2009) and Borges & Gypens (2010). But it has to be taken into account that our model does not include *Phaeocystis*.

### The “no-biology”- run

To distinguish between the physical and the biological effects, we conducted a second long-term simulation without biology. The setup of this second long-term simulation was exactly the same as for the standard run, with the only difference that all biological processes were switched off.

In this simulation the North Sea acted as a permanent source for atmospheric CO<sub>2</sub> (Fig. 2.8). The outgassing occurred in the southern and northern part of the North Sea; while the mean air-sea flux of CO<sub>2</sub> was about -1.0 mol C m<sup>-2</sup>yr<sup>-1</sup> for the total North Sea, the southern North Sea was subject to a stronger mean outgassing of about -1.53 mol C m<sup>-2</sup>yr<sup>-1</sup> and the northern North Sea accounted for -0.69 mol C m<sup>-2</sup>yr<sup>-1</sup>. The release of CO<sub>2</sub> showed a small increase during the simulation period (Fig. 2.8a). This trend is triggered by the northern North Sea, which shows a clearly increasing release of CO<sub>2</sub> to the atmosphere (Fig. 2.8b), while the southern North Sea did not show this signal (Fig. 2.8c). The weakest outgassing occurred in 1996 with a total amount of 292 Gmol C yr<sup>-1</sup> and the strongest outgassing was found in 2006 with 720 Gmol C yr<sup>-1</sup>. The variability in the southern North Sea and the two subregions (Fig. 2.8c,d,e) mainly displays the variability of the river DIC input (Fig. 2.2a).

### Biologically induced air-sea flux

Assuming a superposition of biological and physical effects we calculated the biologically induced air-sea flux of CO<sub>2</sub> (Fig. 2.9) by subtracting the fluxes of the no-biology run from those of the standard run. From Fig. 2.9 it can be seen, that a large amount of CO<sub>2</sub> is taken up in the North Sea due to biology. The net uptake of atmospheric CO<sub>2</sub> due to biology increases slightly during the years, while lowest values occur at the beginning of the simulation period and in 1997. The mean biologically induced uptake was 2.32 mol C m<sup>-2</sup>yr<sup>-1</sup> for the total North Sea, 2.81 mol C m<sup>-2</sup>yr<sup>-1</sup> for the northern North Sea and 1.48 mol C m<sup>-2</sup>yr<sup>-1</sup> for the southern North Sea. In contrast to the total and the northern North Sea, the biological air-sea flux in the southern North Sea is lowest in 1996. The two subregions (Fig. 2.9d+e) are showing no significant differences from each other and match the development of the whole southern North Sea.

## 2.5 Discussion

### 2.5.1 Carbon budget

Our calculated carbon budget for 1995 (Fig. 2.4) differs slightly from the budget in Kühn *et al.* (2010), due to the different model setups, especially in the phytoplankton module, the improved river input and the different meteorological forcing. The NPP in our model is lower than that given by Kühn *et al.* (2010). They found 17.6 mol C m<sup>-2</sup>yr<sup>-1</sup> for 1995 and 17.3 mol C m<sup>-2</sup>yr<sup>-1</sup> for 1996, while our NPP for 1995 is 15.3 mol C m<sup>-2</sup>yr<sup>-1</sup> and 14.5 mol C m<sup>-2</sup>yr<sup>-1</sup> for 1996. Although the NPP is lower in this study, the mean NEP is higher than the Kühn *et al.* (2010) values and with 0.6 mol C m<sup>-2</sup>yr<sup>-1</sup> higher than the NEP calculated by Bozec *et al.* (2006) of -0.1 mol C m<sup>-2</sup>yr<sup>-1</sup>. Our estimated NEP for the upper 30 m is 5.3 mol C m<sup>-2</sup>yr<sup>-1</sup> and thus higher than the estimates of Thomas *et al.* (2005b) (4.0 mol C m<sup>-2</sup> yr<sup>-1</sup>) and Bozec *et al.* (2006) (4.3 mol C m<sup>-2</sup>yr<sup>-1</sup>), while

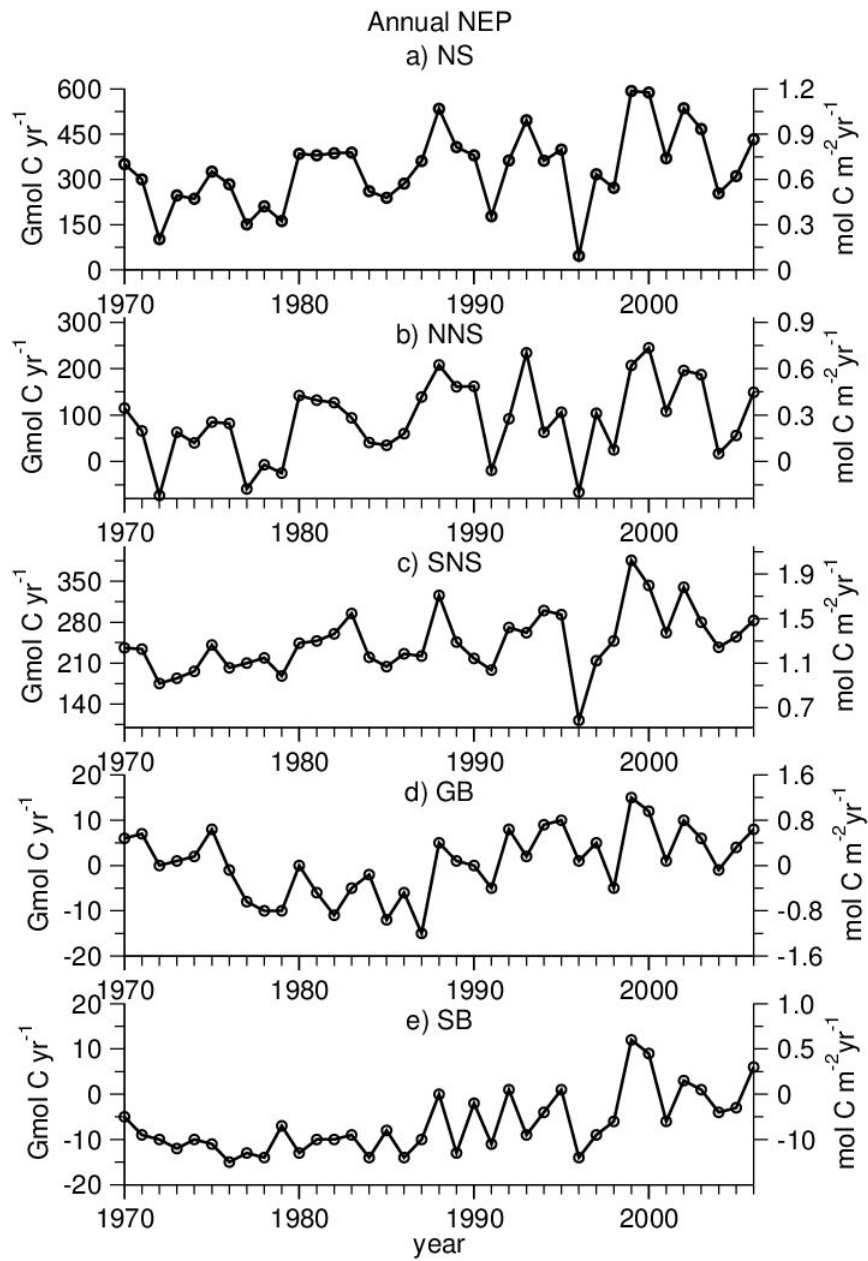


Figure 2.7: Annual NEP for the (a) total North Sea, (b) the northern North Sea, (c) the southern North Sea, (d) the German Bight and (e) the Southern Bight.

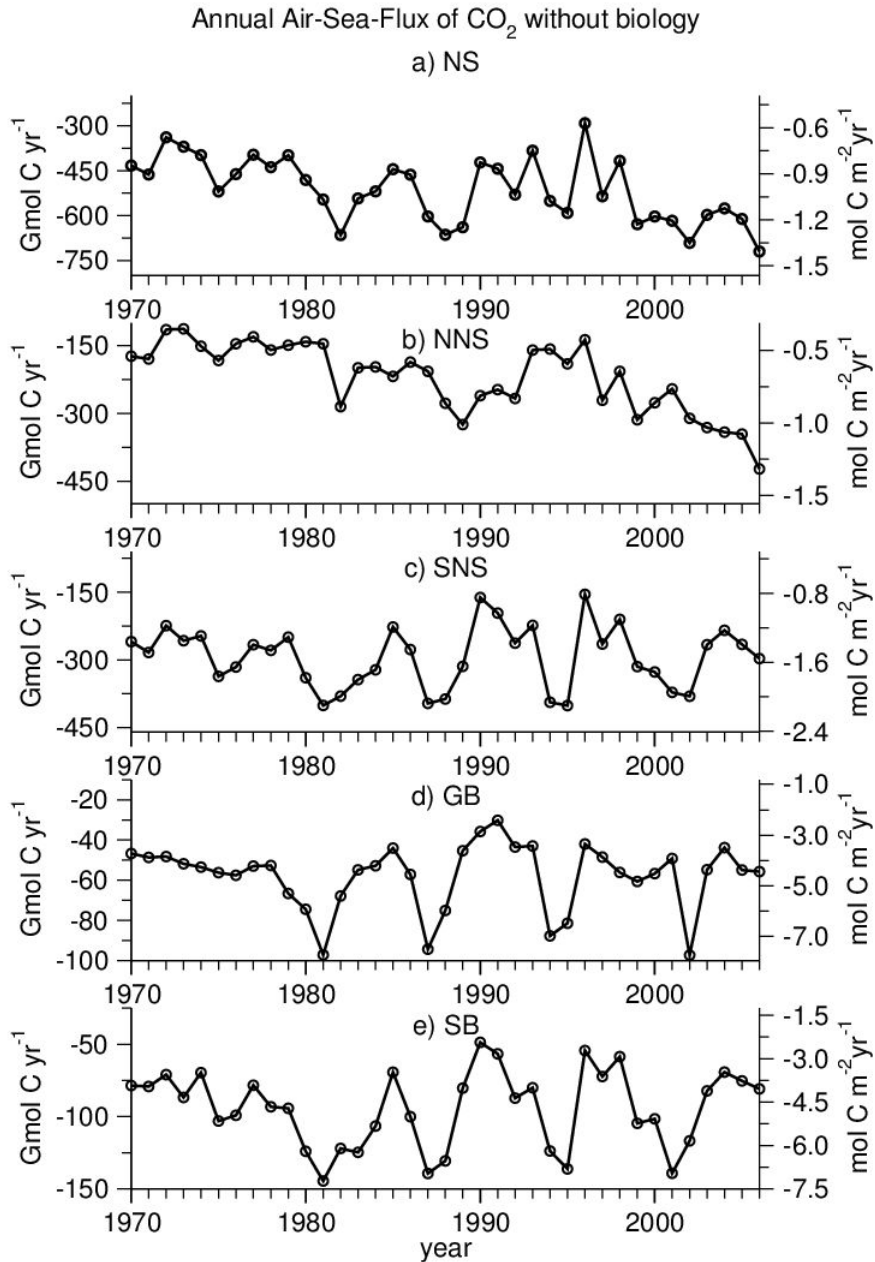


Figure 2.8: Annual air-sea flux of CO<sub>2</sub> without biology for (a) the North Sea, (b) the northern North Sea, (c) the southern North Sea, (d) the German Bight and (e) the Southern Bight.

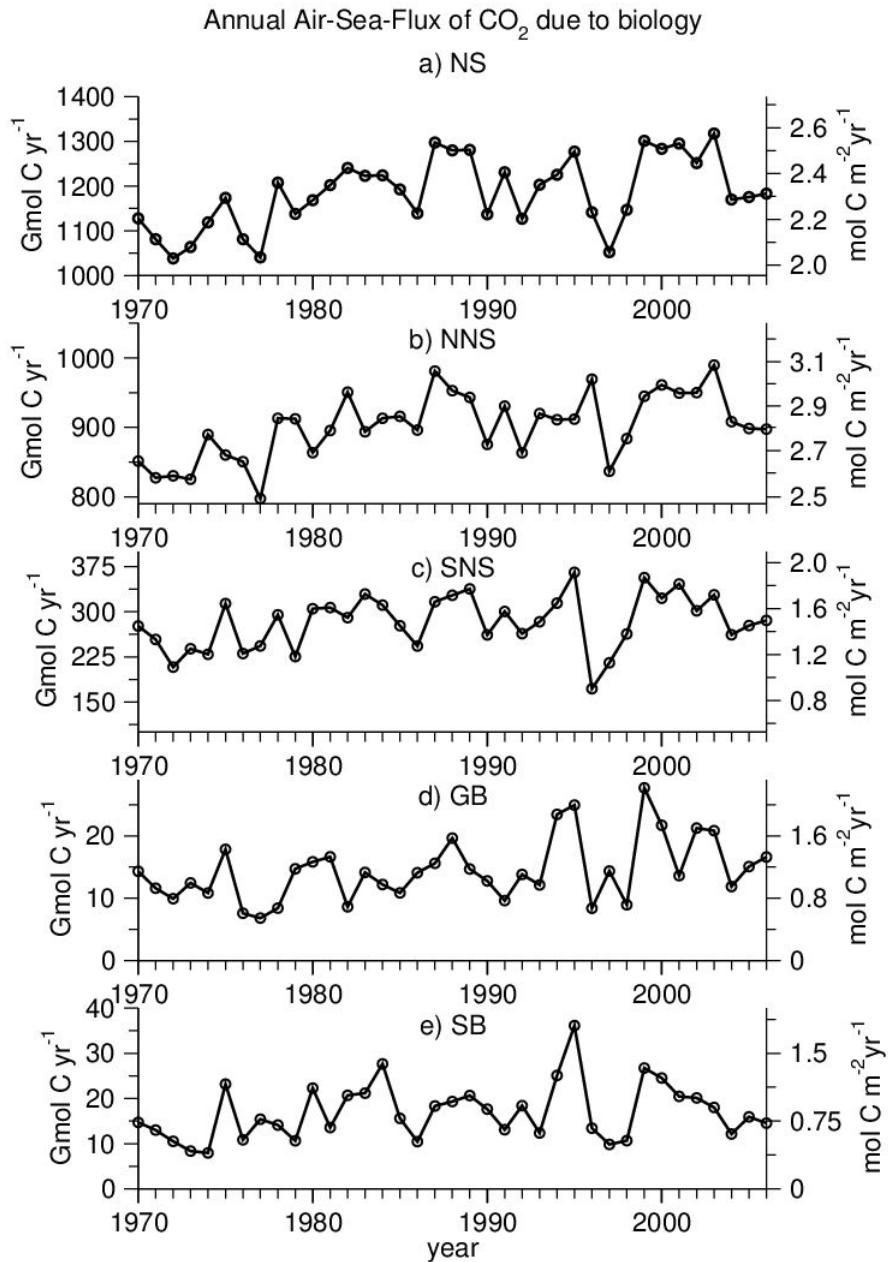


Figure 2.9: Annual air-sea flux of CO<sub>2</sub> due to biology for the (a) North Sea, (b) the northern North Sea, (c) the southern North Sea, (d) the German Bight and (e) the Southern Bight.

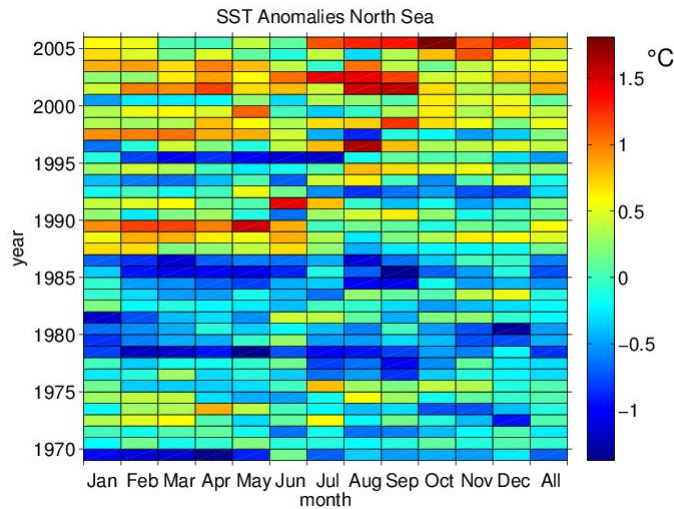


Figure 2.10: Anomalies of SST [C] for every month and the year (called All) for the North Sea

it is lower than that of Kühn *et al.* (2010) ( $6.2 \text{ mol C m}^{-2}\text{yr}^{-1}$ ). But overall, there is quite good correspondence between our NEP estimates and the NEP values from other studies.

### 2.5.2 Physical and biological drivers of the air-sea flux

The time-series of annual values of temperature- and thermocline-related parameters were compared and correlated with the time-series of annual air-sea fluxes of  $\text{CO}_2$  from the standard run, the "no-biology run" and the calculated "only-biology run", respectively. Additionally the correlations between these parameters and the annual net ecosystem production (NEP) integrated over the full water column were analysed. We use the correlation coefficients ( $r$ ) to examine the relationship between two variables and to identify qualitatively the drivers of the system. The idea behind this approach is that meteorological features in the North Sea have a large impact on local marine processes like temperature development or the building of stratified water columns (Sharples *et al.*, 2006). These processes influence the timing and strength of biological activities.

While the correlations generally are not very high, some relationships between the different hydrodynamic parameters and the air-sea fluxes as well as the NEP are instructive.

The SST directly influences the  $\text{CO}_2$  uptake capacity of seawater.  $\text{CO}_2$  is less soluble in warm than in cold water, due to the temperature dependency of the solubility constants. In the physical run, the general warming trend during the simulation period (Fig.2.10) supported an increasing outgassing of carbon dioxide in the northern North Sea ( $r = 0.72$ ). The correlations are weaker for the corresponding winter- ( $r = 0.58$ ) and summer-values ( $r = 0.59$ ). This indicates that the transition times in spring and fall, i.e. the cooling and warming periods, are more important in this context. The warming and cooling tendency of the seawater was quite well correlated with the outgassing tendency of the seawater ( $r = 0.73$  for the NS;  $r = 0.71$  for the NNS;  $r = 0.67$  for the SNS). The year 1996 showed a cold SST anomaly in the first half of 1996, while August of 1997 showed a strong warm anomaly, and the second half of 2006 was very warm as well (Fig. 2.10). These features were visible in the physical air-sea flux with a small outgassing in

the anomalously cold year 1996, increasing outgassing in 1997 and strong outgassing in 2006. The outgassing in the southern North Sea is correlated with the input of dissolved inorganic carbon from the river systems ( $r = 0.85$ ), while the outgassing in the northern part of the North Sea is not correlated with the inflow of inorganic carbon from the North Atlantic ( $r = 0.29$ ) nor to the amount of carbon that is transported from the southern to the northern North Sea ( $r = 0.08$ ) nor with the sum of both. The most important driver for the outgassing in the northern North Sea seems to be the SST.

The correlations between thermocline-dependent parameters and the annual air-sea fluxes are weaker. The largest absolute number relates the maximum thermocline intensity with the physical air-sea flux of the North Sea ( $r = -0.45$ ) followed by the mean thermocline intensity and the physical air-sea flux ( $r = -0.43$ ). The mechanism behind this is again temperature-dependent dissolution of  $\text{CO}_2$ : High temperatures correspond with stronger stratification features. Interesting is that the corresponding only-biological air-sea flux exhibits correlation coefficients ( $r = 0.22$  and  $r = 0.32$ ) which have the opposite sign. Here more intense stratification induces stronger uptake of atmospheric  $\text{CO}_2$ , because of the higher possibility of export of organic carbon into deeper water.

The mean and maximum thermocline depths in the southern North Sea are positively correlated ( $r = 0.29$  and  $r = 0.31$ ) with the physical air-sea flux, which shows that a deeper thermocline goes along with a weaker outgassing or a stronger uptake of atmospheric  $\text{CO}_2$  in the physical run.

In addition to the effect of temperature, the effect of pH must be taken into account. The pH is declining during our simulation period and indicates ongoing ocean acidification due to increasing atmospheric  $\text{CO}_2$  concentrations. An additional effect is caused by the increasing SST, since increasing temperature with constant DIC and TA leads to a lower pH due to the temperature sensitivity of equilibrium constants in the carbonate system. On the other hand increasing temperature with constant TA and  $\text{pCO}_2$  leads to a higher pH. The decline in pH led to a change in the carbonate system equilibrium towards a reduced uptake capacity of atmospheric  $\text{CO}_2$  and thus supports and accelerates the effect of warming SST which weakens the atmospheric  $\text{CO}_2$  uptake capacity of the North Sea. Since the decline in pH is stronger in the northern North Sea, the above mentioned effect partly explains the trend of increased outgassing in the physical air-sea flux of the northern North Sea (Fig. 2.8b). This combined effect of temperature and pH changes is also described by Thomas *et al.* (2007).

From the estimate of the biologically induced air-sea flux, it is clear that biology is an important feature in the efficiency of the carbon shelf pump mechanism in the North Sea. This is in line with Omar *et al.* (2010), who found that biology and mixing were the most important drivers, together with SST, for the variability of the fugacity of carbon dioxide.

The biological air-sea flux is mainly triggered by the NEP ( $r = 0.64$ ). In contrast to the NPP, the NEP is not influenced by the eutrophication, because the heterotrophic respiration balances the higher primary production (Fig. 2.7) in the corresponding years. In 1996, the NEP for the total North Sea reaches a minimum value. This should lead to a very low biology-driven air-sea flux, while in 1997 the NEP reaches an intermediate value of  $317 \text{ Gmol C yr}^{-1}$ , which should induce an intermediate biological air-sea flux, but instead the uptake of atmospheric  $\text{CO}_2$  was minimal in 1997 (Fig. 2.9). The anomalies of primary production (Fig. 2.10) indicate low fixation of carbon by both diatoms and non-diatoms in 1996 and 1997 since river loads of nutrients, especially nitrate (Fig. 2.2d), are quite low in 1996 and are still low in the following year. Additionally, in 1997 the August was very warm. Thus, a combination of the intermediate NEP in 1997

(biological effect) and the warm SST (physical effect) is responsible for the low uptake of atmospheric carbon in that year (Fig. 2.5). When considering the different North Sea regions, the NEP can explain most of the biologically induced air-sea flux in the southern North Sea ( $r = 0.75$ ), while the biological air-sea flux in the northern North Sea is only weakly correlated with the NEP ( $r = 0.39$ ). But since the northern North Sea is stratified during summer, only the mixed layer is able to exchange carbon dioxide with the atmosphere. Therefore, considering only for the upper 20 m of the water column, which is roughly the mean thermocline depth, increases the correlation between NEP and biological air-sea flux in the northern North Sea to  $r = 0.51$ . This finding stresses the importance of the stratification and the spatial separation of primary production and respiration for the air-sea flux.

When we correlated the temperature and thermocline parameters with the NEP, also the NEP showed stronger relationships with temperature-related features (correlation with SST:  $r = 0.51$  (NS),  $r = 0.58$  (SNS) and  $r = 0.42$  (NNS) ) than with thermocline-related ones. For the southern, northern and the total North Sea these positive NEP correlations appear together with positive biological air-sea flux correlations. For the North Sea as a whole and the northern North Sea the maximum stratification intensity ( $r = 0.29$  (NS),  $r = 0.21$  (NNS)) as well as the mean intensity ( $r = 0.2$  (NS),  $r = 0.23$  (NNS)) are positively correlated with the NEP. This can be explained by a more efficient separation of the highly productive upper water column from the lower part. In the southern North Sea the thermocline intensities are negatively correlated with the NEP ( $r = -0.41$  for the maximal intensity and  $r = -0.27$  for the mean intensity).

### 2.5.3 pCO<sub>2</sub> and DIC

In Fig. 2.11 we compare the simulated surface pCO<sub>2</sub> and DIC monthly means for two 1°x1° boxes, one in the southern (box centred at 54° 17 N 07° 35 E) and one in the northern (box centred at 59° 29 N 03° 35 E) part, with corresponding data from three cruises in 2001, 2002 (Thomas *et al.*, 2005b) and 2005 (Thomas *et al.*, 2007).

The available measurements were averaged over the area and the month and the mean and the 17 %- and 83 %-quantiles are given. The measurements and the simulation results correspond quite well, but the simulated pCO<sub>2</sub> in the southern North Sea underestimates the actual values in summer. This, partly to be seen in the DIC concentrations as well, might be due to the fact that we overestimate the SST with our model (Fig. 2.3), which has a stronger effect on pCO<sub>2</sub> in summer than in winter. In the northern North Sea, the model underestimates the drawdown of DIC during late summer, an effect which is due to too low biological production rates during this time. The southern North Sea is partly a source for atmospheric CO<sub>2</sub> (Fig. 2.5c), but from Fig. 2.11b it might as well be a sink due to the biologically induced drawdown in summer. The air-sea flux is horizontally very heterogeneous and the 1°x1° is not representative for the whole southern North Sea, e.g. strong outgassing mainly occurs in the river mouth regions.

To check whether the superposition assumption of biological and physical effects is justified, we compared our biologically induced pCO<sub>2</sub> fluctuations with the biologically induced pCO<sub>2</sub> fluctuations calculated with the method of Takahashi *et al.* (2002). For our approach we calculated pCO<sub>2 bio</sub> by applying the following equation:

$$pCO_{2\_at\_T\_mean\_L} = pCO_{2\_bio} = pCO_{2\_std} - (pCO_{2\_phys} - pCO_{2\_phys\_mean}), \quad (2.7)$$

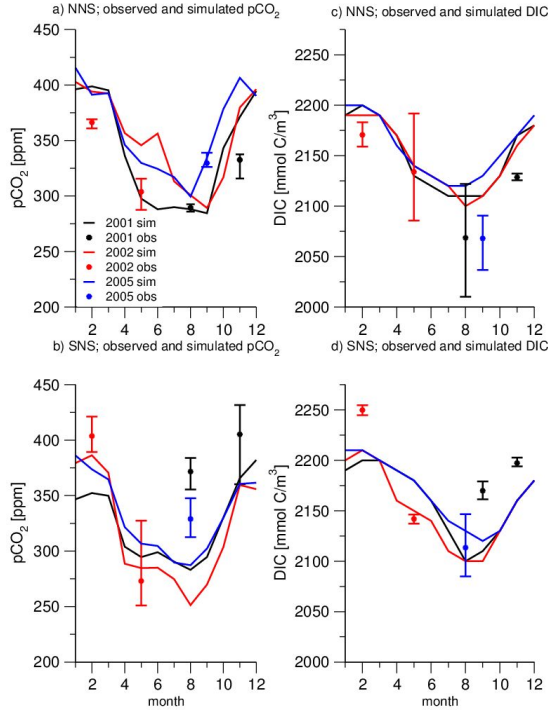


Figure 2.11: Comparison of simulated and measured monthly  $p\text{CO}_2$  and DIC (Thomas *et al.*, 2005b, 2007) for (a+c) the northern North Sea ( $1^\circ \times 1^\circ$  box centred at  $59^\circ 29' \text{N } 03^\circ 35' \text{E}$ ) and (b+c) the southern North Sea ( $1^\circ \times 1^\circ$  box centred at  $54^\circ 17' \text{N } 07^\circ 35' \text{E}$ ). The mean values of the observations are displayed together with their 17 % and 85 % quantile.

where  $p\text{CO}_{2\_at\_T\_mean\_L}$  is the  $p\text{CO}_2$  normalized to a mean temperature. The variability of this normalized  $p\text{CO}_{2\_at\_T\_mean\_L}$  is only due to biology. The  $p\text{CO}_{2\_std}$  is the partial pressure of  $\text{CO}_2$  calculated from the standard simulation and  $p\text{CO}_{2\_phys}$  is the partial pressure of  $\text{CO}_2$  calculated from the simulation without biology with its mean value  $p\text{CO}_{2\_phys\_mean}$ .

For the Takahashi-approach we used the following equation from Takahashi *et al.* (2002):

$$p\text{CO}_{2\_at\_T\_mean\_T} = p\text{CO}_{2\_std} \cdot \exp(0.0432 \cdot (T_{\text{mean}} - T_{\text{std}})), \quad (2.8)$$

where  $T_{\text{std}}$  is the simulated temperature of the standard simulation with its mean value  $T_{\text{mean}}$ . The variability of this calculated  $p\text{CO}_{2\_at\_T\_mean\_T}$  is due to everything but temperature. The results of both calculations for four years in the northern North Sea are given in Fig. 2.12. The comparisons look quite similar for every simulated year, so we have presented the years 1970, 1980, 1990 and 2000 as examples.

The  $p\text{CO}_2$  values calculated with the two methods correspond well. There are some differences, due to the slightly different definitions of the two  $p\text{CO}_2$  values. The Takahashi-approach is including all non-temperature effects, e.g. mixing (Takahashi *et al.*, 2002), while our approach is excluding these effects, as they occur both in the standard run and the run without biology. Additionally, there is certain systematic bias in our calculation of the biological air-sea flux: In the run without biology, the

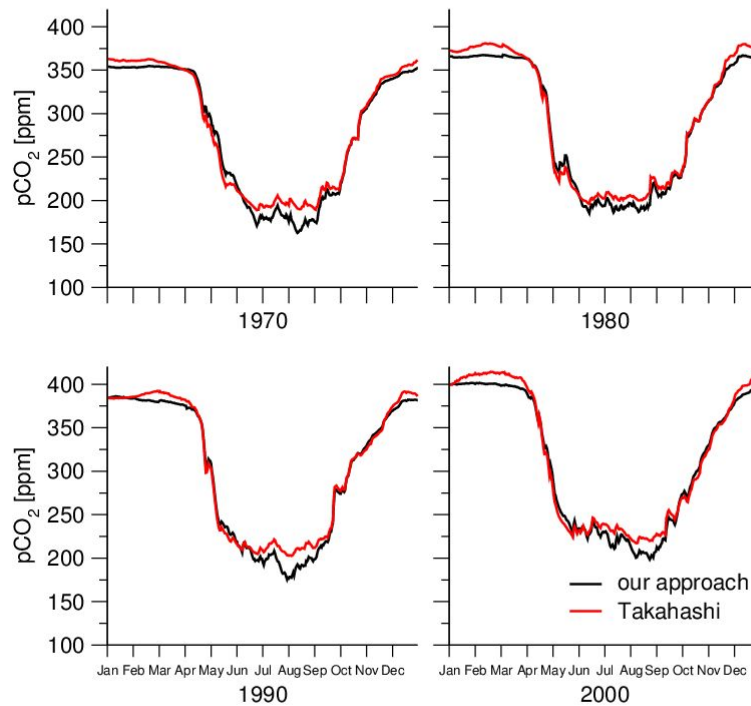


Figure 2.12: Annual cycle of  $p\text{CO}_2$  at mean temperature for 1970, 1980, 1990 and 2000 at one station in the northern North Sea (FLEX,  $58^\circ 55'N$   $0^\circ 32'E$ , see Fig. 2.2). Comparison of our superposition approach versus the approach by Takahashi *et al.* (2002).

temperature effect on  $p\text{CO}_2$  is a bit stronger than in the run with biology. This is due to the effect, that the  $p\text{CO}_2$  level is higher in the run without biology - because no biological drawdown occurs - warming of  $1^\circ$  causes a higher increase in  $p\text{CO}_2$  than in the run with biology. This leads to an overestimation of the biological drawdown when we subtract the two values especially in summer.

#### 2.5.4 River loads and eutrophication

To account for the effect of eutrophication on the carbon fluxes, we conducted a sensitivity run over the simulation period with river loads of 1977. Fig. 2.13 shows the difference between the standard simulation and the sensitivity scenario for the air-sea flux (Fig. 2.13a), the NPP (Fig. 2.13b) and the NEP (Fig. 2.13c) for the total North

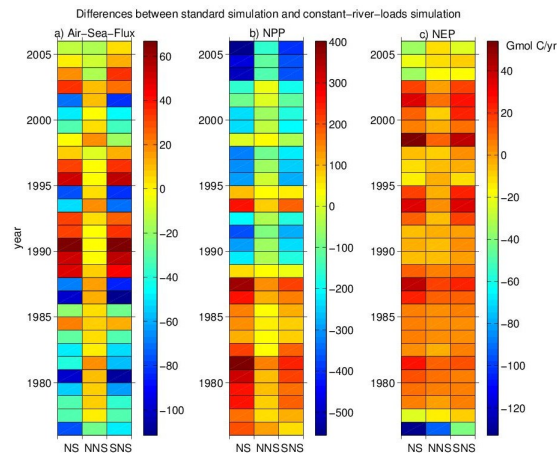


Figure 2.13: Differences between the standard simulation and the simulation with constant river loads for the total North Sea (NS), the northern (NNS) and the southern North Sea (SNS) in Gmol C yr<sup>-1</sup> for (a) the air-sea flux, (b) the net primary production and (c) the net ecosystem production.

Sea (NS), the northern (NNS) and southern (SNS) subregions. The NPP-difference is significantly elevated in the standard simulation during the P-eutrophied years in the late 70's and until 1982. Several additional local maxima exist in 1981, 1988, 1993, 1998 and 2002. They correspond with anomalies in annual riverine nitrogen loads (Fig. 2.2c). This effect is more pronounced in the southern North Sea. The NEP shows a deviating pattern: The P-eutrophied years are not elevated, while the local maxima induced by N-loads also appear in the NEP patterns. This can be explained by the effect of the benthic denitrification in the model which takes reactive nitrogen out of the biological system before it can be remineralised. The strong negative differences in the year 1977 might be biased due to the initialisation of the model, since the sensitivity run started after two years of spin-up directly from 1977. The air-sea flux in the southern North Sea shows negative anomalies in the above listed years, thus a superposing mechanism seems to be responsible. The DIC input of rivers into the North Sea is subject to several interannual oscillations (Fig. 2.2a) which correspond to the time series of water discharge and nitrogen input. During the years of high P-eutrophication there was no additional DIC input by rivers, but during high annual nitrogen loads it was. These DIC loads caused, in the years with high nitrogen loads, enhanced DIC concentrations and thus elevated negative air-sea fluxes of CO<sub>2</sub> (Fig. 2.13a) in the southern North Sea. The importance of the river loads for the interannual variability of the air-sea flux for the whole North Sea in comparison to the other drivers is not so easy to identify. The river loads mostly affect the southern North Sea, while pH, temperature and biology are affecting the whole area. Additionally, the river loads influence the air-sea flux indirectly via biology and directly via DIC loads. The anomalies of the air-sea flux for the total North Sea (Fig. 2.13) are ranging up to about 10 % of the total air-sea flux, which is in the range of the smaller interannual variations as can be seen in Fig. 2.5a. But these anomalies are not in the same order of magnitude as the decreasing trend in the last decade due to temperature and pH and they are not as high as the change from a source for atmospheric CO<sub>2</sub> to a sink as induced by biology.

### 2.5.5 Uncertainties and sensitivities

Due to the lack of data and since our area of interest is not very close to the north-western boundaries of the model area it only was possible to use climatologic values as boundary condition for the hydrodynamic as well as for the biogeochemical part of the model system. One exception is DIC with increasing concentrations over the years due to anthropogenic CO<sub>2</sub> enrichment of the atmosphere. It is known that for the North Atlantic decadal variations of temperature and salinity exist that might go along with variations of nutrient concentrations. These variations are hardly captured for the north-eastern Atlantic by global models (Nunez-Riboni *et al.*, 2011) which could otherwise provide boundary conditions for our modelling approach. Pätsch & Radach (1997) used annual varying interpolated observational data as boundary conditions for a North Sea model. They did not find significant interannual variations in these data aside from a salinity anomaly in the late 1970s. The boundary conditions at the interface between Baltic Sea and North Sea might be more important for our analysis and there is surely an influence on the north-eastern North Sea that we do not capture completely with our simulation.

One of the possible uncertainties considering our results is the parameterisation of the air-sea gas exchange. We have chosen the parameterisation of Wanninkhof (1992). Kühn *et al.* (2010) conducted a sensitivity study and found that a different parameterisation of the wind-dependent gas transfer (Nightingale *et al.*, 2000; Wanninkhof & McGillis, 1999) changed the annual air-sea flux by less than 5 %. This is valid in our model setup and may be regarded as a lower bound since higher error estimates are found in other studies (e.g. Watson *et al.* (2009)).

There exists an alternative time series of atmospheric pCO<sub>2</sub> data from Mace Head (Conway *et al.*, 2011), which is quite close to our area of interest. In a sensitivity study with this data set, we found an increase of the CO<sub>2</sub> air-sea flux compared to our standard run of about 20 Gmol C yr<sup>-1</sup>. This is less than 5 % of the annual value. Nevertheless, the seasonal cycle in Mace Head differs from the seasonal cycle of the Mauna Loa data set. This should be accounted for in studies which will be looking in more detail at the seasonal cycle of pCO<sub>2</sub> in the North Sea.

The simulated annual SST is always higher than the observed SST (Fig. 2.3). We conducted a sensitivity simulation for five consecutive years, in which we changed our solar radiation module to be able to warm not only the first layer but also the deeper layers considering the decline with depth. In this approach the thermocline is about 5 m deeper and SST values are about 0.35 °C closer to the observations. This affects the NEP and the air-sea flux of CO<sub>2</sub>. The effects differ in the southern and the northern North Sea. While in the southern North Sea the NEP and the air-sea flux are more or less the same for the standard and the sensitivity run, in the northern North Sea NEP and air-sea flux are decreasing by 13 %. These effects should be considered in further studies.

We found that the biology is contributing the major effect to the North Sea being a sink for atmospheric CO<sub>2</sub>. This aspect should be examined more explicitly in further studies. Especially the inclusion of calcifying algae should be considered. Concerning the carbonate system, our approach of restoring the alkalinity allows nevertheless to account for shifts in the carbonate system due to biological activity because pH and DIC are calculated freely. But: The prognostic calculation of alkalinity rather than prescribing alkalinity fields is a major issue for more realistic results, because the effects of e.g. nitrate uptake and ammonia release should be taken into account.

If we extend our findings to future scenarios, considering ongoing ocean acidification

and increasing SST, both due to the release of anthropogenic carbon dioxide, our results suggest that the uptake capacity of the North Sea for atmospheric carbon dioxide might show an ongoing decline. This seems even more relevant since no calcite solution from the sediments can be expected for the North Sea and thus no buffering effect for the carbonate system occurs.

## 2.6 Conclusion

Our findings suggest, that biology is the most important feature for the functionality of the carbon shelf pump in the North Sea. Without the fixation of inorganic carbon via photosynthesis, the North Sea would be a continuous source of carbon dioxide for the atmosphere due to the continuous input of carbon species by rivers. In contrast, the interannual variability of the shelf pump is mainly triggered by physical influences, directly via increasing outgassing due to increasing SST and decreasing pH and indirectly via variations of the NEP due to temperature changes. Most interesting was the effect of the low SST in 1996, which directly induced more uptake (or less outgassing) of atmospheric CO<sub>2</sub> but also lowered the NEP thus indirectly inducing less uptake of atmospheric CO<sub>2</sub>. Thus, solubility and biology can counteract each other.

Overall the strength of the shelf pump mechanism was declining during our simulation period from 1970 to 2006, mostly due to temperature and pH effects. Metzl *et al.* (2010) found a declining uptake capacity for atmospheric carbon dioxide for the North Atlantic subpolar gyre as well and identified SST and pH as the main drivers.

The period of high, mainly phosphate-induced, eutrophication during the 1980s had no significant effect on the total air-sea flux because the NEP in contrast to the NPP did not respond very strong to the higher nutrient input. This became specifically clear as we examined the Southern Bight and the German Bight. The regions are highly exposed to river run-off but the NEP did not respond to the eutrophication period. The biologically induced air-sea flux was slightly increasing parallel to river inputs in the first half of the simulation period, but this was directly counteracted by an increasing outgassing obtained from the physical run.

As a more methodological result we found that the calculation of the biologically induced pCO<sub>2</sub> according to Takahashi *et al.* (2002) and our calculation based on the assumption of a superposition of physical and biological effects are in good agreement.

# 3 Comparison of two techniques to separate physically and biologically mediated $p\text{CO}_2$ in seawater

## 3.1 Abstract

In this methodical work we investigate the applicability of two approaches to determine the biologically induced variations of marine  $p\text{CO}_2$ . The first method was proposed by Takahashi et al. (1993), who used data of temperature and  $p\text{CO}_2$  in the North Atlantic to linearise the temperature dependency of  $p\text{CO}_2$ . We compare the Takahashi method with a superposition approach by using model results. The superposition approach assumes that biological, chemical and physical influences on the partial pressure of carbon dioxide are adding up. Thus, the biologically induced  $p\text{CO}_2$  variations are calculated as the difference between a standard run with an ecosystem model and a run in which only physical and chemical processes are taken into account. Both methods agree reasonably for a station in the northern North Sea, characterised by weak dissolved inorganic carbon(DIC) gradients and moderate biological production. The deviations between both approaches are larger for a station in the southern North Sea, characterised by stronger DIC gradients and higher biological activities. In this area the Takahashi approach has not only the problem that sinks and sources of DIC mask the biologically induced  $p\text{CO}_2$  variations but also that the constant for the linearisation ( $l_p=0.0423^\circ\text{C}^{-1}$ ) has to be changed. We show that during strong events which increase the pH ( $>8.3$ ) the  $p\text{CO}_2$  could not be determined correctly with this method. In all other cases the use of the Takahashi constant is valid. Locally and temporally calculated constants which substitute  $l_p$ , lead to deviations in the calculated  $p\text{CO}_2$  smaller than  $2 \mu\text{atm}$ .

## 3.2 Introduction

The partial pressure of  $\text{CO}_2$  in seawater ( $p\text{CO}_2$ ) directly determines the air-sea exchange of  $\text{CO}_2$  and thus has an impact on the concentration of the greenhouse gas in the atmosphere and on the status of marine acidification.

There are different drivers of marine  $p\text{CO}_2$  variability. The most prominent candidates for the causes of these variations are sea surface temperature (SST), biological activities, and chemical reactions. While the contributions of changing temperature and chemical reactions on the  $p\text{CO}_2$  are quite well known and can be calculated by the thermodynamic equilibrium equations of the carbonate system, the direct determination of the biological contribution is not so easy to quantify. Problems arise when the direct effect of biological production and degradation on DIC and total alkalinity (TA) and thus on  $p\text{CO}_2$  are to be budgeted. The biological effects can be manifold since changes in DIC or nutrient concentrations have an influence on the different state variables of the carbonate system. These effects might be overlayed (or hidden) by physical and chemical influences. Additionally, the indirect effect of the contribution of organic bases and acids change

the pH and the corresponding  $p\text{CO}_2$  (Hernandez-Ayon *et al.*, 2007). Because of these problems we searched for methods to estimate the biological influence on  $p\text{CO}_2$  variations in total.

The approach of Takahashi *et al.* (1993) allows to analytically differentiate between the temperature induced  $p\text{CO}_2$  variations and the variations induced by all other drivers. In the absence of external sinks and sources of DIC, the latter drivers can be identified as biological processes. Using observations of temperature and  $p\text{CO}_2$ , these authors calculated the constant  $l_p$ , which linearises the temperature effect on  $p\text{CO}_2$ . The resulting function has already been applied to open-ocean observations (Takahashi *et al.*, 2002) as well as to regional sea observations, giving reasonable results (Thomas *et al.*, 2005b).

From a modellers point of view another possibility arises: While a standard simulation run with a marine ecosystem model includes chemical, physical and biological effects on  $p\text{CO}_2$ , an additional simulation - with the same model setup except that biology is switched off (the physical/chemical run) - represents the  $p\text{CO}_2$  variations due to physical and chemical effects only. Assuming superposition the differences between the simulated  $p\text{CO}_2$  time series are due to biological activities.

When Thomas *et al.* (2005b) applied the Takahashi method to the North Sea by using the constant originally calculated for the North Atlantic ( $l_p=0.0423^\circ\text{C}^{-1}$ ), the question arose to which degree this constant is valid for a shelf sea. As it is not possible to repeat the Takahashi experiment (Takahashi *et al.*, 1993) with the samples of the North Sea from the Thomas *et al.* (2005b) study, we recalculated the Takahashi constant  $l_p^c$  ( $l_p^c \approx l_p$ ) by using the computer program CO2SYS (Lewis *et al.*, 1998) and the available North Sea data from the CANOBA experiment (Thomas *et al.*, 2004).

The aim of this study is to investigate the applicability of the two approaches to calculate the biologically induced variations in the partial pressure of carbon dioxide and to analyse the agreement/disagreement between the results of both methods. Further we try to explain what causes deviations between the two calculated  $p\text{CO}_2$  time series. Therefore, the ecosystem model ECOHAM4 was applied to the Northwest-European Shelf for the years 1970-2006 (Lorkowski *et al.*, 2012). Since the basic mechanisms act similar in every year, we chose the year 2001 as an example. We extracted the simulation results for the offshore station FLEX ( $58^\circ 53' \text{N}$ ,  $0^\circ 35' \text{E}$ ) in the northern North Sea characterised by small lateral gradients in DIC and moderate primary production. Additionally we used the simulation results at the GLOBEC ( $54^\circ 41' \text{N}$ ,  $6^\circ 55' \text{E}$ ) station close to the German Bight in the south-east North Sea with larger horizontal DIC gradients and higher production rates.

### 3.3 Materials and Procedures

Two main factors that change the  $p\text{CO}_2$  have to be differentiated. First, the solubility of  $\text{CO}_2$  in seawater varies due to changes in temperature (Weiss, 1974), second the concentration of  $\text{CO}_2$  itself can change due to physical, chemical and biological processes.  $\text{CO}_2$  is only one state variable of the carbonate system, and changes in the chemical equilibrium may change the  $p\text{CO}_2$ . All carbon species represented in seawater, thus  $\text{CO}_2$ ,  $\text{HCO}_3^-$  and  $\text{CO}_3^{2-}$ , are contained in the model state variable DIC. Together with TA, DIC determines the state of the carbonate system. All variables of the carbonate system can be calculated when these two state variables are known.

In the model TA is treated diagnostically, which means that the observed CANOBA data (Thomas *et al.*, 2004) were temporally and spatially interpolated on the model

grid and prescribed for the simulation. DIC can be changed by biological processes (see BIO in Fig. 3.3 and 3.6): Photosynthesis decreases the DIC concentration, whereas respiration and decomposition increase the DIC concentration in the model. The vertical export of organic particles is not influencing the DIC budget. Physical processes altering the DIC concentration are the air-sea flux of CO<sub>2</sub> (see ASF in Figs. 3.2, 3.3, 3.5, 3.6), and the horizontal and vertical advection (see ADV in Figs. 3.2, 3.3, 3.5, 3.6), which is able to import carbon from the North Atlantic, the Baltic or from the rivers. Vertical mixing (see: MIX in Figs. 3.2, 3.3, 3.5, 3.6) can be very important for supplying remineralised DIC of deeper levels to the upper water column. The CO<sub>2</sub> exchange with the atmosphere is formulated according to Wanninkhof (1992). For this formula we used the wind speed of the NCEP reanalysis data (Kalnay *et al.*, 1996) and the atmospheric partial pressure based on the Mauna Loa data set for 2001. Processes which are not directly included in the model are changes of the carbonate system due to organic bases or acids, TA variations due to internal processes like formations and dissolution of carbonate, nitrate and ammonium fluxes and external TA sources and sinks like river input or exchange with the Wadden Sea. The TA variations mentioned are thought to be included in the measured TA concentrations which were used diagnostically. A detailed description of the model setup with its forcing and boundary conditions can be found in Lorkowski *et al.* (2012).

For the physical/chemical run all biological processes which transfer inorganic matter into organic and vice versa were switched off. The carbonate system is running but variations of DIC are only induced by physical processes as transport or air-sea flux of CO<sub>2</sub>. Additionally, changes in temperature and salinity can influence the solubility in this run as well.

The equilibrium equations of the carbonate system were implemented by using the carbonic acid constants according to Mehrbach *et al.* (1973) as refit by Dickson & Millero (1987). The calcite saturation and the pressure corrections for all equilibrium constants are calculated after Millero (1995), the boric acid constant stems from Dickson (1990), whereas for the ion product of water the formula of DOE (1994) was used. The model works with the seawater pH scale. All equilibrium constants defined with other scales are recalculated into this scale. A description of the CANOBA data set can be found in Thomas *et al.* (2004).

#### Definition - Takahashi method

The Takahashi approach defines a normalised partial pressure of CO<sub>2</sub> related to a mean temperature (Takahashi *et al.* (2002), their equation (1)):

$$p\text{CO}_2^{\text{Ta}}(\text{day}) = p\text{CO}_2(\text{day}) \cdot \exp(\text{lp}(\bar{T} - T)) \quad (3.1)$$

Where  $\bar{T}$  is the annual mean temperature and  $p\text{CO}_2(\text{day})$  is the observed partial pressure of marine CO<sub>2</sub> at temperature  $T$  and day of the year.  $p\text{CO}_2^{\text{Ta}}$  then gives the partial pressure of carbon dioxide which is due to everything but temperature. The temperature dependency of  $p\text{CO}_2$  for North Atlantic surface water is described by Takahashi *et al.* (1993). Their experiments and calculations result in a linear relationship between temperature and the logarithm of  $p\text{CO}_2$ :

$$\text{lp} := \frac{\delta \ln(p\text{CO}_2)}{\delta T} = 0.0423 \pm 0.0002^\circ\text{C}^{-1} \quad (3.2)$$

#### Definition - Superposition method

The superposition approach defines the simulated partial pressure of CO<sub>2</sub> driven by

biological effects only as:

$$p\text{CO}_2^{\text{Su}}(\text{day}) = p\text{CO}_2^{\text{std}}(\text{day}) - (p\text{CO}_2^{\text{phy}}(\text{day}) \cdot \overline{p\text{CO}_2^{\text{phys}}}) \quad (3.3)$$

where  $p\text{CO}_2^{\text{std}}(\text{day})$  and  $p\text{CO}_2^{\text{phy}}(\text{day})$  are the daily simulated pCO<sub>2</sub> values of the standard and the physical/chemical run, respectively.  $\overline{p\text{CO}_2^{\text{phys}}}$  is the annual mean pCO<sub>2</sub> of the physical/chemical run.

The question is, whether the constant  $lp$  is also valid for North Sea surface waters. To test this we wanted to directly calculate the coefficient  $lp$  for North Sea data. Unfortunately it is not possible to repeat the experiment by Takahashi *et al.* (1993) for the North Sea samples gathered in 2001 and 2002 (Thomas *et al.*, 2004) in the laboratory. Using CO2SYS with the choice of constants described above we recalculated table A1 of Takahashi *et al.* (1993): With the given TA and DIC concentration and the salinity of their experiment we calculated pCO<sub>2</sub> (and  $\ln(p\text{CO}_2)$ ) values for the temperatures 2.1 °C, ..., 24.5 °C. The linear best fit through the data with temperature on the x-axis and  $\ln(p\text{CO}_2)$  on the y-axis then gave us the corresponding  $lp^c$  value. In a second step we repeated this for each station of the CANOBA experiment by determining the linear factor  $lp^c$  ( $=\Delta\ln(p\text{CO}_2)/\Delta T$ ) for the observed DIC and TA concentrations and the corresponding observed salinity of the North Sea for the temperature range of T: 2 - 20 °C, which is typical for the North Sea. For this calculation we used the carbonate system module of ECOHAM (Lorkowski *et al.* 2012), which has been tested against CO2SYS. The latter calculations were performed by a module of ECOHAM because data handling within the model domain showed much better performance than the application of CO2SYS.

## 3.4 Assessment

### 3.4.1 Comparison of the two methods

For the comparison we applied both methods to our simulation results of the North Sea ecosystem, as described by Lorkowski *et al.* (2012) for the year 2001. First we focus on the annual time series at station FLEX (58° 53 N, 0° 35 E) with a water depth of 135 m situated in the northern North Sea distant from terrestrial sources of biogeochemical tracers and without notably high biological productivity. Second we discuss the simulation results at the GLOBEC station close to the German Bight (54° 41' N, 6° 55' E) in the south-eastern North Sea (depth: 38 m) with larger horizontal DIC gradients and, due to the adjacent coast, with high anthropogenic loads of nutrients and DIC (Pätsch & Kühn, 2008; Kühn *et al.*, 2010) and thus higher production rates. For both stations we show the time series of the different pCO<sub>2</sub> values together with the sea surface temperature SST. To understand the reasons for DIC changes we additionally discuss the temporal development of the DIC budgets and DIC itself. For a better overview we grouped together all biological fluxes and all advective fluxes, respectively. Additionally the influence of the air-sea flux of CO<sub>2</sub> and the vertical mixing of DIC is discussed.

#### FLEX

While Fig.3.1a shows the two pCO<sub>2</sub> series, which reflect mainly the biological influence over the year calculated with the two different methods, the time series of the SST, the pCO<sub>2</sub> series of the standard and the physical/chemical run are shown in Fig. 3.1b.

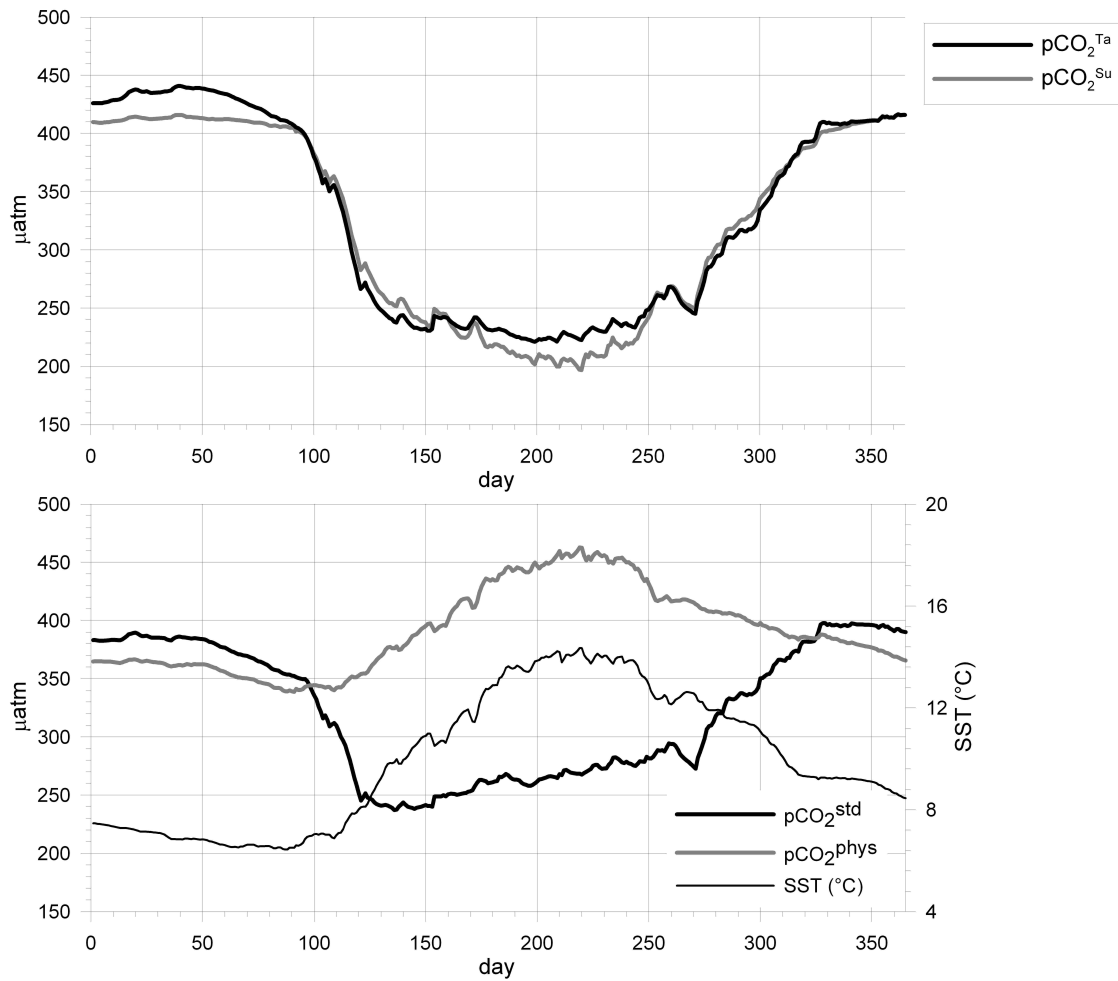


Figure 3.1: (a): Time series of estimated pCO<sub>2</sub> variations induced by biology for the station FLEX (58° 53 N, 0° 35 E). pCO<sub>2</sub><sup>Ta</sup> after Takahashi *et al.* (2002); pCO<sub>2</sub><sup>Su</sup>: superposition method; (b): Time series of SST ( $^{\circ}\text{C}$ ), pCO<sub>2</sub> of the standard run (pCO<sub>2</sub><sup>std</sup>) and pCO<sub>2</sub> of the physical/chemical run (pCO<sub>2</sub><sup>phys</sup>) at station FLEX.

DIC ( $\text{mmol kg}^{-1}$ )	$p\text{CO}_2$ ( $\mu\text{atm}$ )	$\Delta p\text{CO}_2/\Delta T$ ( $\mu\text{atm}/^\circ\text{C}$ )
2100	443.8	18.9
2050	337.5	14.5

Table 3.1: Temperature sensitivities of  $p\text{CO}_2$  at different  $p\text{CO}_2$  levels. The data were calculated by CO2SYS (TA=2300  $\mu\text{mol kg}^{-1}$ , T=15°C).

Both time series in Fig. 3.1a exhibit amplitudes of about 200  $\mu\text{atm}$  in the year 2001. The amplitudes of the  $p\text{CO}_2^{\text{Su}}$  and  $p\text{CO}_2^{\text{Ta}}$  series are larger than those of the standard run and the physical/chemical run, respectively (Fig. 3.1b). This shows that the biologically and physically/chemically induced signals partly cancel each other out within the standard run.

The time series in Fig. 3.1a run mostly parallel, the values for  $p\text{CO}_2^{\text{Ta}}$  are slightly higher than those for  $p\text{CO}_2^{\text{Su}}$  except in the time interval 100-150 and during some events in fall. The SST (Fig. 3.1b) is lowest in March (day 60-90) and highest in August (day 200-235). The timing of these SST extremes coincides with those of the  $p\text{CO}_2$  of the physical/chemical run. High values in winter, an abrupt decline in spring (day 95-120), low values in summer and an increase in fall are the characteristics for  $p\text{CO}_2^{\text{std}}$ .

In the superposition method we assume that in both simulations (standard and physical/chemical) all effects except the biology-induced ones are identical. But this is not completely fulfilled: Temperature-induced  $p\text{CO}_2$  variations in summer have a smaller effect in the standard run (with lower simulated  $p\text{CO}_2$  in summer) than in the run without biology (with higher simulated  $p\text{CO}_2$  in summer), thus they actually depend on the season and the simulated  $p\text{CO}_2$  itself. This effect is demonstrated in Tab. 3.1, in which the temperature sensitivity of  $p\text{CO}_2$  is shown for different  $p\text{CO}_2$  levels. The values were calculated using CO2SYS.

With this argument the small deviations between the  $p\text{CO}_2$  of both methods can be explained: During the temperature increase (day 100-220; Fig. 3.1b) the  $p\text{CO}_2^{\text{phys}}$  is higher than the  $p\text{CO}_2^{\text{std}}$ . This implies that the temperature induces a stronger increase in  $p\text{CO}_2^{\text{phys}}$  than in the  $p\text{CO}_2^{\text{std}}$  especially in June and July where the  $p\text{CO}_2$  differences are largest (Fig. 3.1b). Subtracting the two leads to an underestimation of  $p\text{CO}_2^{\text{Su}}$ , which is largest around day 220 (Fig. 3.1a). During the temperature decrease from day 220 to day 320,  $p\text{CO}_2^{\text{phys}}$  is higher than  $p\text{CO}_2^{\text{std}}$ . This implies that the temperature-driven decrease of  $p\text{CO}_2^{\text{phys}}$  is higher than the decrease in  $p\text{CO}_2^{\text{std}}$ , which overestimates  $p\text{CO}_2^{\text{Su}}$ . From day 220 to day 320 both approaches converge again. During the period of decreasing temperature from day 320 to day 90, the  $p\text{CO}_2^{\text{phys}}$  is lower than the  $p\text{CO}_2^{\text{std}}$ . This implies that the temperature-driven decrease of  $p\text{CO}_2^{\text{phys}}$  is lower than the temperature-driven decrease of  $p\text{CO}_2^{\text{std}}$ , which leads to an underestimation of  $p\text{CO}_2^{\text{Su}}$ .

The temporal cumulative DIC budget of the upper level (0-10 m) for the physical/chemical run (Fig. 3.2) exhibits small DIC variations ( $\Delta \text{DIC} < 170 \text{ mmol C m}^{-3}$ ) mostly driven by horizontal advection. The air-sea flux of  $\text{CO}_2$  and the vertical mixing, both governed by concentration gradients have the tendency to cancel out each other. The picture changes drastically for the budget of the standard run (Fig.3.3), in which the largest flux is the NEP (net ecosystem production,  $1050 \text{ mmol C m}^{-3} \text{ yr}^{-1}$ ). The NEP is approximately balanced by the uptake of atmospheric  $\text{CO}_2$  ( $168 \text{ mmol C m}^{-3} \text{ yr}^{-1}$ ) and vertical mixing ( $823 \text{ mmol C m}^{-3} \text{ yr}^{-1}$ ). The variations in DIC are larger than in the physical/chemical run ( $\Delta \text{DIC} > 260 \text{ mmol C m}^{-3}$ ). From the budget of the standard run at FLEX (Fig.3.3) it becomes clear that the size of the summer draw down

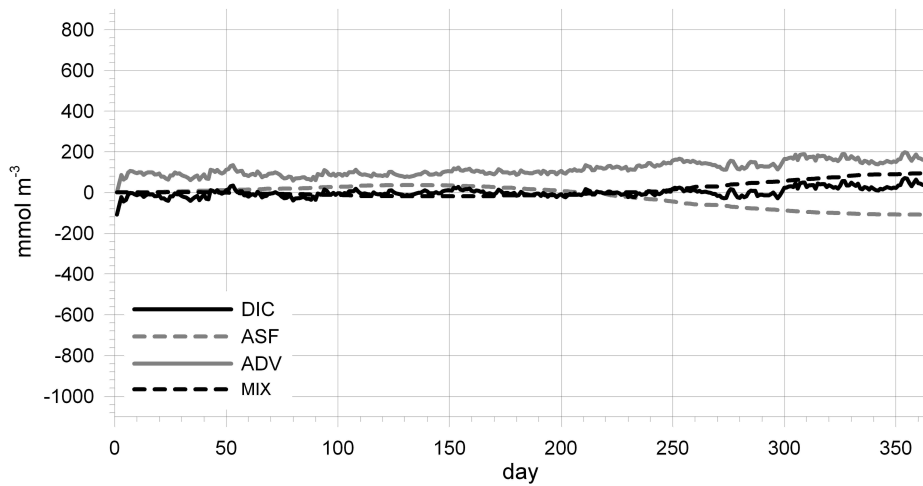


Figure 3.2: Temporal cumulative DIC budget of the upper level (0-10 m) for the physical/chemical run at FLEX. DIC - normalised DIC concentration, ASF - CO<sub>2</sub> cumulative air-sea exchange, ADV - cumulative horizontal advection, MIX - cumulative, vertical mixing for the surface layer.

of near- surface DIC which can be addressed to the NEP cannot provide an estimate for the magnitude of the NEP, because other fluxes like vertical mixing or the uptake of CO<sub>2</sub> from the atmosphere fill up the DIC pool in the same time as the NEP lowers DIC (Kühn *et al.*, 2010).

## GLOBEC

At this station the annual amplitudes of the pCO<sub>2</sub><sup>Ta/Su</sup> series (Fig. 3.4a) are larger than at the northern station FLEX (Fig. 3.1a);  $\Delta pCO_2^{Ta}$  exceeds 290  $\mu\text{atm}$ . For pCO<sub>2</sub><sup>Su</sup> this corresponds to the large amplitude of pCO<sub>2</sub><sup>phys</sup> in Fig 3.4b. The latter one is partly governed by the SST with an amplitude of 13.3°C, which is larger than the  $\Delta\text{SST}$  of 6.9°C at FLEX.

Both time series of pCO<sub>2</sub> start and end more or less at the same pCO<sub>2</sub> level (Fig. 3.4a). In contrast to pCO<sub>2</sub><sup>Su</sup>, pCO<sub>2</sub><sup>Ta</sup> rises above 470  $\mu\text{atm}$  during the first 55 days. This strong increase in pCO<sub>2</sub><sup>Ta</sup> can be attributed to the advection of DIC, which is simulated both in the physical/chemical run (Fig. 3.5) and the standard run (Fig. 3.6). An additional source during the first 55 days is the air-sea flux in the physical/chemical run (Fig. 3.5). In the following time period of day 75 - 220 the decrease of pCO<sub>2</sub><sup>Su</sup> is stronger than that of pCO<sub>2</sub><sup>Ta</sup>. This is because the temperature-induced pCO<sub>2</sub><sup>phys</sup> rise during this period is overestimated. The latter argument follows the discussion above concerning Tab. 3.1.

For the southern station GLOBEC (Fig. 3.4b) the SST maximum in summer and the maximum of pCO<sub>2</sub><sup>phys</sup> do not coincide like at FLEX (Fig. 3.1b). In this shallow area the Total Alkalinity increases in summer due to benthic ammonium release, which is even displayed in the diagnostic TA. These high Total Alkalinity values induce a shift in the carbonate system which lowers the CO<sub>2</sub> concentrations and thus pCO<sub>2</sub> decreases.

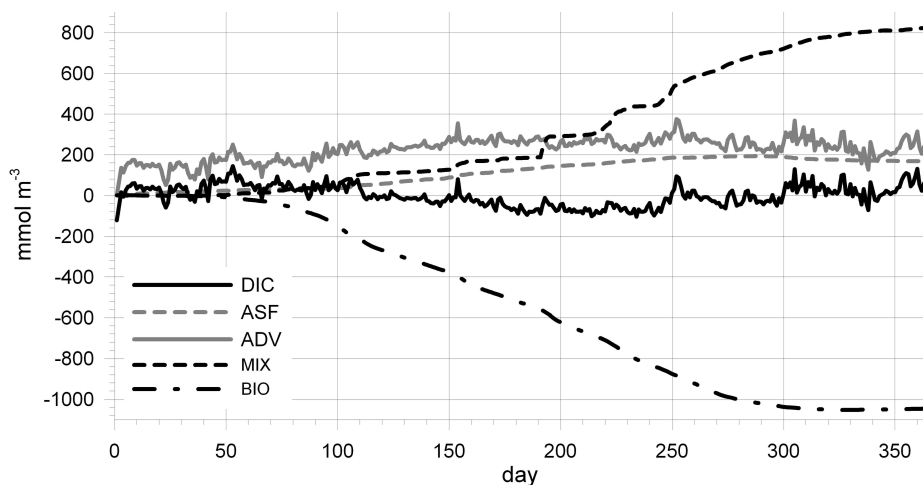


Figure 3.3: Temporal cumulative DIC budget of the upper level (0-10 m) for the standard run at FLEX with DIC - normalised DIC concentration, ASF -  $\text{CO}_2$  cumulative air-sea exchange, ADV - cumulative horizontal advection, MIX - cumulative, integrated vertical mixing, BIO - cumulative net ecosystem production.

### 3.4.2 Determination of constants for the North Sea

The resulting  $p\text{CO}_2$  values (Tab. 3.2) recalculated with CO2SYS after the values of Takahashi (their table A1) are a bit smaller than the original values of Takahashi. This might be due to the fact that marine organic acids or bases and other substances that have an impact on the carbonate chemistry are neglected by CO2SYS (Millero *et al.*, 2002; Hernandez-Ayon *et al.*, 2007; Koeve *et al.*, 2010). Another contribution to the deviations between calculated  $p\text{CO}_2$  values and the values by Takahashi is based on the choice of equilibrium constants for the calculations: Using the original values by Mehrbach *et al.* (1973) resulted in higher  $p\text{CO}_2$  values than applying the refitted ones by Dickson & Millero (1987). Using the calculated  $p\text{CO}_2$  data for the linearisation (equation 2) the resulting  $\text{lp}^c$  value of  $0.0431^\circ\text{C}^{-1}$  is a bit higher than the  $\text{lp}$  of Takahashi *et al.* (1993). But since the difference between the two values is smaller than 2 %, indicating the validity of the calculation with CO2SYS, we decided to calculate  $\text{lp}^c$  values for the whole North Sea from the CANOBA data set (Thomas *et al.*, 2004).

The horizontal distribution of the  $\text{lp}^c$  values is shown in Fig. 3.7. In winter (November 2001, February 2002) they exhibit small variations. For most of the area they are larger than  $\text{lp}$  (Eq. 3.2). In May 2002 and August 2002 the  $\text{lp}^c$  field (Fig. 3.7) is more heterogeneous. The lowest  $\text{lp}^c$  value can be found in the German Bight in May ( $\text{lp}^c = 0.04109^\circ\text{C}^{-1}$ ). Since for the calculation of  $\text{lp}^c$  a linear fit with temperature on the x-axis and  $\ln(p\text{CO}_2)$  on the y-axis is made for every data point, the deviation between the local best fit and the  $\ln(p\text{CO}_2)$  of the observed value can be given as a temperature difference. In Fig. 3.8 the mean deviations [ $^\circ\text{C}$ ] between the logarithm of the temperature-depending  $p\text{CO}_2$  and the best fit show again more or less homogeneous patterns for November and February with values of about 0.1. Higher variability can be found in May and August.

Two examples for this best fit and the deviation of the observed value are given in Fig. 3.9. We compare the situation of a relatively high  $\text{lp}^c$  value of the open North Sea in August ( $55^\circ 59' \text{N}$ ,  $5^\circ \text{E}$ ) with the situation in May in the German Bight ( $54^\circ 24' \text{N}$ ,  $8^\circ 6' \text{E}$ ), where the lowest  $\text{lp}^c$  value was found (Fig. 3.9). Additionally the two

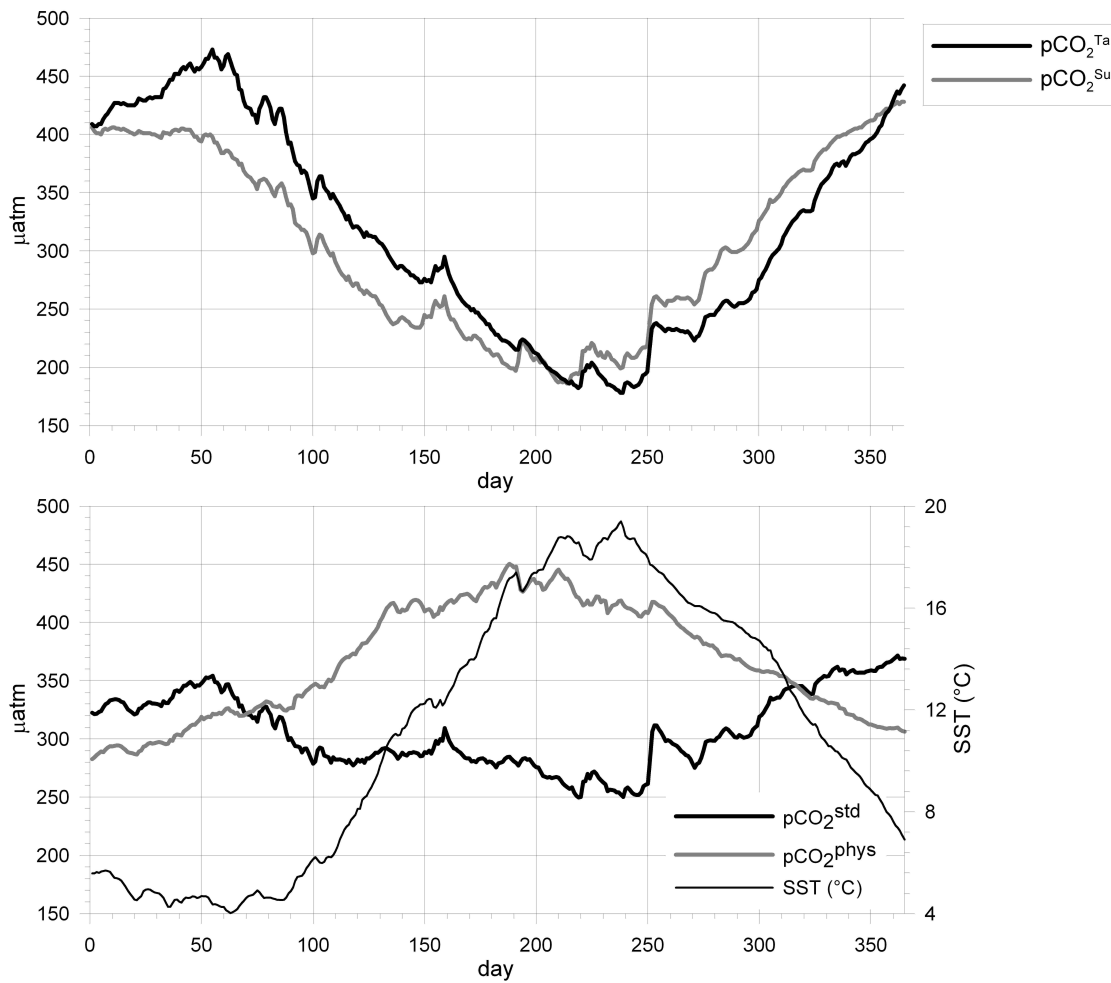


Figure 3.4: (a): Time series of estimated pCO<sub>2</sub> variations induced by biology for the station GLOBEC (54° 41' N, 6° 55' E). pCO<sub>2</sub><sup>Ta</sup> after Takahashi *et al.* (2002); pCO<sub>2</sub><sup>Su</sup>: superposition method; (b): Time series of SST (°C), pCO<sub>2</sub> of the standard run (pCO<sub>2</sub><sup>std</sup>) and the pCO<sub>2</sub> of the physical/chemical run pCO<sub>2</sub><sup>phys</sup> at station GLOBEC.

Temp. (°C)	pCO <sub>2</sub> (μatm) CO2SYS	pCO <sub>2</sub> (μatm) Takahashi <i>et al.</i> (1993)	ln(pCO <sub>2</sub> ) CO2SYS	ln(pCO <sub>2</sub> ) Takahashi <i>et al.</i> (1993)
2.1	255.0	267.0	5.541	5.587
6.33	309.2	322.1	5.734	5.775
10.05	364.2	376.1	5.898	5.930
15.01	449.8	461.6	6.109	6.135
18.00	508.8	526.3	6.232	6.266
20.0	551.7	571.0	6.313	6.348
24.5	659.0	688.2	6.491	6.534
			lp <sup>c</sup> =0.0431 °C <sup>-1</sup>	lp = 0.0423 °C <sup>-1</sup>

Table 3.2: Comparison of the relationship between temperature and pCO<sub>2</sub> and ln(pCO<sub>2</sub>) and the resulting linear coefficients lp<sup>c</sup> and lp using Tab. A1 by Takahashi *et al.* (1993) and CO2SYS. (DIC = 2074 μmol kg<sup>-1</sup>; TA = 2270 μmol kg<sup>-1</sup>; S = 35.38 psu; dissociation constants of carbonic acid by Mehrbach *et al.* (1973) as refit by Dickson & Millero (1987).

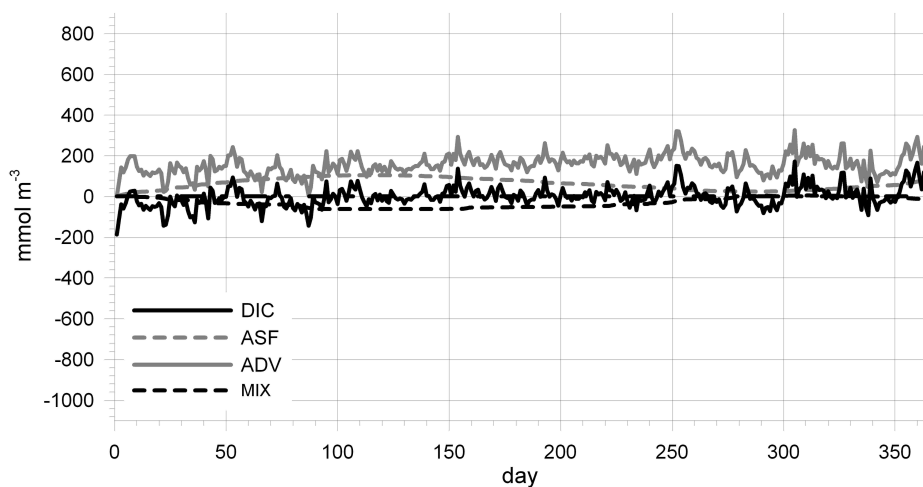


Figure 3.5: Temporal cumulative DIC budget of the upper level (0-10 m) for the physical/chemical run at GLOBEC. DIC - normalised DIC concentration, ASF -  $\text{CO}_2$  cumulative air-sea exchange, ADV - cumulative horizontal advection, MIX - cumulative vertical mixing for the surface layer.

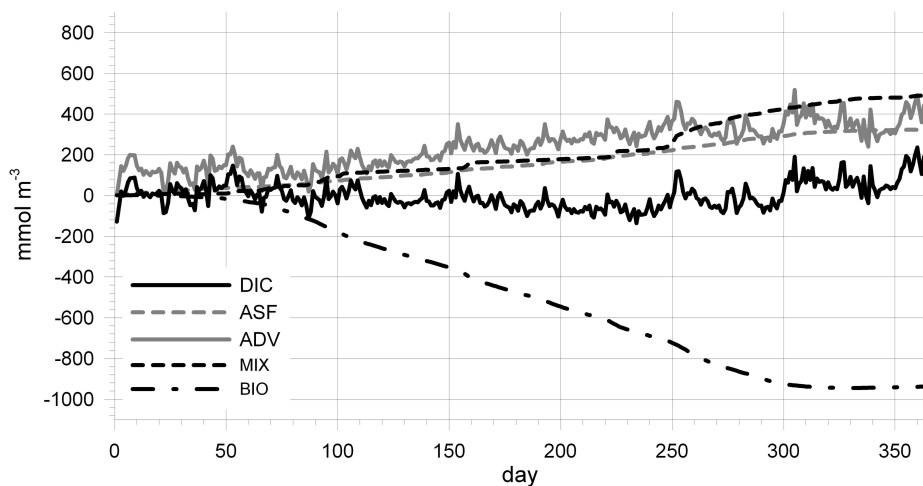


Figure 3.6: Temporal cumulative DIC budget of the upper level (0-10 m) for the standard run at GLOBEC with DIC - normalised DIC concentration, ASF -  $\text{CO}_2$  cumulative air-sea exchange, ADV - cumulative horizontal advection, MIX - cumulative vertical mixing for the surface layer, BIO - cumulative net ecosystem production.

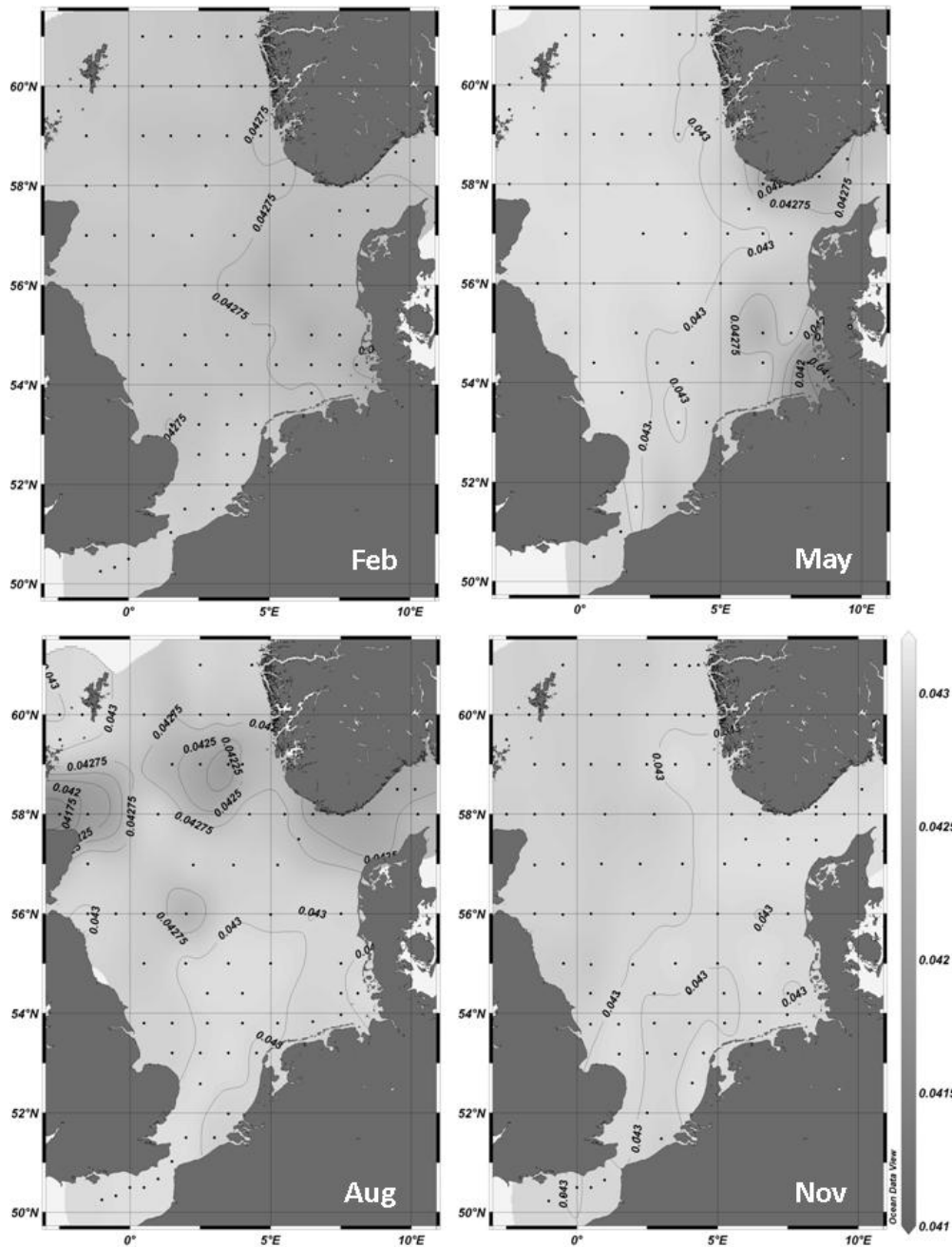


Figure 3.7: Horizontal distributions of the linear coefficient  $lp^c$  [ $^{\circ}\text{C}^{-1}$ ] calculated by the carbonate module of ECOHAM using observed DIC and TA concentrations and corresponding observed salinity for the range of temperatures 2 - 20 $^{\circ}\text{C}$  for February and May 2002 and August and November 2001.

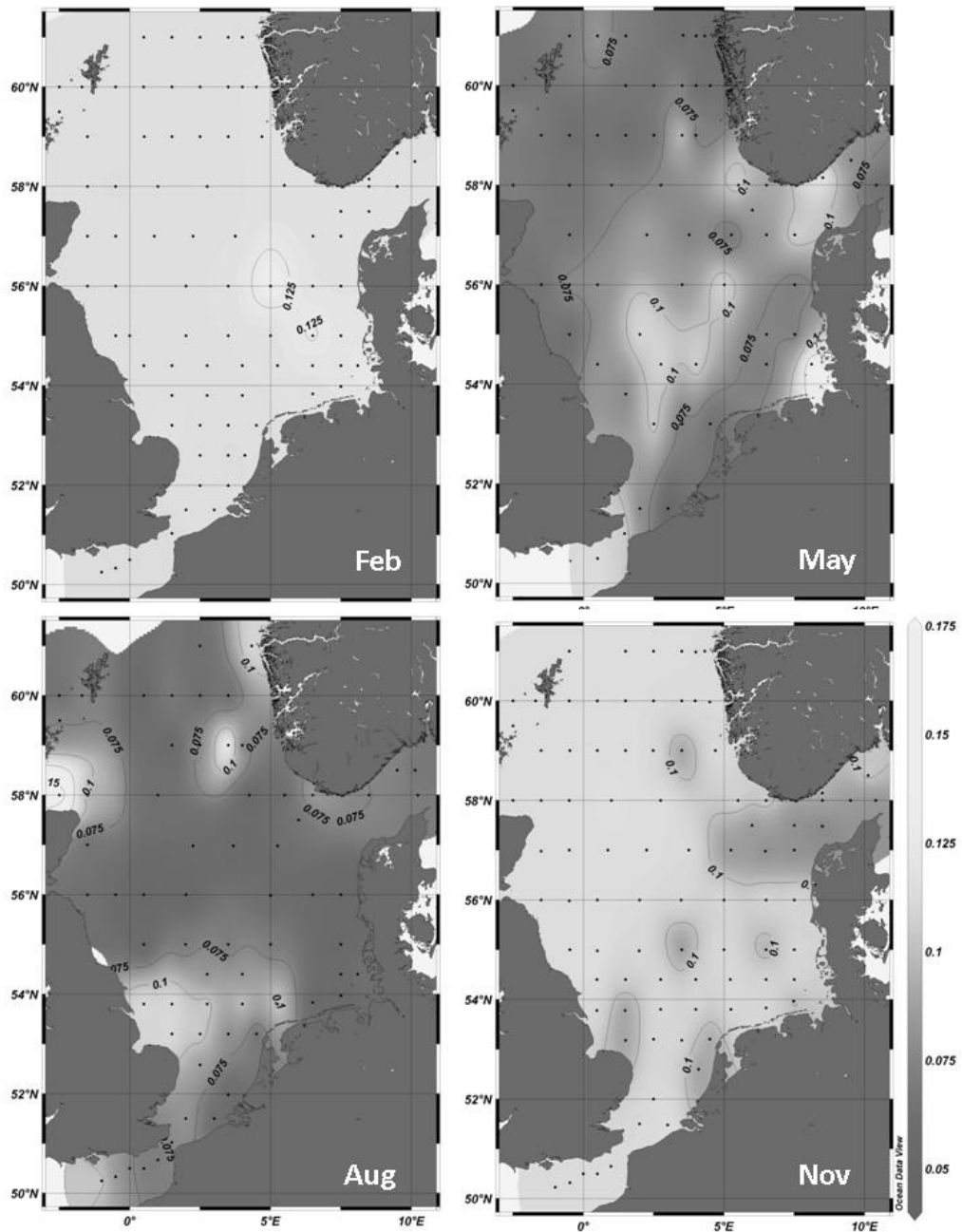


Figure 3.8: Horizontal distributions of the mean deviations [ $^{\circ}\text{C}$ ] between the calculated logarithm of the temperature-dependent  $p\text{CO}_2$  and the line of best fit, see Fig. 3.9

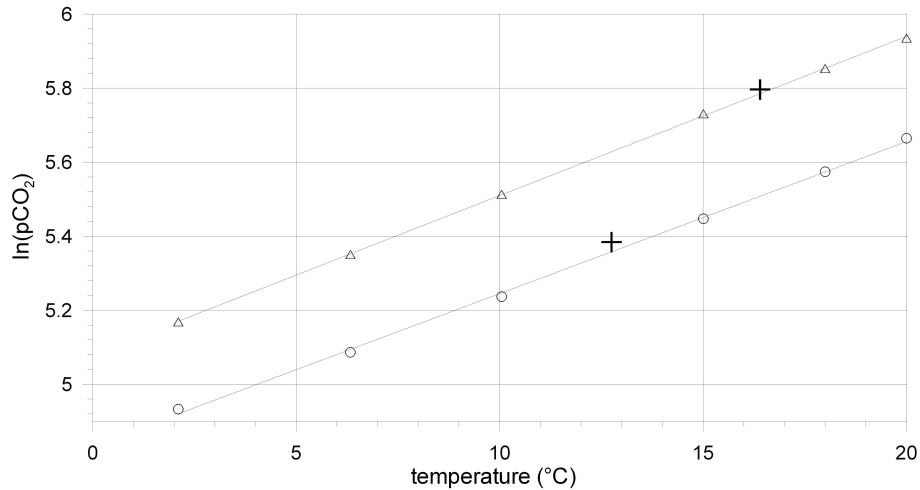


Figure 3.9: Comparison of the situation of a relatively high  $lp^c$  value of the open North Sea in August (55.98°N, 5°E) (triangles) with the situation in May in the German Bight (54.4°N, 8.1°E) (circles), where the lowest  $lp^c$  value was found (pH>8.3). The two values indicated by crosses represent corresponding observations of  $pCO_2$ .

values of the logarithm of the observed marine  $pCO_2$  are inserted as crosses. Both values are higher than the corresponding values of the  $lp^c$  derived logarithms. In case of the situation in August this deviation is smaller than in May. Both water columns were not in equilibrium with the atmospheric  $pCO_2$ : In August the marine  $pCO_2$  was 36  $\mu atm$  and in May even 160  $\mu atm$  lower than the atmospheric level. In May the German Bight water exhibited a pH of 8.297 whereas the corresponding value in the open North Sea in August was only 8.111. Fig. 3.10 shows the temperature dependency of the logarithm of the  $CO_2$  concentration for both situations. Obviously for the open North Sea station there is a nearly linear relationship between temperature and  $\ln(CO_2)$ . For the German Bight situation the relation is by no means linear (Fig. 3.10, solid black curve).

### 3.5 Discussion

The Takahashi method apparently linearises the temperature effect and then removes the corresponding signal from the data. Variations remaining must then be attributed to other effects. These effects include biological, chemical and other ones. When the non biological effects are small compared to the biological effect it appears to be sound to call the remaining signals to be biologically induced. In the following section we assume that the remaining signal is due to biological effects, and discuss situation where this holds and situations where this assumption is no longer valid. Applying the superposition method we assume that the biological effects do not interact with all other effects changing the  $pCO_2$ . We show that this assumption may fail in summer but holds during the rest of the year. The following discussion highlights particular situations where these assumptions hold or fail.

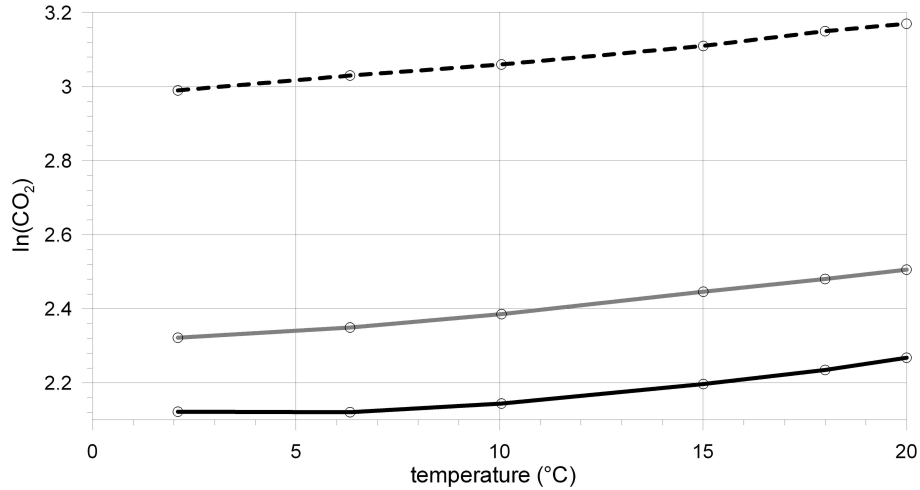


Figure 3.10: Temperature dependency of the logarithm of the  $\text{CO}_2$  concentration for the station in the open North Sea in August (grey line), and for the German Bight in May (solid black line). Additionally the situation of an artificial station with low pH-values is shown (dotted black line).

The influence of organic bases on  $p\text{CO}_2$  variations (Hernandez-Ayon *et al.*, 2007) is significant for water masses with high concentrations of DOC (dissolved organic carbon). For the discussion of the model derived data these acids do not play a role, as they are not included in the model.

The examination of the two methods, which allow to determine the biologically induced  $p\text{CO}_2$  variations, shows that both methods must be treated carefully. The Takahashi approach for identifying the biological impact on the  $p\text{CO}_2$  cannot be applied correctly to water bodies with sources and sinks of DIC which do not result from biological activities. From the budgets of DIC (Figs. 3.2,3.3,3.5,3.6) it is obvious that the high-frequency variations of DIC are related to the net effect of advection of DIC. When this flux causes strong variations in DIC the Takahashi method clearly fails (Fig. 3.6, day 1-40). But also the assumption of a superposition of physical-chemical and biological processes leads to difficulties: Temperature-induced variations of the  $p\text{CO}_2$  are larger for high  $p\text{CO}_2$  values than for lower ones. This implies that the physical/chemical run without summer depletion of DIC due to biological production, which exhibits higher  $p\text{CO}_2$  values than the standard run, is exposed to higher variations of  $p\text{CO}_2$  induced by temperature. This shows that the physical processes are not identical in both runs. So, the assumption that those processes and variations cancel out by subtracting the physical/chemical run from the standard run cannot be completely fulfilled.

In a sensitivity experiment we applied correction terms for the superposition method (Eq. 3.3), which corrects for too strong or too low temperature dependencies of the  $p\text{CO}_2$ . The daily correction terms took into account the tendency and rate of change of  $p\text{CO}_2$  of the physical/chemical run, the temperature change and the deviation between  $p\text{CO}_2$  of the standard run and the physical/chemical run. For some time intervals this helps but as the mean  $p\text{CO}_2$  is shifted, the temporal benefit is overwritten by an overall shift of  $p\text{CO}_2^{\text{Su}}$ . Previdi *et al.* (2009) circumvented this problem by decomposing the

total DIC variations into partial Taylor sums reflecting the different drivers. This method is able to identify the contribution of these drivers to change DIC from one state into another.

With the distribution of the  $lp^c$  values which substitute the  $lp$  value by Takahashi it is now possible to estimate the error which is induced when the constant  $lp$  is used instead of varying  $lp^c$  values. Applying the  $lp^c$  values for station FLEX we found strongest deviations from the original  $pCO_2^{Ta}$  series of  $-1.07$  and  $0.51 \mu\text{atm}$ . For station GLOBEC the deviations fall in the range of  $-1.27$  and  $1.04 \mu\text{atm}$ .

The Takahashi method appears to be robust in respect of the linearisation of the temperature dependency of the marine  $pCO_2$  and exhibits very low methodical errors. This means that the deviation between spatially and temporally calculated constants in the exponent of Takahashi's equation (Eq. 3.1) and the original constant determined by Takahashi *et al.* (1993) leads to deviations of the calculated  $pCO_2$  smaller than  $\pm 2 \mu\text{atm}$ . Only in areas with high pH values ( $>8.3$ ) due to e.g. biological production the double linearisation of the Weiss - approximation (Weiss, 1974) and the carbonate dynamics is not satisfying (Fig. 3.10, dashed line). On the other hand, the method works well in situations with lower pH values. This can be seen in Fig. 3.10 in the 'acidification' curve where artificial assumptions with pH values between 7.81 and 8.09 were applied ( $TA = 2300 \text{ mol kg}^{-1}$ ,  $DIC = 2150 \text{ mol kg}^{-1}$ ,  $S = 35 \text{ psu}$ ) giving an almost linear development.

### 3.6 Comments and recommendations

The Takahashi method and the superposition approach correspond quite well in areas without sinks and sources. Deviations occur when the annual cycle of  $pCO_2$  of the standard run and the physical/chemical run deviate strongly, because the superposition approach neglects the different effect of a change in temperature on different  $pCO_2$  levels. Generally the Takahashi approach is not applicable in areas with sinks and sources of DIC. This could be verified for areas with strong horizontal gradients where allochthonous sources like rivers exist. In case of autochthonous sources, as uptake of atmospheric  $CO_2$  or vertical DIC entrainment by mixing, the methods do not deviate. In this case the  $pCO_2$  curves do not reflect the biologically induced  $pCO_2$  alone, because both mentioned sources (mixing and exchange with the atmosphere) are not recognized by both methods. This recommends to take  $pCO_2^{Su}$  and  $pCO_2^{Ta}$  as lower bounds for biologically induced  $pCO_2$  changes.



## 4 The impact of coccolithophores on the carbon budget of the North Sea

### 4.1 Abstract

The dynamics of calcifying coccolithophores were successfully implemented as a third phytoplankton group into the ecosystem model ECOHAM for the North Sea (47° 41'–63° 53' N, 15° 5' W - 13° 55' E). The state variables for the biomass and the calcite are both treated prognostically. The results were validated with data from a cruise in 1999. We then analysed how the coccolithophores and the calcification influence the carbon fluxes by comparing the simulation with coccolithophores and a simulation without calcification. Additionally to the standard simulation, we examined the influence of ballasted zooplankton faecal pellets, doubled atmospheric CO<sub>2</sub> and higher SST on the carbon budget of the North Sea. Calcification lowers the air-sea flux as expected but the effect is dampened because additional carbon is exported to the sediment as newly formed particulate inorganic carbon (PIC). Acidification in a high CO<sub>2</sub> world weakens calcification as well as the export, but the air-sea gradient is still the most important trigger for the uptake of atmospheric CO<sub>2</sub>. The mechanism for the termination of the coccolithophore bloom still remains unclear.

### 4.2 Introduction

The North Sea (Fig. 4.1) is located on the North European Continental Shelf (47° 41'–63° 53' N, 15° 5' W - 13° 55' E). It provides a link between the anthropogenically influenced coastal area and the North Atlantic ocean and plays a specific role in the marine and global carbon cycle via the “carbon shelf pump” mechanism, which describes the interplay between the biological pump, the solubility pump, and the lateral advection of organic and inorganic carbon into the adjacent deep ocean (Tsunogai *et al.*, 1999). The North Sea is nowadays subject to warming of sea surface temperature (SST) (Wiltshire & Manly, 2004) and ocean acidification (Blackford *et al.*, 2008). Due to this rapidly changing environmental factors, it is crucial to understand the triggers of natural variabilities in such a system. Lorkowski *et al.* (2012) (from here on called L12) analysed in a long-term simulation the drivers of the variability of the air-sea flux of carbon dioxide in the North Sea. They found that the North Sea has taken up carbon dioxide during the last 30 years, but that this sink for atmospheric carbon dioxide is decreasing. This decrease is mainly governed by the northern North Sea.

The northern North Sea is quite often subject to blooms of coccolithophores (e.g. Holligan *et al.* (1989, 1993a); Burkill *et al.* (2002); van der Wal *et al.* (1995); Archer *et al.* (2001); Rees *et al.* (2002); Widdicombe *et al.* (2002); Wilson *et al.* (2002)). They are the most important marine calcifiers, accounting for about 80 % of marine calcification (Müller *et al.*, 2008). Their calcification impacts the carbonate system: For one mol of calcium carbonate formation, DIC decreases by one mol and TA decreases by two mol, shifting the carbonate system equilibrium towards CO<sub>2</sub>. Therefore, blooms of

coccolithophores might influence the uptake capacity for atmospheric CO<sub>2</sub> of the North Sea. This process is the so-called "carbonate counter pump". The L12 study does not consider this process in detail, thus we decided to implement a new phytoplankton group, the coccolithophores, into ECOHAM4 to directly analyse the effect of calcification on the carbon fluxes in the North Sea.

Additional to the effect of calcification on pCO<sub>2</sub>, the calcium carbonate is often discussed in connection to sinking fluxes as mineral ballast (Francois *et al.*, 2002; Klaas & Archer, 2002; Armstrong *et al.*, 2002). This ballasting effect might enhance the sinking of organic carbon and thus influence the export of carbon into the deep water. It also might reduce the decreasing effect of calcification on the air-sea flux due to the increasing vertical carbon export (Buitenhuis *et al.*, 2001). The interaction between calcification and ballast export in a high CO<sub>2</sub> world was examined by Hofmann & Schellnhuber (2009) who found lower export due to lower calcification, which will partly reduce the negative feedback of decreasing calcification on rising atmospheric pCO<sub>2</sub>. One possible occurrence of this ballasting effect may be the agglutination of TEP and coccoliths to form marine snow aggregates (Harlay *et al.*, 2009). Another theory assumes that the coccoliths, which were ingested by zooplankton increase the sinking velocity of their faecal pellets and lead to a faster transport of organic material into deeper water (Honjo, 1976; Buitenhuis *et al.*, 2001). These ballasted faecal pellets can be found in sediment traps (De La Rocha & Passow, 2007). We implemented the ballasting effect on zooplankton faecal pellets when they feed on a coccolithophore bloom for a sensitivity run and monitored the differences in export fluxes and the carbon budgets between this ballast simulation and the standard run.

The change of calcification in times of rising temperatures and rising atmospheric pCO<sub>2</sub> is still under debate. Several studies report on decreasing calcification in a high CO<sub>2</sub> world (e.g. Riebesell *et al.* (2000); Delille *et al.* (2005); Engel *et al.* (2005); Zondervan *et al.* (2001)), whereas Iglesias-Rodriguez *et al.* (2008) found an increase in calcification during high pCO<sub>2</sub> conditions. Langer *et al.* (2006) found that the response on species basis is highly diverse. We investigated this effect by conducting a high CO<sub>2</sub> simulation in which we doubled the atmospheric pCO<sub>2</sub> as expected for the year 2100 in the IPCC scenario IS92a (IPCC, 2001).

Some implementations of coccolithophores in biogeochemical models already exist (e.g. Tyrrell & Taylor (1996); Gehlen *et al.* (2007), or Gregg & Casey (2007)) and we used some of their parameters and processes to implement them into ECOHAM4. Additionally we used one specific study, the so called DISCO cruise, which was conducted in 1999 (Burkill *et al.*, 2002) to calibrate our model. The main goal of this cruise was to analyse the DMS production of coccolithophores. DMS can act as cloud condensation nuclei and the formation of DMS is another interesting aspect in the ecology of coccolithophores, but goes beyond the scope of this study. Here we describe the implementation of coccolithophores and show the calibration and validation. Afterwards we analyse several different simulation runs, with and without coccolithophores, with and without ballast, simulations to analyse the temperature and pCO<sub>2</sub>-sensitivity and sensitivity tests with varying calcification rates.

### 4.3 The model

The general structure of the model ECOHAM is kept as in Lorkowski *et al.* (2012). We extended the biogeochemical module of ECOHAM4 by implementing new state variables for coccolithophores and included a prognostic alkalinity. The model was run for the

year 1999 with two years of spinup. The hydrodynamics were simulated by HAMSOM (Backhaus, 1985; Pohlmann, 2006), including freshwater input by the most important rivers and a prognostic calculation of salinity (Pohlmann, 2006).

#### 4.3.1 Forcing, boundary conditions and river input

The meteorological forcing and boundary conditions are the same as in the L12 study, of course only for the year 1999. We used mean monthly atmospheric  $p\text{CO}_2$  data for the year 1999 measured at Mace Head from NOAA (Conway *et al.*, 2011). The river set up was changed in comparison to L12. Dissolved inorganic carbon (DIC) and Total Alkalinity (TA) would drastically increase near the river mouths without freshwater input. Therefore, we included daily freshwater input. We aimed at obtaining a consistent data set for the most important rivers including all carbon species and all nutrients together with freshwater input. The rivers, their location and the data sources are given in Tab. 4.1. For the carbon species of the Norwegian rivers we had no data available and assumed that they are similar to the northern UK rivers.

#### 4.3.2 Prognostic Alkalinity, calcite saturation and dissolution of calcite

We included a prognostic treatment of Total Alkalinity (TA) into the model to obtain a more precise calculation of the carbonate system and the dynamics of the counterpump. Therefore, we implemented the above mentioned riverine input of TA and changes of TA due to biogeochemical processes. The biogeochemical part is determined by calcite-, nitrate- and ammonium- related processes. The respective theoretical background is best described in the study of Wolf-Gladrow *et al.* (2007). The coccolithophores influence the TA in several ways. The uptake of carbonate ions ( $\text{CO}_3^{2-}$ ) during calcification, the pelagic and benthic dissolution of calcite have to be named explicitly. Vice versa, changes in TA influence the calcification via the carbonate saturation state. A strong correlation between  $\text{CO}_3^{2-}$  concentration and the occurrence of coccolithophores has been found for the Bering Sea (Merico *et al.*, 2004). In every timestep we calculate the concentration of carbonate ions from DIC and TA after Zeebe & Wolf-Gladrow (2001) (their Eq. 1.1.11). As the calcium ion is available in abundance, the carbonate ion concentration determines the calcite saturation state  $\Omega$  (calculated after Zeebe & Wolf-Gladrow (2001), their Eq. 1.1.25) of seawater, which then influences calcification (see below, A1 Eq. 13.12). Both  $\Omega$  and the benthic and pelagic dissolution of calcite are dependent on the solubility product  $K_{\text{sp}}$  according to (Millero, 1995). The dissolution of calcite as implemented in ECOHAM is also described in Pätzsch *et al.* (2002).

#### 4.3.3 Implementation of coccolithophores

In the former ECOHAM4 version, the coccolithophores were implicitly included in the second phytoplankton state variable, the flagellates or more precisely non-diatoms, by assuming a fixed constant calcite to organic carbon ratio. Now we calculate the state variables coccolithophores and calcite both prognostically with varying organic carbon to calcite ratio. The parametrisation for the coccolithophores is given in Tab. 4.2. The value for the minimal organic carbon to calcite carbon ratio (Tab. 4.2) was calculated by considering a coverage of 20 liths per cell, 13 pg org. C per cell and 0.39 pg C per lith (Harlay *et al.*, 2010).

Name	River mouth position	Data source
Elbe	54° 05' N 08° 35' E	Freshwater from Pätsch & Lenhart (2008); Nutrients and carbon species see Lorkowski <i>et al.</i> (2012)
Ems	53° 41' N 06° 35' E	as above
Nordzeekanal	52° 29' N 04° 15' E	as above
Ijssel E	53° 29' N 05° 15' E	as above
Ijssel W	53° 17' N 04° 55' E	as above
Nieuwe Waterweg	52° 05' N 03° 55' E	as above
Haringvlet/Rhine	51° 53' N 03° 35' E	as above
Schelde	51° 29' N 03° 15' E	as above
Weser	53° 53' N 08° 15' E	as above
Humber	53° 17' N 00° 35' E	Nutrients and carbon species see Lorkowski <i>et al.</i> (2012); Freshwater from O'Driscoll <i>et al.</i> (2012)
Thames	51° 41' N 01° 15' E	as above
Moray Forth	58° 05' N 03° 25' W	Carbon species calculated like Firth of Forth; Nutrients from Heath <i>et al.</i> (2002); Freshwater from O'Driscoll <i>et al.</i> (2012)
Spey	58° 05' N 02° 45' W	as above
Firth of Forth	55° 53' N 02° 25' W	Nutrients from Heath <i>et al.</i> (2002); Carbon species calculated after Neal (2002); Freshwater from O'Driscoll <i>et al.</i> (2012)
Tees	55° 05' N 01° 05' W	as above
Tyne	54° 41' N 00° 25' W	as above
Wash	53° 53' N 00° 15' E	as above
Norway 1	59° 05' N 05° 15' E	Carbon species calculated from UK; Nutrients from OSPAR (2000); Freshwater from O'Driscoll <i>et al.</i> (2012)
Norway 2	58° 17' N 05° 55' E	as above
Norway 3	57° 53' N 06° 55' E	as above
Norway 4	58° 17' N 08° 55' E	as above
Norway 5	58° 53' N 10° 15' E	as above
Seine	49° 29' N 00° 25' W	Nutrients and carbon species see Lorkowski <i>et al.</i> (2012); Freshwater from Lenhart <i>et al.</i> (2010)

Table 4.1: Names of rivers, river mouth positions and data source.

name	value	source
half saturation constant nitrate uptake	0.25 mmol N m <sup>-3</sup>	half of value for diatoms after Gregg & Casey (2007) as for non-diatoms
half saturation constant ammonium uptake	0.05 mmol N m <sup>-3</sup>	
half saturation constant phosphate uptake	0.05 mmol P m <sup>-3</sup>	
growth rate at 10°	1.0 d <sup>-1</sup>	
exudation fraction	0.05	
mortality rate	0.035 d <sup>-1</sup>	
mortality at quadratic loss term	0.01	
Grazing preference for microzooplankton	0.25	
N:P ratio	32.0	Tyrrell & Taylor (1996)
maximum calcification rate	1.0 mmol calcite C (mmol org C d) <sup>-1</sup>	
minimum ratio of organic carbon to calcite carbon	1.6 mmol org C (mmol calcite C) <sup>-1</sup>	calculated after Harlay <i>et al.</i> (2010)
half saturation for light, primary production	30 W m <sup>-2</sup>	Zondervan (2007)
half saturation for light, calcification	17 W m <sup>-2</sup>	Zondervan (2007)
half saturation, dependence on $\Omega$	0.4	Gehlen <i>et al.</i> (2007)

Table 4.2: Parameter names and values. If available, a literature source is given.

The complete set of equations with descriptions for the implemented coccolithophores is given in the appendix A5. The most significant differences between the coccolithophores and the other two phytoplankton groups are that the coccolithophores are not light inhibited at high radiation levels (Nimer *et al.*, 1991) (A5: Eq. 13.9), they are able to use very low phosphate concentrations and can additionally take up organic phosphorus (A5: Eq. 13.22). The growth is limited not only by light, nutrients and temperature, but also by the calcite saturation state (Gehlen *et al.*, 2007). The calcification depends on light intensity and the calcite saturation state as well (Eq. 13.11). They are grazed by microzooplankton (Merico *et al.*, 2004). The detachment of coccoliths consists of two parts. First the detachment occurs at a constant rate (A5: Eq. 13.23), and second, if a specific minimum organic carbon to calcite ratio is reached, all additional coccoliths will be detached and enter the detritus pool (Tyrrell & Taylor, 1996) (A5: Eq. 13.25).

### 4.3.4 Sinking and mineral ballast

The ballasting effect of ingested coccoliths on zooplankton faecal pellets is implemented by adding a new detritus group with a higher sinking velocity of 100 m/d (Kriest, 2002). The corresponding equations are given in the appendix A6.

It is assumed, that all ingested calcite, but only 25 % of the ingested organic carbon (Lorkowski *et al.*, 2012) is transferred into fecal pellets. The excretion of heavy detritus by zooplankton (A6: Eq. 14.6) is parameterised by calculating the ratio of ingested (= excreted) calcite carbon to excreted organic carbon (A6: Eq. 14.5). This ratio then gives the portion of organic material that belongs to the new detritus group. The portion of excreted organic nitrogen and excreted organic phosphorous that is entering the new detritus group is calculated by multiplying with the respective element ratios.

### 4.3.5 Climate change scenarios

To account for the effect of changing environmental conditions, we conducted one simulation with doubled mean monthly atmospheric CO<sub>2</sub> concentration (double). To investigate the effect of temperature, the biological set up of the standard simulation was subjected to a warm and a cold forcing set up (warm/cold). To obtain a consistent set of forcing without the need to rerun the hydrodynamic model, we used the forcing set of the coldest year from the L12 study which was 1979 and the warmest year of the L12 study, which was 2006 but used the same river set up as for the standard simulation from 1999. The differences in SST between the warm and the cold simulation is about 1.67 °C in the annual mean, while the annual mean SST of 1999 is only 0.24 °C lower than the annual mean SST in the warm simulation and 1.43 °C higher than the mean annual SST in the cold simulation. Finally, to analyse the combined effect of higher temperature and atmospheric CO<sub>2</sub>, we conducted one simulation with the warm forcing set up and the doubled monthly mean atmospheric CO<sub>2</sub> concentrations (double+warm).

## 4.4 Results

### 4.4.1 Validation/Calibration

We used a data set of the British Oceanographic Data Center (BODC) to validate and calibrate the model. The data were obtained during a measurement campaign of a coccolithophore bloom in the northern North Sea in 1999 (Burkill *et al.*, 2002). We

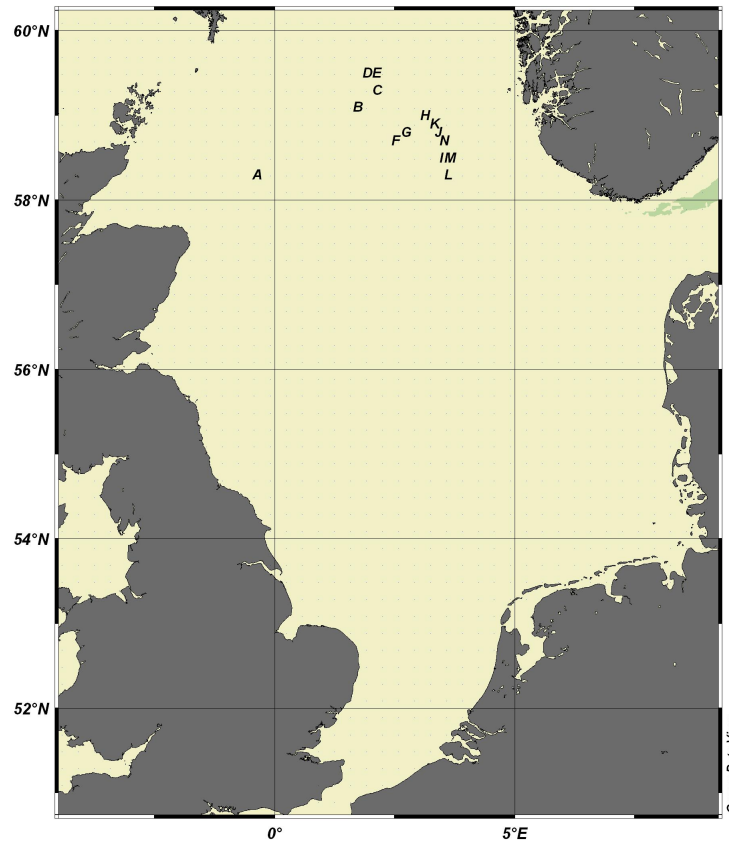


Figure 4.1: Location of the 14 water columns used for model validation.

used the temperature and salinity data for validation and the calcite measurements for calibration. The available data span over two weeks in June 1999 and contain 43 water columns, which corresponds to 14 of our model grid water columns (Fig. 4.1).

We averaged the data which fell into one model grid cell. Since the different water columns were sampled during different days of the cruise (usually 1 to 3 days) the data were averaged over this short time interval as well. Model results for every single one of the corresponding 14 water columns were averaged over the two weeks of the measurement campaign. The model-data-comparison for salinity can be seen in Fig. 4.2. The model underestimates the measured salinity slightly, but the general pattern and the profiles are represented reasonable. The deviations in the surface salinity are more pronounced in the station closer to the Norwegian Coast, therefore differences in the river run-off might lead to the underestimation of salinity in the upper 25 m.

The modelled temperature profiles are reproducing the stratification as observed during the cruise (Fig. 4.3), although surface temperature is a bit overestimated, while the temperature in the deep is underestimated by the model. The mismatch between model and data, especially in the surface might be due to the fact, that we average the data over the 10 m model layer thickness. Strong gradients which might be in the data influence this average.

Since all parameters influencing the calcification except the maximum calcification rate are constrained by literature values (Tab. 4.2), we tuned only the calcification rate,

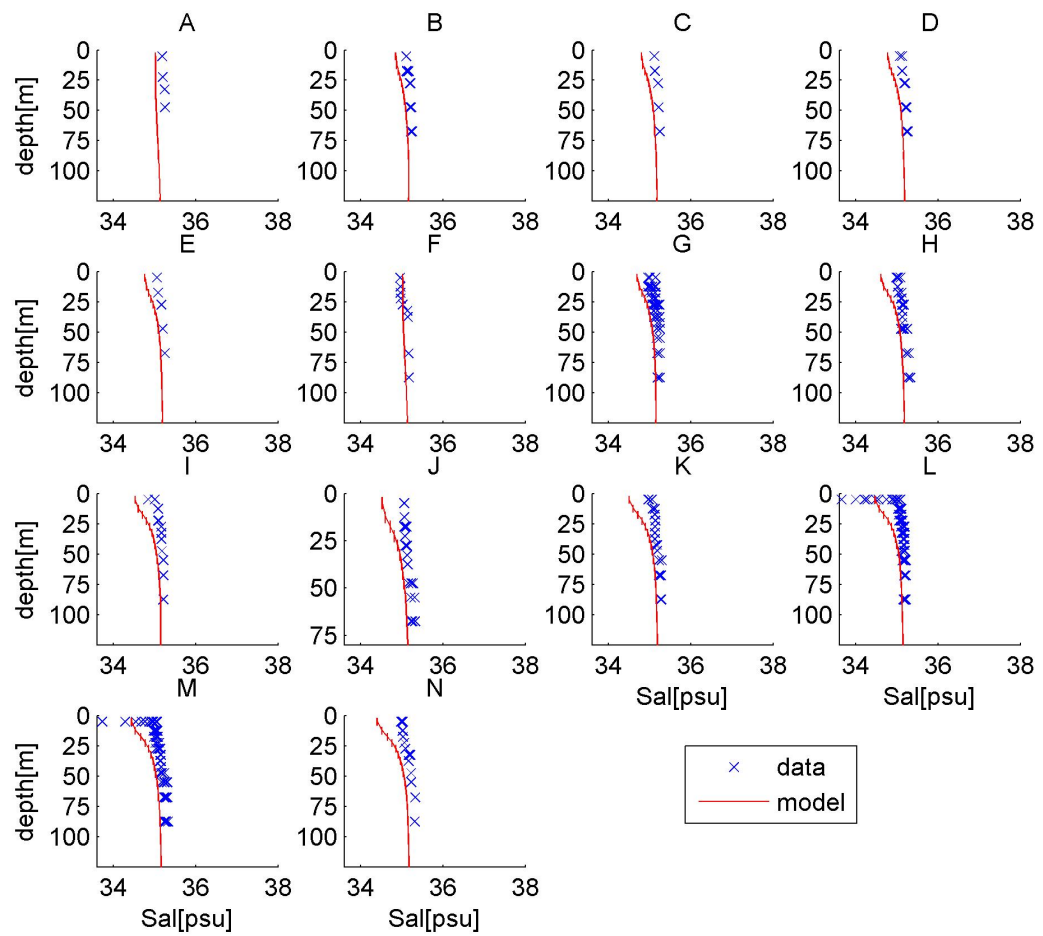


Figure 4.2: Model-data comparison for the salinity profiles of the BODC water columns (Fig. 4.1).

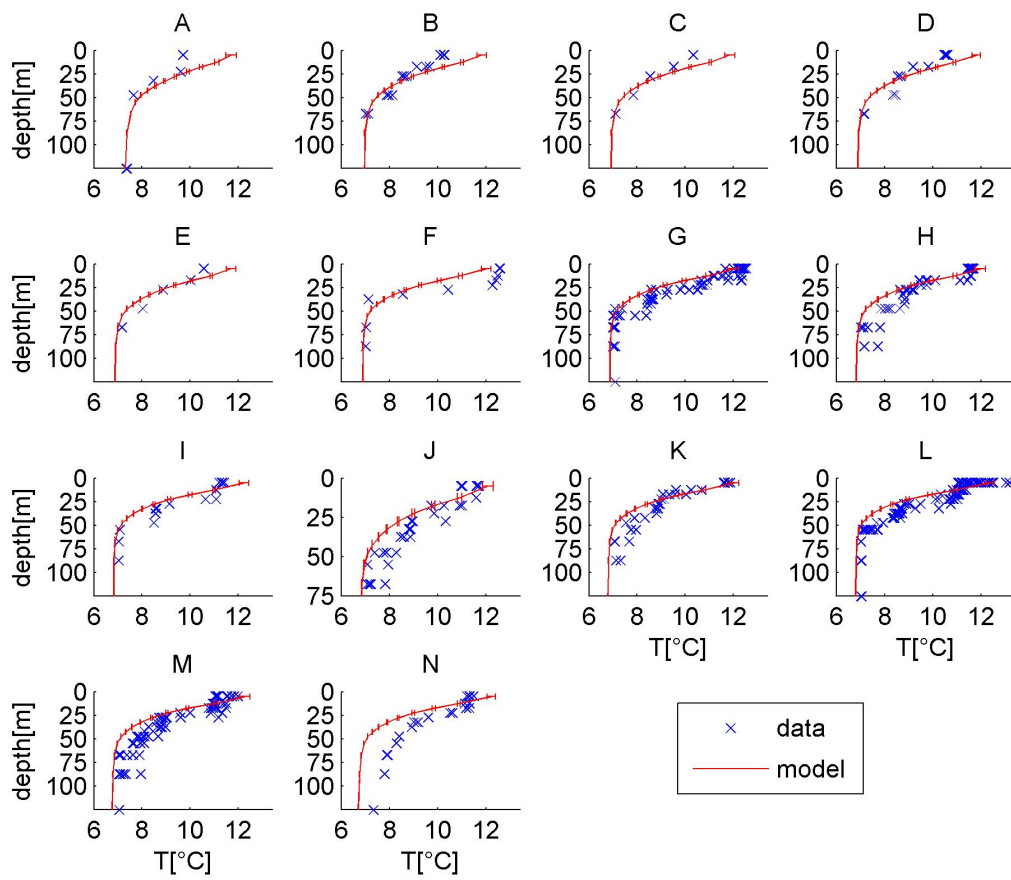


Figure 4.3: Validation of the temperature profiles for the BODC water columns.

to fit the data best. The calcite measurements were originally counts of coccospheres. To compare them with our modelled calcite concentrations, we had to multiply the number of coccospheres by the number of liths per cell (10-50 liths per cell after Tyrrell & Taylor (1996)) and the weight of one coccolith ( $0.39 \pm 0.07$  pg C per lith after Harlay *et al.* (2010)). We used the values plus and minus the standard deviation, which gave us a range of values for the validation of modelled calcite. The comparison can be seen in Fig. 4.4.

The modelled living calcite reaches mostly the upper range of the data estimates in the upper 50 m, while it underestimates the observations below 50 m. One reason for this may be, that the model clearly distinguishes between calcite associated with living cells and "dead" calcite and because due to the concentration-based model formulations we can not distinguish between complete detrital coccospheres and detrital coccoliths. In the calibration plot we only show the modelled "living" calcite, while the data contain whole coccospheres, which can be dead or alive. Therefore the observed calcite in the deeper water may as well be already calcite detritus.

The horizontal variability in the model is lower than in the data. This can especially be seen in the water column A (Fig. 4.1), which is distant to the other water columns. The modelled horizontal distribution nevertheless shows some heterogeneity (Fig. 4.5), with a bloom in the northern North Sea and smaller blooming patches in the southern North Sea. These features can also be seen in satellite pictures from Holligan *et al.* (1989).

#### 4.4.2 Carbon fluxes

We conducted several different simulations to estimate the effect of coccolithophores on the North Sea carbon budget. One was with the old two phytoplankton groups (2groups), one with coccolithophores (standard) and one with coccolithophores and the ballasting effect on zooplankton faecal pellets (ballast).

Fig. 4.6 shows the vertically and horizontally integrated biomass of the three phytoplankton groups in the North Sea. The diatoms display a prominent spring and autumn bloom, while the non-diatoms dominate during summer. The coccolithophores contribute the lowest biomass and start blooming latest. The beginning of the coccolithophore bloom agrees with observations (Harlay *et al.*, 2010).

The modelled cumulative air-sea flux for the three simulations is given in Fig. 4.7. In all simulations the North Sea takes up CO<sub>2</sub> during most of the time. In the first half of the year, the simulations with coccolithophores take up more atmospheric CO<sub>2</sub> because the winter inventories of DIC are lower in this simulation since more "last year"-carbon is stored in the sediments (see below). After the start of the coccolithophore bloom and the resulting calcification in June (about day 150), the uptake becomes smaller for the runs with coccolithophores and even a short outgassing event occurs around day 270. At the end of the year, the air-sea flux for the standard simulation with coccolithophores is lower ( $756 \text{ Gmol C yr}^{-1}$ ) than in the 2groups-simulation ( $959 \text{ Gmol C yr}^{-1}$ ). The difference between the ballast- and the standard simulation is comparatively small ( $11 \text{ Gmol C yr}^{-1}$ ). The North Sea is a sink for atmospheric CO<sub>2</sub> at the end of the year for all three simulations. The air-sea flux from the standard simulation is in the range of the L12 simulation and is with about  $1.5 \text{ mol C m}^{-2} \text{ yr}^{-1}$  only slightly higher than values from Thomas *et al.* (2004) of  $1.38 \text{ mol C m}^{-2} \text{ yr}^{-1}$ . The addition of coccolithophores led to a reduction in the air-sea flux of 22 % which is higher than values from Suykens *et al.* (2010), who found a decrease of the air-sea flux of 12 % due to calcification during a coccolithophore bloom in the Bay of Biscay.

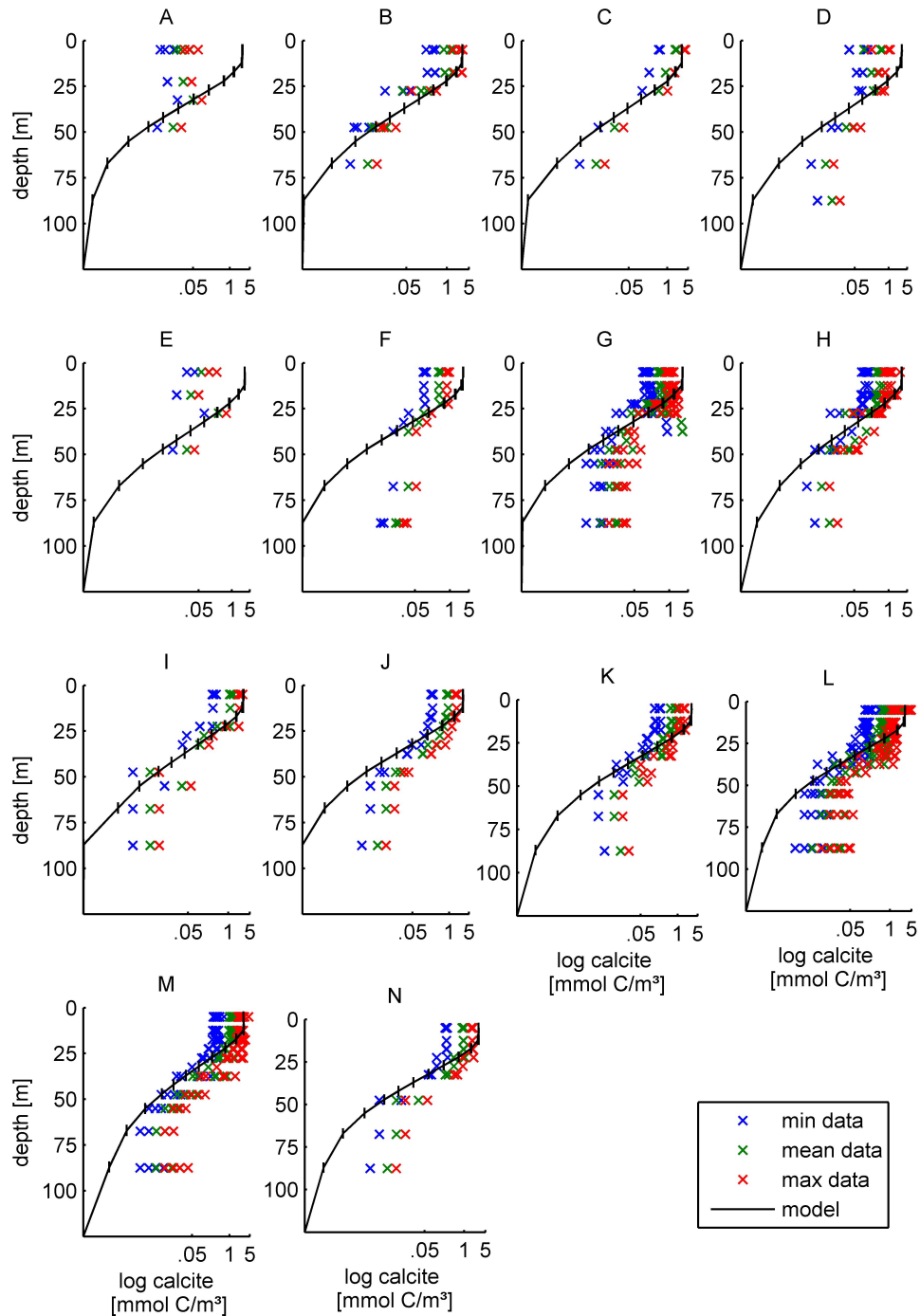


Figure 4.4: Model-data comparison for calcite. The fourteen water columns from Fig. 4.1 are shown.

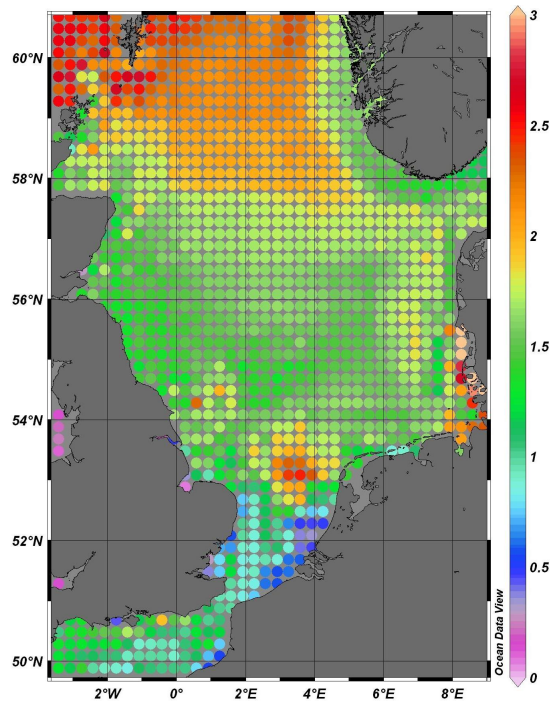


Figure 4.5: Modelled horizontal distribution of surface coccolithophore calcite [ $\text{mmol C m}^{-3}$ ] in June 1999.

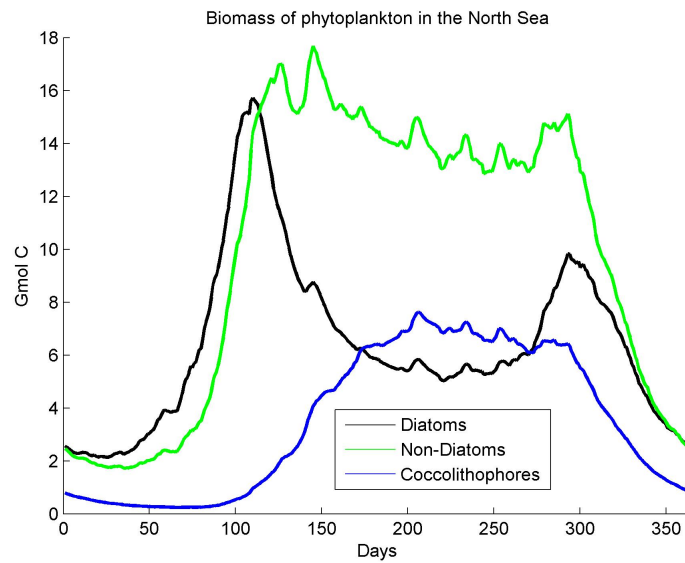


Figure 4.6: Vertically and horizontally integrated biomass of the three phytoplankton groups for the whole North Sea in Gmol C.

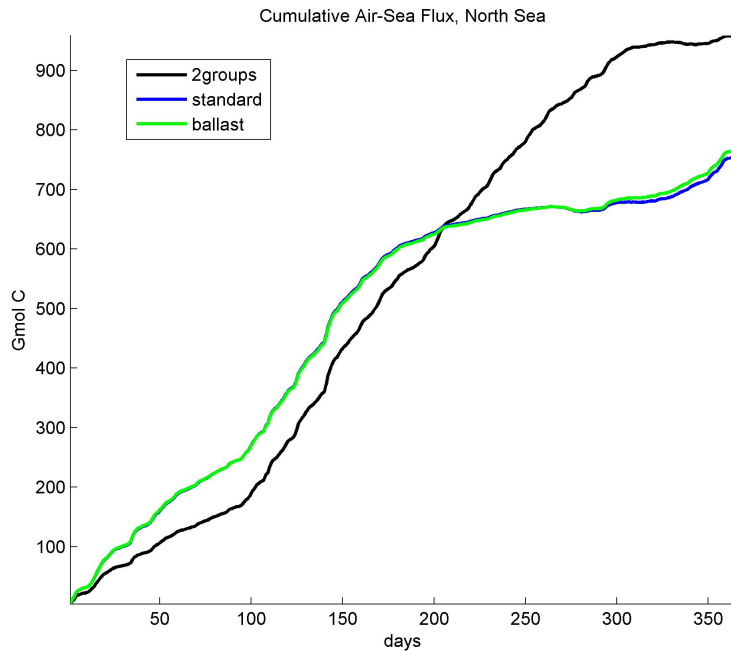


Figure 4.7: Cumulative air-sea flux of the North Sea for the different simulations.

The total Net Primary Production (NPP) (Fig. 4.8) as well as the Net Ecosystem Production (NEP; NPP minus respiration) (Fig. 4.9) do not vary significantly between the simulations. The values for the NEP are in the range of values calculated by Lorkowski *et al.* (2012), and, by relating it to the area of the North Sea (511724 km<sup>2</sup>), with 0.1 mol C m<sup>-2</sup> yr<sup>-1</sup> lower than values from Kühn *et al.* (2010) (0.6 mol C m<sup>-2</sup> y<sup>-1</sup>) and slightly higher than values from Bozec *et al.* (2006) (-0.1 mol C m<sup>-2</sup> yr<sup>-1</sup>). The cumulative NEP (Fig. 4.9) is differing slightly between the simulations, especially in the second half of the year. But the NEP for the year in total is almost the same for all simulations. Fig. 4.8 shows the cumulative NPP for the whole North Sea. While the total NPP of the standard simulation is only slightly higher than for the 2groups simulation, the largest difference occurs in the NPP of the Non-diatoms. In the standard simulation, the coccolithophores replace some production of the Non-diatoms group, because the coccolithophores are physiologically closer to the Non-diatoms, which also displays in the parametrisation. In the study of Lorkowski *et al.* (2012) the coccolithophores were considered to be included implicitly into the Non-diatoms. The total NPP for the standard run fits in the range of values from the L12 simulation, which found an annual mean of 7898 Gmol C yr<sup>-1</sup> for annual cumulated NPP, while our total NPP for the standard simulation is 7325 Gmol C yr<sup>-1</sup>.

The amount of calcification for the standard run is 1574 Gmol C yr<sup>-1</sup> and 1530 Gmol C yr<sup>-1</sup> in the ballast simulation. Thus, in the standard run, the amount of calcification of total inorganic carbon incorporation was 17.7 %. This is higher than the upper bound of 2-16 % found in the DISCO cruise within the coccolithophore bloom (Rees *et al.* , 2002).

The total net export of total carbon via the Norwegian Trench does not differ much between the simulations, the most important trigger for this export is the amount of water, which is the same in all three simulations (not shown). This is valid also for the export in the deep below 100 m water depth. The net export of the different carbon

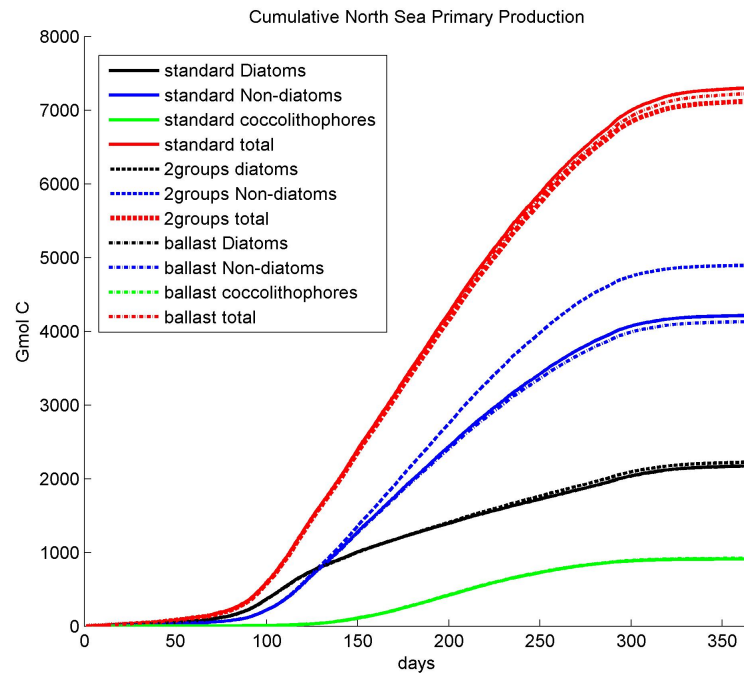


Figure 4.8: Cumulative NPP of the North Sea for the different groups and simulations. The solid line represents the standard simulation, the dashed line the 2groups simulation and the dashed dotted line the ballast simulation. The red curves or showing the total NPP, the blue curves represent the NPP by non-diatoms, the black curves are showing the NPP of diatoms and the green curves visualise the NPP of coccolithophores.

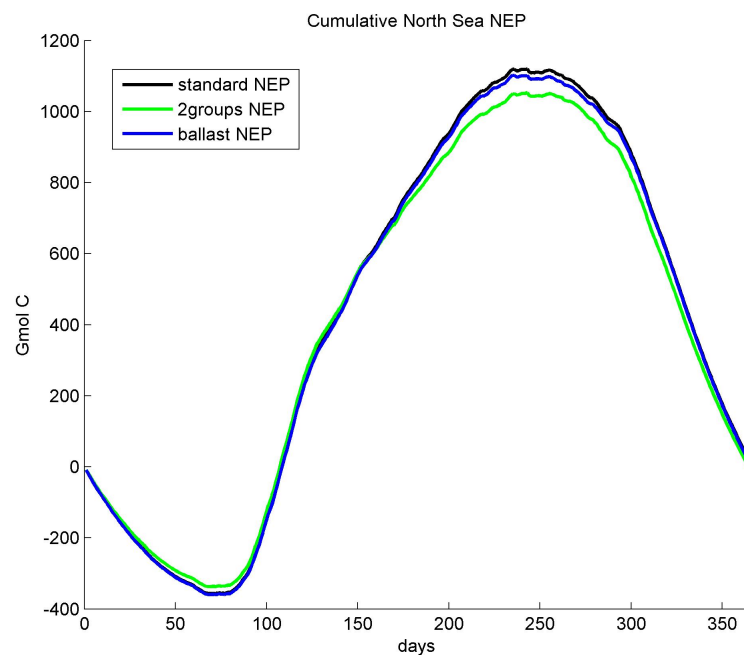


Figure 4.9: Cumulative NEP of the North Sea for the different groups and simulations.

	2groups	standard	ballast
DIC	1075.0	913.5	929.9
TOC	103.4	122.0	115.6
Cal	0	-0.4	-0.3

Table 4.3: Horizontal net export of DIC, total organic carbon (TOC) and calcite (Cal) in  $\text{Gmol C yr}^{-1}$ .

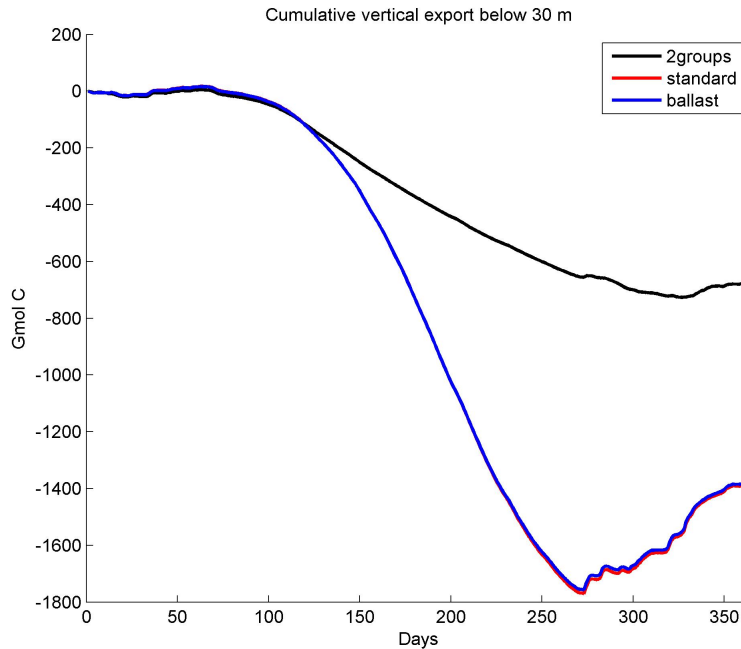


Figure 4.10: Cumulative vertical export below 30 m of TC in  $\text{Gmol C yr}^{-1}$  of the North Sea for the different simulations.

components is given in Tab. 4.3

Fig. 4.10 shows the cumulative vertical export of TC below 30 m for the whole North Sea. The difference between the simulation with two phytoplankton groups and the two simulations with three phytoplankton groups is quite large, while the difference between the standard and the ballast simulation is comparatively small.

Fig. 4.11 shows the vertical export below 30 m for the different simulations subdivided into TOC, DIC and PIC. The upwelling of DIC rich water in the second half of the year can be seen. The difference in the export of TOC between the three simulation is small, with the highest export of TOC for the ballast simulation. The export of PIC is even a bit smaller in the ballast simulation than in the standard simulation, because the calcification in the ballast simulation is slightly smaller ( $1530 \text{ Gmol C yr}^{-1}$  in the ballast run compared to  $1574 \text{ Gmol C yr}^{-1}$  in the standard run). From Fig. 4.11 it gets clear, that the difference between the 2groups simulation and the two simulations with three phytoplankton groups in the vertical export of total carbon in Fig. 4.10 results from the additional export of PIC - partly dampened by the enlarged DIC reflux - which does not exist in the 2groups simulation.

The cumulative pelagic dissolution of calcite is nearly the same for the ballast and the standard run (Fig. 4.12), whereas the benthic dissolution is a bit higher for the standard

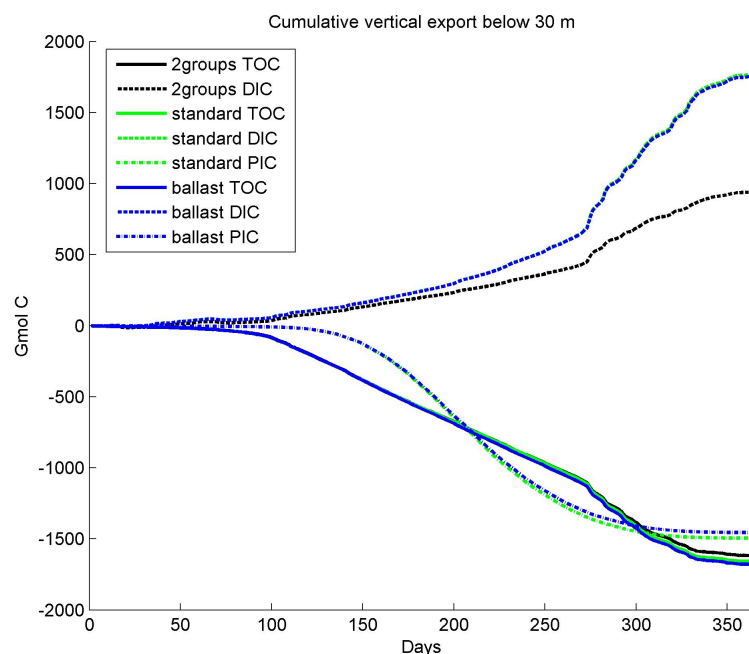


Figure 4.11: Cumulative vertical export of DIC, TOC, PIC in  $\text{Gmol C yr}^{-1}$  of the North Sea for the different simulations.

run than for the ballast simulation (Fig. 4.12).

The total benthic remineralisation of carbon and thus the release of DIC from the sediment into the water column is highest in the ballast simulation ( $789 \text{ Gmol C yr}^{-1}$ ) and lowest in the 2groups simulation ( $753 \text{ Gmol C yr}^{-1}$ ). The DIC release from the sediment in the standard simulation is  $787 \text{ Gmol C yr}^{-1}$ .

The amount of carbon that is stored in the sediment at the end of the year is  $51.4 \text{ Gmol}$  organic carbon (OC) and  $167.8 \text{ Gmol}$  of particulate inorganic carbon (PIC) for the ballast simulation,  $50.5 \text{ Gmol}$  OC and  $173.4 \text{ Gmol}$  PIC for the standard simulation and  $42.3 \text{ Gmol}$  OC for the 2groups simulation. The PIC content in the sediment is about 10 % of calcification, which is in the range of observation-based estimates that globally about 15 % of the  $\text{CaCO}_3$  formed is stored in the sediments (Balch *et al.*, 1996), while the OC content is about 0.5 % of total NPP, and thus in the range of less than 1 % as reported by several studies (Radach & Lenhart, 1995; de Haas *et al.*, 2002; Luff & Moll, 2004; Thomas *et al.*, 2005a).

### Climate change scenarios

The calculated carbon fluxes for the double  $\text{pCO}_2$ , the cold, the warm and the warm/double  $\text{pCO}_2$  scenarios in comparison with the standard simulation are given in Tab. 4.4.

The doubling of the monthly mean atmospheric  $\text{CO}_2$  concentrations in the standard run results in an increased annual uptake of atmospheric  $\text{CO}_2$  by 135 % (Tab. 4.4). The export of DIC via the Norwegian Trench is about  $1049 \text{ Gmol C}$  higher than in the standard run and the horizontal export of TOC is a bit smaller than in the standard run for the double  $\text{CO}_2$  simulation. Calcification and NPP of coccolithophores decreases, as well as the NEP (Tab. 4.4). The production of diatoms and non-diatoms changes only

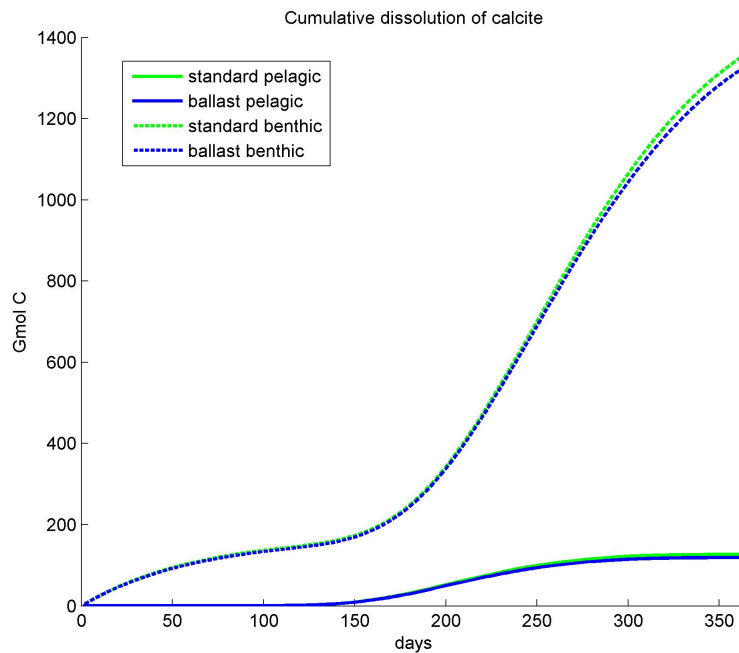


Figure 4.12: Cumulative benthic and pelagic calcite dissolution for the standard and the ballast run for the North Sea.

slightly, with higher values in the double  $\text{CO}_2$  simulation (Tab. 4.4).

The comparison of the warm versus the cold year shows (Tab. 4.4), that NPP and calcification increases with temperature, although it is still lower in the warm simulation than in the standard simulation. The NEP decreases drastically in the cold simulation, whereas the air-sea flux is lowest in the warm simulation. In the cold simulation TOC is imported into our budget area, which is not the case for every other simulation.

The combination of doubled atmospheric  $\text{CO}_2$  and the warm forcing set leads to reduced NPP for the coccolithophores and the lowest calcification (Tab. 4.4). The air-sea flux is quite high, but lower than in the double simulation. The horizontal export of DIC is highest for this simulation.

	double [Gmol C y <sup>-1</sup> ]	cold [Gmol C y <sup>-1</sup> ]	warm [Gmol C y <sup>-1</sup> ]	double+warm [Gmol C y <sup>-1</sup> ]	standard [Gmol C y <sup>-1</sup> ]
NPP diatoms	2194	2147	2159	2173	2183
NPP non-diatoms	4356	4003	4104	4230	4230
NPP coccolithophores	703	818	880	673	912
Calcification	1188	1363	1520	1140	1574
NEP	32	-156	7	-5	43
Air-sea flux	1782	1023	521	1600	755
Horizontal net DIC export	1962	1239	1173	2284	913
Horizontal net TOC export	111	-71	95	84	122
Community respiration	7222	7120	7136	7080	7282
Benthic DIC release	756	759	758	755	760
Sediment OC content at end of year	49	48	49	48	50
Sediment PIC content at end of year	70	152	173	72	173

Table 4.4: Comparison of the carbon fluxes for the simulation with doubled atmospheric CO<sub>2</sub>, the cold year, the warm year, the warm/doubled atmospheric CO<sub>2</sub> and the standard run in Gmol C yr<sup>-1</sup>.

The vertical export of DIC, TOC and PIC is given in Fig. 4.13. For the double pCO<sub>2</sub> simulation the export of TOC is close to the export of the standard simulation, while the upwelling of DIC is smaller for the double pCO<sub>2</sub> simulation as well as the export of PIC. In the cold simulation, the vertical export of PIC is smaller than in the warm simulation (Fig. 4.13), but in both cases, the PIC export is lower than in the standard simulation. In the cold simulation more organic carbon is exported below 30 m than in the other simulations, while the upwelling of DIC is smaller for the cold simulation compared to the standard and the warm simulation. The smallest export of TOC and PIC occurs for the double+warm simulation, which is in agreement with the findings of Hofmann & Schellnhuber (2009). This simulation also generates the lowest DIC upwelling in autumn/winter (Fig. 4.13).

The benthic dissolution of calcite is considerably lower in the double pCO<sub>2</sub> run and the double+warm run compared to the standard run (Fig. 4.14), whereas the pelagic dissolution of calcite is higher in the double pCO<sub>2</sub> simulation. Considering the temperature effect, the benthic as well as the pelagic dissolution of calcite is higher in the warm year simulation than in the cold year simulation (Fig. 4.14).

#### 4.4.3 Calcite saturation and pH

In Figs. 4.15 and 4.16 the seasonal, depth-resolved development of the calcite saturation state  $\Omega$  and pH for the different simulations is given. The diagram shows the water column G (Fig. 4.1) as an example since other water columns behave similar. The ballast simulation is not shown because there is no visible difference between the ballast and the standard run for this two variables. The modelled profile for  $\Omega$  in the standard simulation is in the same range as profiles from a cruise in the Bay of Biscay (Harlay *et al.*, 2010). The effect of calcite dissolution can be seen when comparing the 2groups simulation and the standard simulation (Fig. 4.15, 4.16). In autumn, there is a source for carbonate ions from the sediment due to benthic calcite dissolution. The most significant impact has the double atmospheric pCO<sub>2</sub> simulation and the warm+double simulation. pH and  $\Omega$  are both significantly lower compared to the standard simulation, indicating that acidification decreases  $\Omega$  (Gehlen *et al.*, 2007). The effect of temperature on  $\Omega$  and pH is small (Merico *et al.*, 2006) in comparison to the effect of pCO<sub>2</sub>. The cold and the warm year do not differ much. pH is generally a bit higher in the cold than in the warm year, whereas the calcite saturation is a bit higher in the warm year.

## 4.5 Discussion

### 4.5.1 Carbon fluxes

Our model results show a decrease in the uptake of atmospheric CO<sub>2</sub> when coccolithophores and their calcification were included in the model. This decrease is not due to a change in the biological production, since NPP and NEP do not change significantly between the three simulations (Figs. 4.8,4.9), but is the direct effect of the carbonate counter pump. Thus, the study contributes to the ongoing discussion of whether coccolithophore blooms are sources or sinks for atmospheric CO<sub>2</sub> (e.g. Buitenhuis *et al.* (1996); Riebesell *et al.* (2000); Iglesias-Rodriguez *et al.* (2008); Murata (2006)). The strength of the decrease definitely depends on the calcification rate, which was chosen in the standard simulation to fit the observations. If we decrease this rate by 50 % to 0.5 d<sup>-1</sup>, the annual cumulated calcification decreases by 50 % and the uptake of atmospheric CO<sub>2</sub> increases by 16 %. If the calcification rate is increased by 50 %, the annual cumulated calcification increases by 50 % and the uptake of atmospheric CO<sub>2</sub> decreases by 16 %.

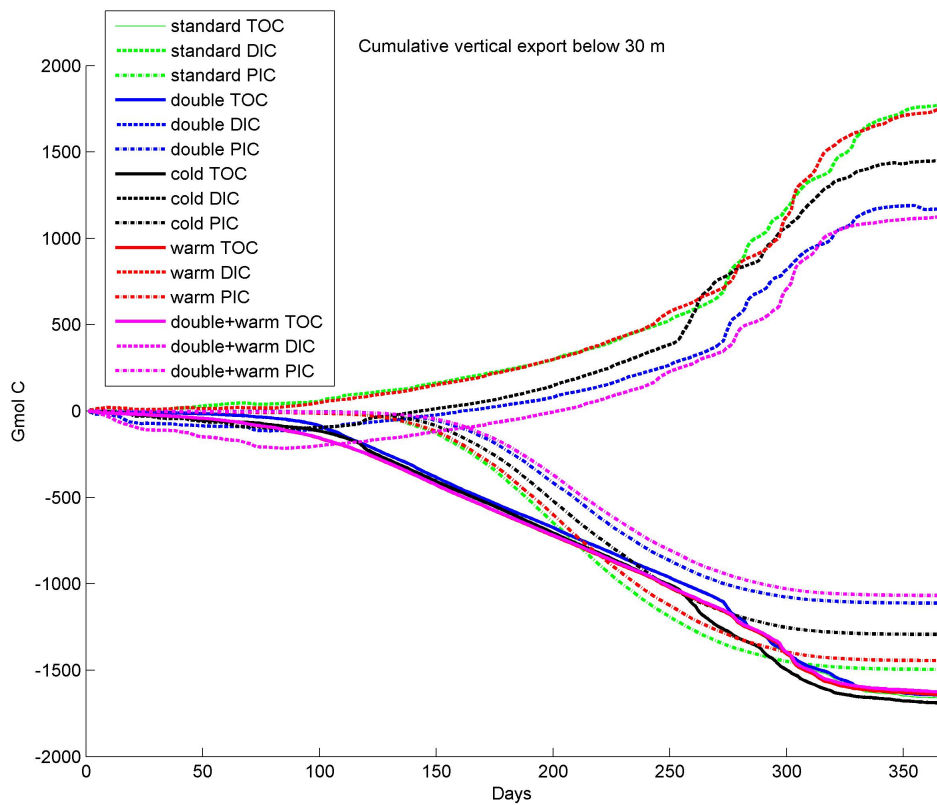


Figure 4.13: Comparison of the vertical export of DIC, TOC and PIC for the standard simulation (green), the double pCO<sub>2</sub> simulation (blue), the cold year simulation (black), the warm year simulation (red) and the warm/double pCO<sub>2</sub> simulation (magenta).

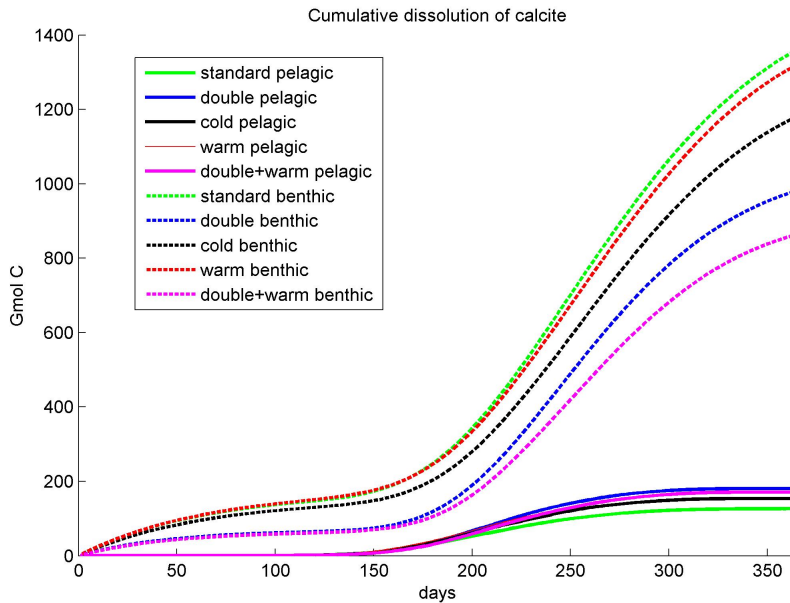


Figure 4.14: Cumulative benthic and pelagic calcite dissolution for the standard, the double  $p\text{CO}_2$ , the cold, the warm year simulation and the warm/double  $p\text{CO}_2$  simulation for the North Sea.

the annual cumulated calcification increases by 47 % and the uptake of atmospheric  $\text{CO}_2$  decreases by 18 %. For comparison, the change in  $\text{CO}_2$  uptake in relation to the 2groups simulation is 26 % without calcification. Nevertheless, regarding the amount of calcification in the standard run itself, it could be expected that the effect on the air-sea flux would be much higher, but the high export of PIC may partly compensate the release of  $\text{CO}_2$  during the calcification (Buitenhuis *et al.*, 1996). The sensitivity test with the ballasted zooplankton pellets could not change this picture significantly, due to the only small additional particle flux in comparison to other modeled fluxes. The ballast simulation did show a slightly higher export of organic carbon to the sediment (Fig. 4.10), which resulted in a higher organic carbon content in the ballast simulation at the end of the year. Still, the parameterisation of this process might be improved and will give more reliable results, when observation data are available. Additionally, we did not account for the effect of calcite dissolution in the zooplankton gut (Harris, 1994), which might change the density and thus the sinking velocity of zooplankton fecal pellets.

The vertical export of PIC has a significant effect on the vertical export of total carbon in our model. This indicates, that when coccolithophore blooms occur, the vertical export of carbon can only be estimated correctly when calcification is included. The magnitude of this effect might differ, depending on the amount of calcification and the sinking velocity. From our calibration it can be seen, that we obtained the right order of magnitude for the calcification, at least where data were available. The duration of the bloom might also play a role and a shorter bloom would surely reduce the vertical export of PIC. It would be very useful to have a good data set to include the optimal parameterisation of this effect.

The strength of the carbon shelf pump, as the mechanism which transports carbon from the North Sea into the adjacent deep ocean is only slightly affected by the inclusion

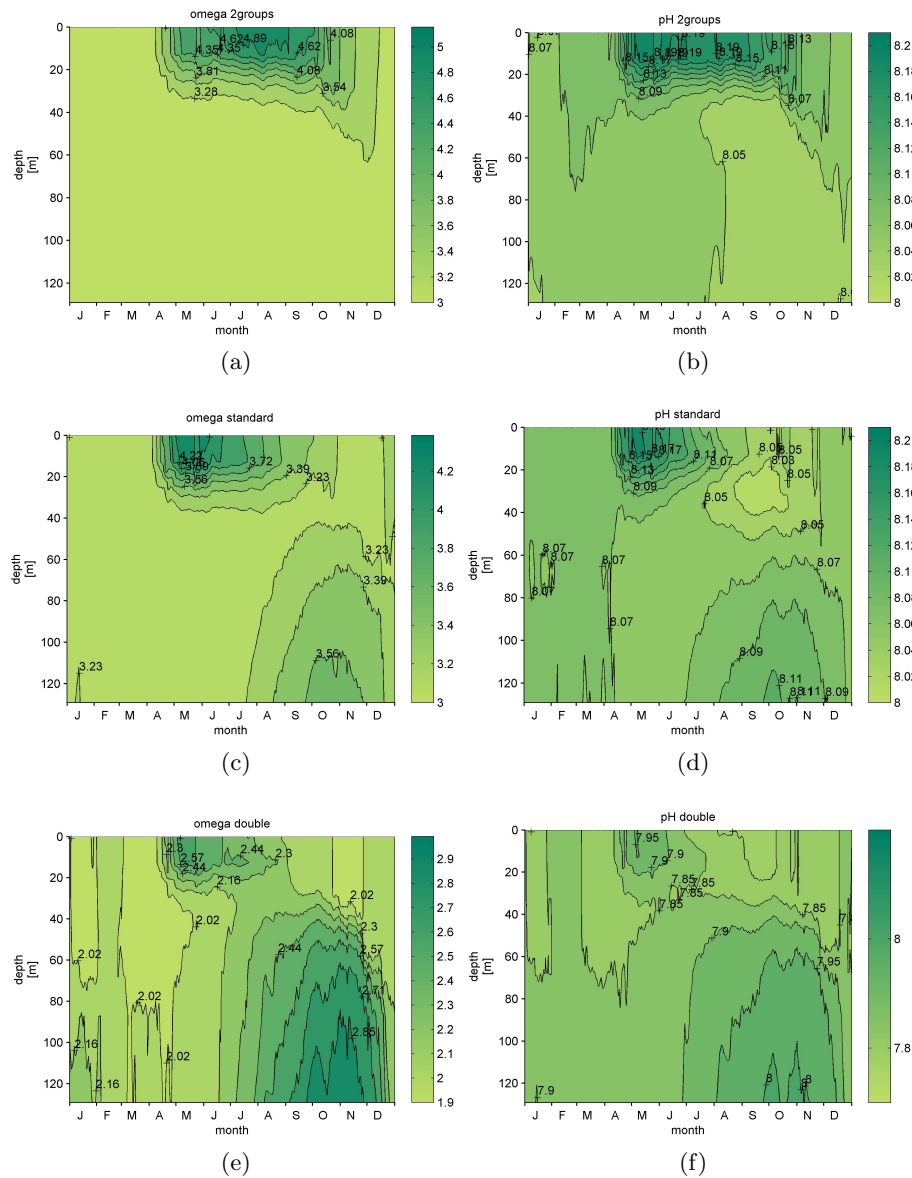


Figure 4.15: Comparison of  $\Omega$  and pH for the different simulations part 1. The water column G (see Fig. 4.1) was chosen here as an example. Please note that the scales on the colourbars differ between the plots. Although it is a bit more laborious to compare the plots, it was not possible to plot them all with the same scaling due to reasons of visualisation.

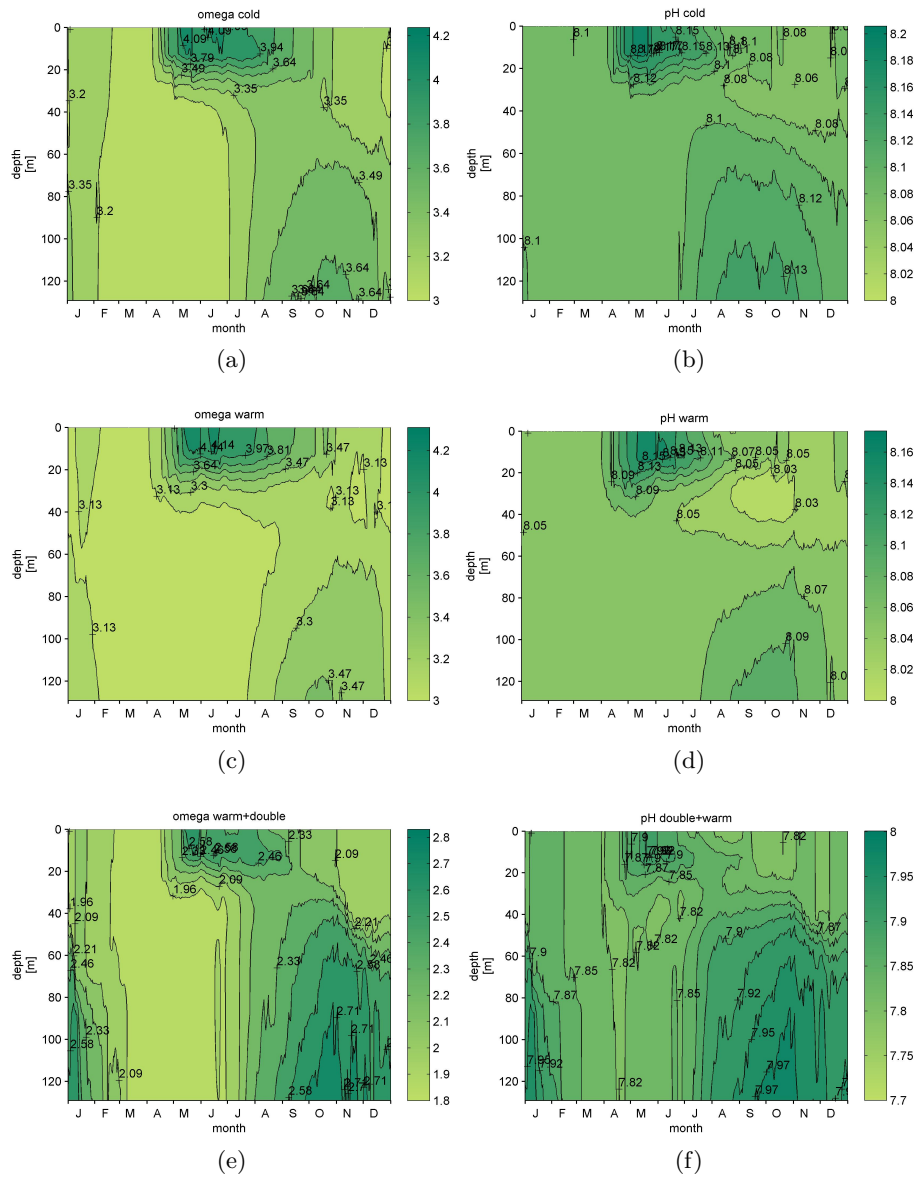


Figure 4.16: Comparison of  $\Omega$  and pH for the different simulations part 2. The water column G (see Fig. 4.1) was chosen here as an example. Please note that the scales on the colourbars differ between the plots. Although it is a bit more laborious to compare the plots, it was not possible to plot them all with the same scaling due to reasons of visualisation.

of the coccolithophores (Tab. 4.3). Due to the lower uptake of atmospheric CO<sub>2</sub>, about 10 % less DIC is exported via the Norwegian Trench. The small horizontal import of calcite (Tab.4.3) originates from blooms in our model area, which are lying outside of our budgeting area (Fig.4.1) for example in the Celtic Sea or in the North Atlantic south of Iceland.

The doubling of atmospheric CO<sub>2</sub>, as expected in the IPCC scenario IS92a for the year 2100 (IPCC, 2001), results in a large increase of the air-sea flux simply due to the stronger concentration gradient between seawater and atmosphere. In addition, it might be that, despite the spinup period, the system was still not completely in equilibrium, which would also lead to high uptake of atmospheric CO<sub>2</sub>. While the NPP of the calcifiers decreases (Tab. 4.4) due to the increasing acidification of the seawater (Fig. 4.15, 4.16), the NPP of the non-calcifiers increases because the coccolithophores use less resources. Consequently, also the PIC export decreases (Fig. 4.13) and the PIC content of the sediment decreases (Tab. 4.4). The additional CO<sub>2</sub> from the atmosphere is almost completely exported via the Norwegian Trench (Tab. 4.4). Due to the lower PIC content in the sediment, there is also a smaller benthic dissolution of calcite, which might act as a buffer for ocean acidification (Fig. 4.14), whereas the pelagic dissolution is higher in the double CO<sub>2</sub> simulation than in the standard simulation as a result of the changed carbonate equilibrium in the acidified seawater. This simulation shows, that in a high CO<sub>2</sub> world, the uptake of atmospheric CO<sub>2</sub> is still mainly controlled by the air-sea gradient. The decreasing calcification might enhance the uptake capacity a little bit, but for the overall budget this seems to play an insignificant role. Another aspect has to be mentioned: While we see a decreased calcification, we do not see an increase in total NPP as observed e.g. by Zondervan *et al.* (2001), because our system is not DIC limited in the standard run, and nutrient limitation does not differ much between the simulations.

In the temperature simulations, two effects come into play. First, the dissolution of CO<sub>2</sub> in seawater is temperature-dependent: CO<sub>2</sub> dissolves better in cold water. Second, the primary production rates are temperature-dependent via the Arrhenius-function. Although NEP is lowest in the cold simulation, the air-sea flux is highest in comparison to the warm and the standard simulation (Tab. 4.4). The low NEP results from the fact that the production rates in ECOHAM4 are temperature-dependent, while the respiration rates are not (Lorkowski *et al.*, 2012). The direct effect of temperature on the CO<sub>2</sub> dissolution can also be seen in the warm simulation, where the air-sea flux is lowest. Calcification is affected via the temperature-dependent production rate, leading to a weaker carbonate counter pump in the cold simulation. Since the temperature difference between the warm and the standard simulation is not very large, it is quite remarkable that the air-sea flux is considerably smaller in the warm simulation, while the DIC export via the Norwegian Trench is higher. This might result from the lower biological production in the warm simulation compared to the standard simulation (see NEP Tab. 4.4), leaving more DIC in the water column for export, but it has also to be taken into account that the hydrodynamics of the simulations are slightly different. Since the amount of water leaving the North Sea via the Norwegian Trench is the most important factor for the export, the water masses need to be known to judge this numbers correctly. In the standard simulation the outflow of water via the Norwegian Coastal Current is 42 km<sup>3</sup> yr<sup>-1</sup>, in the cold simulation 44 km<sup>3</sup>yr<sup>-1</sup> and in the warm simulation again 42 km<sup>3</sup>yr<sup>-1</sup>. Thus, the higher export in the cold simulation might be due to the larger volume of water that is exported, but the difference between standard run and the warm run can not be due to differences in the volume of exported water.

The combined effect of doubled atmospheric CO<sub>2</sub> and a warmer mean annual SST results in even lower pH and  $\Omega$  values (Fig. 4.15, 4.16). Thus, the calcification and the NPP of coccolithophores is lowest in this simulation, as well as the vertical export of PIC, whereas a large amount of DIC remains in the water column and gets exported into the North Atlantic (Tab. 4.4). This high export in comparison to the warm and the standard simulation can not be due to the amount of water that is exported, because it is the same in the three simulations. This simulation shows that in a warm and high CO<sub>2</sub> world calcification decreases and the uptake of atmospheric CO<sub>2</sub> still mainly follows the concentration gradient. The effect of a warmer temperature lowers this uptake capacity, as can be seen when directly comparing the double and the warm+double simulation. Thus, from our simulation results one can infer that there is still potential for the uptake of atmospheric CO<sub>2</sub> by the North Sea, although the structure of the ecosystem might change during this time. The storage of carbon in the sediment decreases due to lower calcification (Tab. 4.4) and the effectiveness of the long-term storage of carbon depends on the fate of the horizontally exported carbon into the North Atlantic. If this carbon is reaching deeper water, it will be stored for a long time, but the amount of DIC in the mixed layer might be quickly released to the atmosphere again. Due to our limited model area we are not able to track the DIC into the North Atlantic.

#### 4.5.2 Uncertainties and Sensitivities

While the beginning of the coccolithophore bloom corresponds with observations (Harlay *et al.*, 2010), one of the shortcomings of the model is the termination of the coccolithophore bloom. Observations indicate that blooms do not last much longer than 40 days (Holligan *et al.*, 1993b). In our model they exist over a much longer period until late autumn. Nevertheless the results give a good indication of the impact on carbon fluxes, but should be regarded as an upper limit because of the longer bloom duration. The mechanisms for the termination of a coccolithophore bloom are still under debate. Several causes, as for example viral infection, may be involved (Joassin *et al.*, 2011). Since our model does not contain viruses, this effect can not be simulated. Further, Harlay *et al.* (2009) suggest that the termination might be due to particle aggregation triggered by TEP and thus faster sinking rates. Together with grazing by zooplankton this may quickly terminate a bloom of coccolithophores. Some first sensitivity test in which we included TEP formation and particle aggregation according to Schartau *et al.* (2007) have indicated a strong impact of this process on the export of carbon. But due to time limitations and missing validation data, we did not go into the details within this study.

The factor  $\text{lim}_{\text{dep}}$  is only an artificial parametrisation to avoid coccolithophore blooms in too shallow water. It was introduced, because it could not be completely identified, which factor limits the blooms in shallow water. Turbulence might be a factor, as well as salinity or optical properties. Iida *et al.* (2002) suggested the stratification and the related nutrient supply as a controlling factor in the Bering Sea. Another aspect might be, that our model does not contain *Phaeocystis* as an explicit group, which might inhabit the ecological niche in the shallower water and outcompete coccolithophores in natural assemblages. Gregg & Casey (2007) already found for a global model, that the distribution of coccolithophores strongly depends on the distribution of the other phytoplankton groups and the competition between the different groups. The introduction of *Phaeocystis* into the model might help to clarify this question.

It is known, that coccolithophores are able to take up organic phosphate in case of inorganic phosphate depletion (Benner & Passow, 2010). We included this in the model,

but found that the inorganic phosphate concentrations in the model never get as low as to activate this uptake of organic phosphate. This depends of course on the parametrisation of the process, but we did not find sufficient information in the literature to validate our specific parametrisation of this process.

We did not consider the effect of changing optical properties of seawater in the presence of coccolithophores. Due to their calcite shells they can change the albedo, and the penetration of light into the water column. This aspect should be considered in further studies, since it might have an influence on the SST.

It will be challenging to conduct a long-term simulation as in Lorkowski *et al.* (2012) with this new phytoplankton compartment, due to several still unresolved questions: Coccolithophores are known to show strong temporal and spatial variability (Iida *et al.*, 2002), of which the triggering mechanisms are not completely understood yet. One aspect might be that coccolithophores are known to have an advanced life cycle (Müller *et al.*, 2008), which might also effect their interannual and spatial variability as Hense (2010) suggests for harmful algae blooms and cyanobacteria.

## 4.6 Conclusion

We presented an ecosystem model for the North Sea including coccolithophores. The simulated features of the coccolithophores show reasonable results in comparison the observations, regarding the onset, magnitude and vertical profile of the bloom. While the carbonate counter pump weakens the air-sea flux of CO<sub>2</sub> as expected, the feedback of calcification on the CO<sub>2</sub> concentrations is weakened by an export of PIC and storage of PIC in the sediment. The inclusion of ballasted zooplankton faecal pellets led to no significant changes in comparison with the standard simulation. In the climate change scenarios, acidification decreases calcification and the production of coccolithophores, but for the air-sea flux, the concentration gradient between seawater and atmosphere is of greater importance. The combination of high SST and high atmospheric CO<sub>2</sub> decreases the air-sea flux as well as the calcification, but the export of DIC via the Norwegian Trench increases.

## 5 Interannual variability of the air-sea flux - some additional aspects on the influence of temperature, salinity and atmospheric CO<sub>2</sub>

As already explained in chapter 2 the decreasing uptake capacity for atmospheric CO<sub>2</sub> is mainly governed by SST and pH. To substantiate these findings two additional sensitivity tests were conducted, which due to time and space limitation were not included in the manuscript. Fig. 5.1 shows the long-term simulation without biology and always the same annual cycle of SST from 1972. Thus the rise in SST from 1970 to 2006 (Fig. 2.3) is neglected.

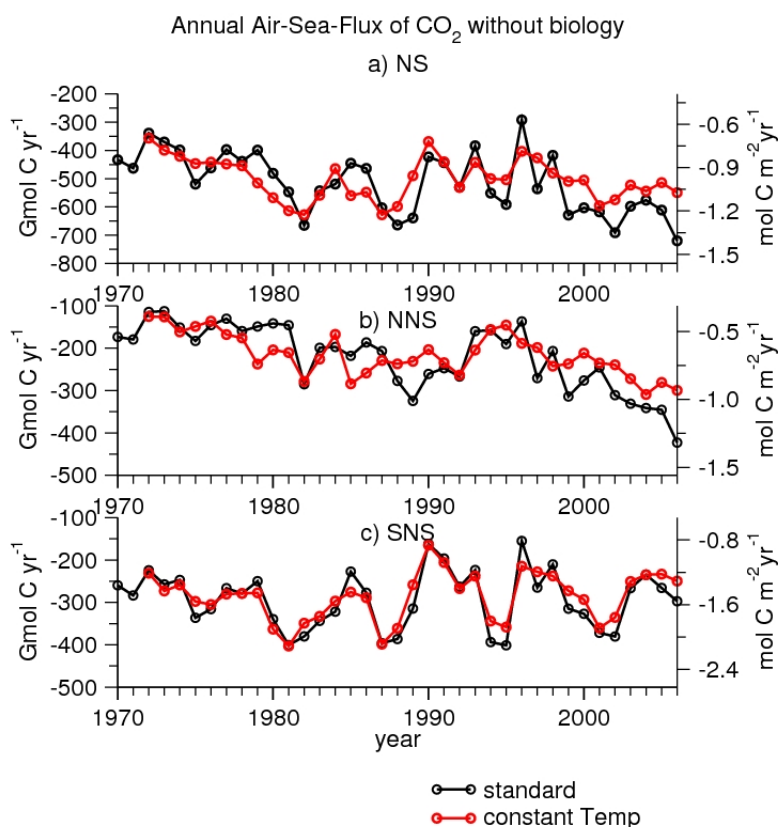


Figure 5.1: Annual air-sea flux for the total, the southern and the northern North Sea for the simulation without biology with the standard temperature setup and the repeatedly used annual cycle of SST of 1972.

The outgassing is decreasing in the constant temperature simulation, especially in the

northern North Sea, stressing the conclusions in chapter 2, that the rising SST is partly responsible for the decreasing uptake capacity for atmospheric  $\text{CO}_2$  in the North Sea. For this simulation it has to be taken into account, that the atmospheric  $\text{CO}_2$  increases as in the standard run.

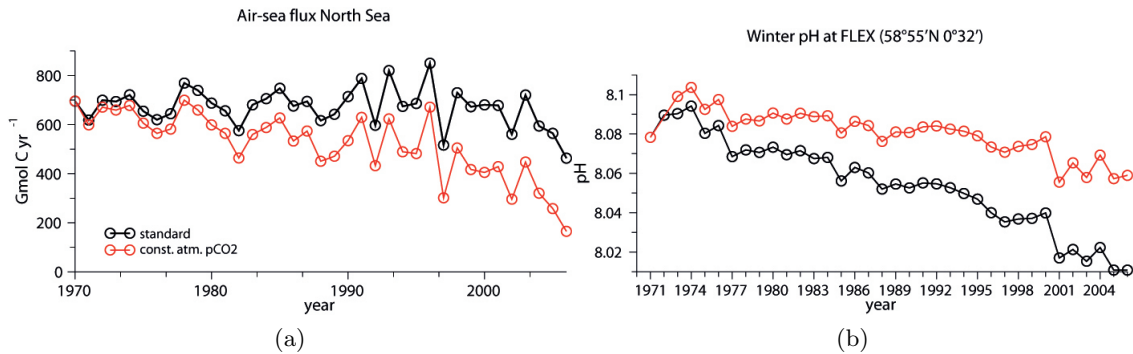


Figure 5.2: a) Annual air-sea flux for the North Sea for standard simulation and a simulation with the atmospheric  $\text{CO}_2$  concentrations from 1970. b) pH at a station in the northern North Sea for the standard simulation and the simulation with constant atmospheric  $\text{CO}_2$ .

The influence of rising atmospheric  $\text{CO}_2$  concentrations on the long term trend in uptake capacity gets obvious when regarding the results of the sensitivity test in Fig. 5.2. They show the resulting air-sea flux and pH for a simulation with constant atmospheric  $\text{CO}_2$  from 1970. The uptake of atmospheric  $\text{CO}_2$  is lower during the whole time, and shows almost the same decreasing trend as the standard simulation, which might on the first glance be a contradiction to the results in chapter 2. But it has to be taken into account, that an important figure for the uptake of atmospheric  $\text{CO}_2$  is the gradient between seawater and atmosphere and this gradient is smaller in the constant atmospheric  $\text{CO}_2$  simulation. The trend in temperature is the same as in the standard simulation and it can be seen from Fig. 5.2b, that the pH is decreasing in this simulation as well, although not as strong as in the standard run. This decrease in pH can be attributed to the temperature effect on pH, since higher temperatures lead to a change in the equilibrium constants of the carbonate system, resulting in more acidic water. Thus these findings add additional information to the picture, telling that the uptake capacity for atmospheric  $\text{CO}_2$  is still decreasing, despite the constant  $\text{pCO}_2$  in the atmosphere, due to changes in SST and the resulting pH change (Fig. 5.2b), but that the uptake in the standard simulation is a bit higher than we would expect compared to the constant atmospheric  $\text{CO}_2$  simulation. The increasing gradient of  $\text{pCO}_2$  between atmosphere and ocean due to rising atmospheric  $\text{CO}_2$  concentrations dampens the strength of the decreasing trend in uptake capacity due to temperature and pH effects alone. Ballantyne *et al.* (2012) analysed the development of land and ocean  $\text{CO}_2$  sinks over the past 50 years and questioned the decline in oceanic uptake projected by several models (e.g. Schuster & Watson (2007); Le Quere *et al.* (2007)). They stated that the global  $\text{CO}_2$  sink had increased during the past 50 years, which might be due to the increasing concentration gradient. The constant  $\text{CO}_2$  simulation partly supports this hypothesis, showing that the uptake would have declined more if the atmospheric  $\text{CO}_2$  stayed constant, but the temperature had increased. From these sensitivity simulations it seems that the effect of temperature is more important for the decline in the uptake capacity for atmospheric  $\text{CO}_2$  of the North Sea than the increasing atmospheric  $\text{pCO}_2$ .

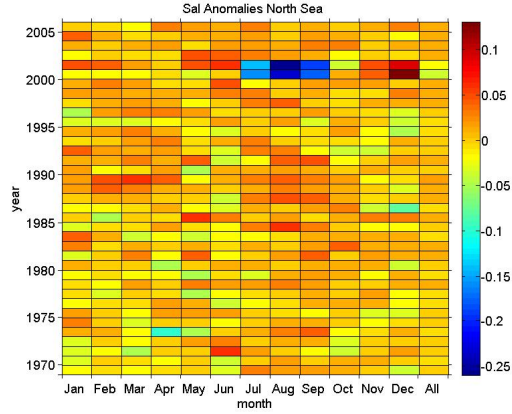


Figure 5.3: Anomalies of salinity for the North Sea [psu]. The anomalies are given for every month and the year in total (All).

year	Annual air-sea flux [Gmol C yr <sup>-1</sup> ] Reference run	Annual air-sea flux [Gmol C yr <sup>-1</sup> ] -1 psu run
1970	-433	-388
1971	-463	-421
1972	-339	-301
1973	-370	-326
1974	-398	-356
1975	-519	-475
1976	-461	-428
1977	-397	-354
1978	-439	-396
1979	-398	-356
1980	-481	-447

Table 5.1: Comparison of the air-sea flux in the simulation without biology for the standard salinity set up and the set up with a salinity of 1 psu lower than in the reference run.

While the atmospheric CO<sub>2</sub> concentration determines the magnitude of the air-sea flux itself, the changes in temperature determine the trend.

The salinity influences the air-sea flux because the equilibrium constants for the dissolution of CO<sub>2</sub> in seawater are salinity-dependent. To test the influence of salinity in comparison to the influence of temperature, pH and river input, a sensitivity simulation with the model from chapter 2 was conducted, again without biology. The model ran from 1970 to 1980 with a salinity that was 1 psu lower than in the standard simulation. This is a large variation in comparison to the salinity variability in the original long-term simulation (Fig. 5.3), which ranges up to 0.25 psu per month. Additionally, the salinity from the years 1970 to 2006 does not show a trend which could have influenced the uptake capacity of the North Sea for atmospheric CO<sub>2</sub>. The low variability in the standard run can partly be attributed to the fact that salinity is not calculated prognostically, but is restored with a relaxation factor to climatology. The differences in the annual air-sea flux are given in Tab. 5.1. The outgassing is always a bit lower than in the original

simulation. The differences are ranging up to 10 %. Given that the salinity variability in the standard simulation is about 25 % of the variability in the sensitivity simulation, the influence of salinity is minor in comparison to e.g. SST. Projection runs for the North Sea suggest an increasing salinity for the southern North Sea of 1 psu as a result of changing westerly winds due to climate change (Schrum, 2001) . Following the results, above the increased salinity would decrease the uptake capacity of the southern North Sea resulting in a more pronounced source for atmospheric CO<sub>2</sub> than in the standard simulation. The effect of warming SST and lower pH would further increase this source. The projection for the northern North Sea suggests a small decrease of surface salinity of 0.2 psu (Schrum, 2001). This decrease would strengthen the sink for atmospheric CO<sub>2</sub> in the northern North Sea and thus slightly counteracting the still dominant effect of warmer SST and lower pH.

## 6 Final Discussion

### 6.1 The role of the North Sea in the global carbon cycle

In the long-term simulation from 1970 to 2006 as well as in the simulations with coccolithophores, the North Sea acts as a sink for atmospheric CO<sub>2</sub> as also found by Thomas *et al.* (2004) for the years 2001/2002. The mean uptake was 1.31 mol C m<sup>-2</sup> yr<sup>-1</sup>, which agreed with the results from Thomas *et al.* (2004) of 1.38 mol C m<sup>-2</sup> yr<sup>-1</sup>. While the southern North Sea oscillated between being a source and a sink as also found by Gypens *et al.* (2004) and Gypens *et al.* (2011), the northern North Sea was a sink for atmospheric CO<sub>2</sub> during the whole simulation period. The water circulating through the North Sea is leaving enriched with carbon. Thus the North Sea efficiently exports carbon from the atmosphere and from rivers into the North Atlantic.

### 6.2 What is influencing the export of carbon from the North Sea into the North Atlantic?

The most important factor for the amount exported carbon into the adjacent North Atlantic is the amount of water that is leaving the North Sea via the Norwegian coastal current. Since almost all water is leaving the North Sea via this current, the outflow mainly depends on the inflow from the North Atlantic and this inflow is correlated to the North Atlantic Oscillation (NAO, compare chapter 2). This is in line with findings by Eden & Willebrand (2000), who found the NAO responsible for changes in the prominent features of the circulation in the North Atlantic. In the mean the modelled export in the long-term simulation is 1.31 Sv with a maximum of 1.5 Sv and a minimum of 1 Sv, which is in the range of estimates by Otto *et al.* (1990). Therefore, small changes in the carbon concentration of the exported water do play a minor role, compared to the changes in the amount of water that is exported. In the mean, the water that is leaving the North Sea contains 0.03 mol C m<sup>-3</sup> more carbon than the water entering the North Sea, which fits quite well to the value of 0.024 mol C m<sup>-3</sup> estimated by Thomas *et al.* (2004), resulting in an efficient export of carbon from the North Sea into the North Atlantic. The results from chapter 4 showed that when coccolithophores and a prognostic calcification were included and the circulation pattern was kept the same, the export of DIC into the North Atlantic decreased by about 10 % while the export of organic carbon increased by about 10 % in comparison to the simulation without coccolithophores. It has to be kept in mind, that the export of DIC is one order of magnitude higher than the export of OC, resulting in an overall decrease in export of total carbon by 10 %.

### 6.3 The driving mechanisms for the interannual variability of the air-sea flux in the North Sea and their interaction

Several factors were identified to influence the interannual variability of the air-sea flux of CO<sub>2</sub>. The overall decreasing trend of the uptake of atmospheric CO<sub>2</sub>, simulated

in the long-term simulation, was induced by the increasing SST and the decreasing pH. This is also described by Thomas *et al.* (2007) and Metzl *et al.* (2010). The sensitivity simulation with the constant atmospheric  $p\text{CO}_2$  showed that the increasing atmospheric  $\text{CO}_2$  enhances the acidification, but also dampened the effect of increasing temperature on the uptake of atmospheric  $\text{CO}_2$ . The NEP was responsible for the biological contribution to the air-sea flux and years with low NEP led to a lower air-sea flux. The effect of the NEP was sometimes counteracting the effect of temperature, e.g. in 1996, when low SST led to higher uptake of atmospheric  $\text{CO}_2$ , whereas the low NEP in 1996 dampened this effect and the resulting uptake ranged at an intermediate level. The influence of river input on the air-sea flux was observed to act on two levels. The air-sea flux was directly depending on the amount of DIC that was brought into the system by rivers, especially in the southern North Sea, whereas the nutrient loads of the rivers, especially the nitrogen loads influenced the NEP, which then impacts on the air-sea flux. The influence of salinity is of minor importance, since the variability of about 0.25 psu during the long-term simulation is too low to show a significant impact. Still, a decreasing salinity leads to lower outgassing in the physical simulation, and thus would result in a higher uptake of atmospheric  $\text{CO}_2$ . The dependence of the interannual variability of the air-sea flux on changes in calcification was not examined in the long-term simulation, but the sensitivity runs with the newly implemented coccolithophores and changing calcification rates showed that the air-sea flux reacts as expected: When the calcification increases, the uptake of atmospheric  $\text{CO}_2$  decreases and vice versa.

### **6.4 How can the impact of biology on the air-sea flux of $\text{CO}_2$ be identified?**

Two methods were used to calculate the biologically induced air-sea flux. One was the superposition method. It was assumed that biological and physical/chemical effects on the air-sea flux add up to the total. Therefore, the results from long term simulations with and without biology were used and the subtraction of the physical air-sea flux from the standard air-sea flux led to the biologically induced air-sea flux. This approach induces an error by not accounting for the different impact of changes in temperature on  $p\text{CO}_2$  at different  $p\text{CO}_2$  levels. The second approach was introduced by Takahashi *et al.* (1993), who linearised the impact of temperature on changes in  $p\text{CO}_2$ . This approach, when applied to identify the biological impact, produces incorrect estimates when external sinks and sources are present. Despite their respective weaknesses both methods agree quite well.

### **6.5 The influence of the coccolithophores on the carbon fluxes and the continental shelf pump**

The influence of coccolithophores -the calcification and the increasing export of organic matter due to ballasting - on the carbon pump is currently under debate (e.g. Buitenhuis *et al.* (2001); Armstrong *et al.* (2002); Murata (2006)). During calcification  $\text{CO}_2$  is released into the water column, which locally can increase  $p\text{CO}_2$  (Harlay *et al.* , 2010). The simulations showed that in the North Sea, the air-sea flux of  $\text{CO}_2$  does decrease due to calcification, but not as strong as expected when regarding the amount of calcification. The increased vertical export of PIC and storage of PIC in the sediment does partly compensate for the released  $\text{CO}_2$ , as also suggested by Buitenhuis *et al.* (2001). The

ballasting of organic material was only partly investigated by including the effect of ballasted zooplankton faecal pellets (Honjo, 1976) into the model. The implemented parametrisation of this process did not have a significant impact on the carbon fluxes. The horizontal export of carbon was slightly affected, when coccolithophores were present and the export of total carbon decreased by 10 %. Our model results suggest that coccolithophores and the carbonate counter pump weaken the efficiency of the continental shelf pump in the North Sea, but further studies will be needed to quantify this impact.

## 6.6 Does the explicit modelling of coccolithophores lead to improved model results?

One uncomfortable question to be posed is whether the implementation of coccolithophores was worth the effort. Is it leading to "better" results in comparison to the ECOHAM version without the prognostic simulation of coccolithophores and calcification, but with a constant ratio of organic carbon to calcite for the non-diatom state variable?

When only regarding the air-sea flux, the answer might be "No": The annual cumulative air-sea flux for the year 1999 is 756 Gmol C yr<sup>-1</sup> for the simulation with coccolithophores and 959 Gmol C yr<sup>-1</sup> for the 2groups simulation without coccolithophores in chapter 4, while the annual cumulative air-sea flux for 1999 in the long term simulation with a constant calcite to organic carbon ratio is 672 Gmol C yr<sup>-1</sup>. Although it has to be taken into account that the comparison between the long-term simulation and the simulations with coccolithophores is not really valid because the hydrodynamics were not identical and the river loads differ between the simulations. Additionally, the prognostic calculation of TA in the simulations with coccolithophores influences the carbonate system. Despite the differences, the result for the long term-simulation is closer to the simulation with coccolithophores than to the 2groups simulation. The answer might also be "No", when regarding the negligible effect of ballasted zooplankton faecal pellets as implemented in the model in chapter 4. But the answer is definitely "Yes", when the impact of climate change is to be analysed. Without the prognostic calcification, it would not be possible to estimate the strength of the negative feedback of calcification on ocean acidification and the impact of changes in the vertical carbon export. Before this study it was not known how strong the impact of coccolithophores on the carbon budget of the North Sea, and thus on the continental shelf pump, might be and how the system would possibly change due to ocean acidification and a warmer SST. Although the model has still some uncertainties and issues waiting to be solved, it is possible to gain answers to those questions now (as described in chapter 4) which would not be possible without the implementation of a prognostic calcification.

## 6.7 What changes in the carbon fluxes can be expected due to climate change and ocean acidification?

The projections of increasing temperature, rising atmospheric CO<sub>2</sub> concentrations (IPCC, 2001), ongoing ocean acidification and the increasing salinity in the southern North Sea and decreasing salinity in the northern North Sea (Schrum, 2001) would lead to several, partly counteracting changes in the North Sea if the model results would be extrapolated into the future. The increasing SST would lead to a further

reduction in the uptake of atmospheric  $\text{CO}_2$ , while the temperature effect on pH would further decrease pH and thus enhance this decrease in uptake, while the increasing atmospheric  $\text{pCO}_2$  would partly dampen this effect, because the gradient of  $\text{pCO}_2$  between atmosphere and ocean may not decrease as strongly when seawater  $\text{pCO}_2$  AND atmospheric  $\text{pCO}_2$  increase. The decrease in pH due to the increase in SST and atmospheric  $\text{CO}_2$ , decreases calcification and thus leads to a negative feedback on rising atmospheric  $\text{pCO}_2$ . Nevertheless, the response of calcification is still under debate and it is not clear whether calcification increases (Iglesias-Rodriguez *et al.* , 2008) or decreases (Riebesell *et al.* , 2000) during ocean acidification. The decrease in export of inorganic carbon or ballasted organic carbon due to decreasing calcification might even counteract the negative feedback and turn it into a positive feedback. The decreasing salinity in the northern North Sea would slightly enhance the uptake of atmospheric  $\text{CO}_2$  and counteract the impact of rising SST, but the stronger increase in salinity in the southern North Sea enhances the release of  $\text{CO}_2$  into the atmosphere. The double  $\text{CO}_2$  scenario in chapter 4 showed an enhanced shelf pump with a higher air-sea flux and a higher vertical export of DIC, but it might be that this effect is enlarged due to a unbalanced gradients between the different carbon pools. The changes in river input due to a changing climate are hard to estimate, because discharge, DIC, TA and nutrient concentrations might change. All in all the behaviour of the total North Sea system is hard to guess and yet so important to know, since changes in the carbonate chemistry and in temperature might also effect higher organisms and change the ecosystem as a whole. Therefore, a lot more research is needed to be able to quantify all expectable changes and their interactions.

## 7 Conclusion

This work investigates the important aspects of the carbon cycle of a continental shelf sea, namely the North Sea, using the ecosystem model ECOHAM. In a long-term simulation from 1970 to 2006 it was found that the North Sea is a sink for atmospheric CO<sub>2</sub> and that shelf pump mechanism is working in the North Sea. The variability of the export of carbon into the adjacent North Atlantic and thus the strength of the shelf pump is mostly dependent on the variability of the amount of water that is exported into the North Atlantic via the Norwegian Coastal Current. The fact that the North Sea is taking up atmospheric CO<sub>2</sub> is only due to biology, since without biological production, the North Sea is a source for atmospheric CO<sub>2</sub> due to the input of carbon via rivers. Nevertheless, the period of high phosphate input via rivers - while enhancing biological production - did not affect the air-sea flux significantly. This was found to be due to the fact that the biological air-sea flux is mainly dependent on the NEP, which does not show an increase during the period of eutrophication because respiration increases parallel to primary production. The long-term simulation showed that the uptake of atmospheric CO<sub>2</sub> by the North Sea was decreasing, especially in the last ten years of the simulation period. This decrease can be attributed to an increase in SST, since CO<sub>2</sub> dissolves better in cold water, and the decrease in pH due to the temperature effect on pH and the ongoing acidification. The increasing atmospheric CO<sub>2</sub> concentrations on the one hand dampened the effect of increasing SST by keeping the air-sea flux on a higher level than it would be with constant atmospheric CO<sub>2</sub>, but on the other hand decreased pH and thus enhanced the impact of the rising SST on the air-sea flux. The influence of river input on the interannual variability acts mainly in the southern North Sea, where years with high DIC loads could be identified to decrease the uptake capacity for atmospheric CO<sub>2</sub>, whereas years with high nitrogen loads tend to increase NEP and thus the biological air-sea flux. The differentiation between the biologically and physically/chemically induced air-sea flux was made by the assumption that biological and physical/chemical aspects add up to the total air-sea flux. This assumption was shown to be valid although some errors are introduced because the temperature effect on pCO<sub>2</sub> differs at different pCO<sub>2</sub> values. In a comparative study it was shown that the approach by Takahashi *et al.* (1993) to separate the biological effects on the air-sea flux gave comparable results in areas without external sinks and sources.

The coccolithophores were successfully implemented in ECOHAM. It was shown that the calcification slightly decreases the air-sea flux, an impact which was found to be dampened by the export of PIC into the deep water and the sediment when calcification was included. In warming and acidification scenarios it could be seen that the calcification decreases with high CO<sub>2</sub> values, thus leading to a negative feedback on rising atmospheric CO<sub>2</sub> concentrations while the decreasing vertical export of PIC led to a positive feedback. The export of carbon into the North Atlantic was - besides the amount of water that is exported - mostly determined by the atmospheric CO<sub>2</sub> concentrations leading to high export in a high CO<sub>2</sub> world.

Altogether this study contributes to a better understanding of the marine carbon cycle by highlighting the different drivers of carbon flux variability and especially the

different influence of the physical, chemical and biological drivers. It was shown that without biology the shelf pump system in the North Sea would not work and that different phytoplankton groups contribute differently to the carbon budget because of their different characteristics as, e.g. the calcification. The strength of the sink for atmospheric CO<sub>2</sub> was estimated for the different North Sea regions, contributing to the calculation of global estimates for the marine carbon cycle. The influence of a changing environment was analysed and will thus help to understand which developments might be expected in the future.

## 8 A0: The carbon cycle as implemented in ECOHAM

The carbon cycle as implemented in ECOHAM is shown in Fig. 8.1. Two versions were used, one without coccolithophores and one with coccolithophores and a prognostic calculation of TA.

In Fig. 8.1a the carbon cycle without coccolithophores is shown: Dissolved inorganic carbon (DIC) is taken up by phytoplankton. Diatoms are grazed by mesozooplankton while and flagellates (or more strictly non-diatoms) are grazed by microzooplankton, which itself is grazed by mesozooplankton. Dead phytoplankton and excreted material is entering one of the two detritus pools, which have different sinking velocities. The microbial loop is represented by bacteria, which remineralise the organic material. The bacteria are grazed by microzooplankton. The excess production of phytoplankton is channelled into the semi-labile organic carbon (SOC) pool, which is degraded to labile dissolved organic carbon (DOC). Particulate organic carbon which is reaching the sediment is stored as benthic detritus. Calcification is only implicitly included via a constant ratio of organic carbon to calcite carbon of the non-diatoms. The model includes a fully resolved carbonate system. The implementation of coccolithophores (Fig. 8.1b) led to some changes in the representation of the carbon cycle. They are characterised as a third phytoplankton group and are grazed by microzooplankton. They directly produce the calcite shells and contribute to the detritus compartments as the other phytoplankton groups. Of course, this implementation is only a simplification of reality. The marine foodweb is highly diverse ranging from a variety of primary producers with different physiology and functions, which are here classified by two (later three) groups to small and large heterotrophic organisms, from protozooplankton up to fish and marine mammals. The higher the trophic level, the more diverse and complex are the respective organisms and the more difficulties occur when modelling these organisms. To try to correctly represent the primary production and eventually the next trophic level together with a closure term is therefore the mostly used approach in biogeochemical ecosystem modelling. ECOHAM includes in addition to the carbon cycle the biogeochemical cycles of the macronutrients nitrate, ammonium and phosphate, as well as silicate for the diatoms and it includes an oxygen cycle. In this study the cycles of trace metals as e.g. iron are not included in the model, because iron limitation does not play a role in the North Sea, although recently an iron cycle was implemented into one version of ECOHAM for the North Pacific (Lindenthal *et al.*, 2012). The different cycles are interrelated in ECOHAM by a fixed stoichiometry, mainly the Redfield ratio (Redfield, 1934), as another simplification. In nature, the stoichiometry varies between species and even one single phytoplankton may have a variable C:N:P ratio. But since the phytoplankton is already categorised into only two or three groups, the simplified fixed elemental ratio is acceptable.

The prognostic calculation of calcification in the model version with coccolithophores (Fig. 8.1b) and the estimation of the resulting impact on the carbonate system is not possible without a prognostic representation of TA. The TA determines together with DIC the calcite saturation state (Zeebe & Wolf-Gladrow, 2001)(their Eq. 1.1.11), which

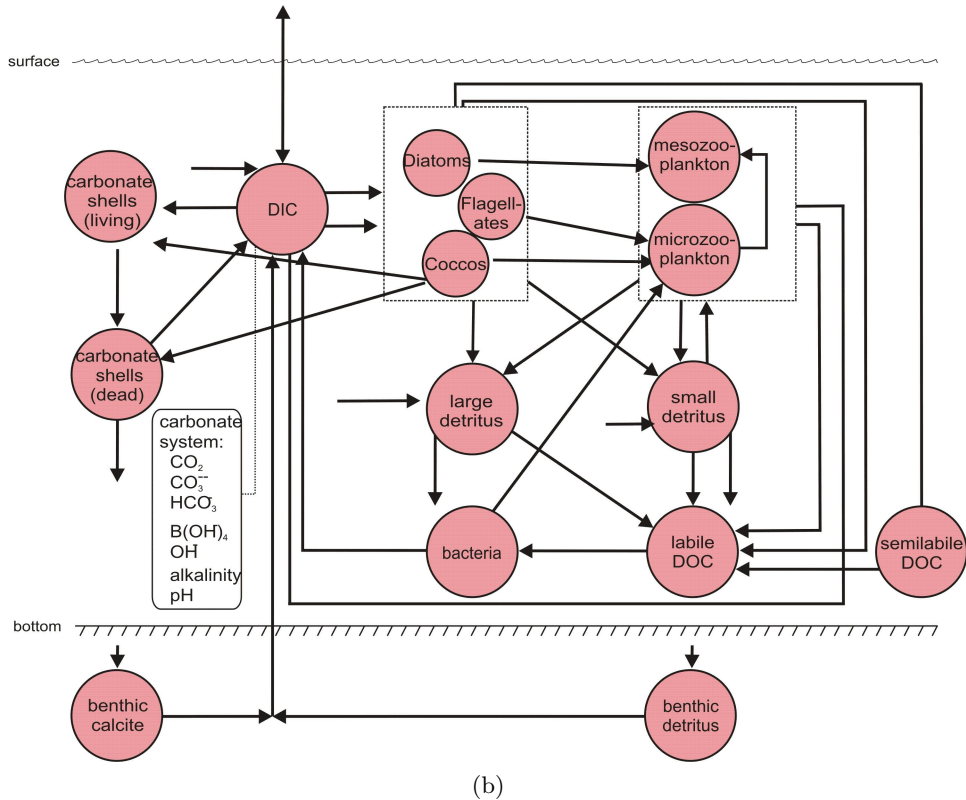
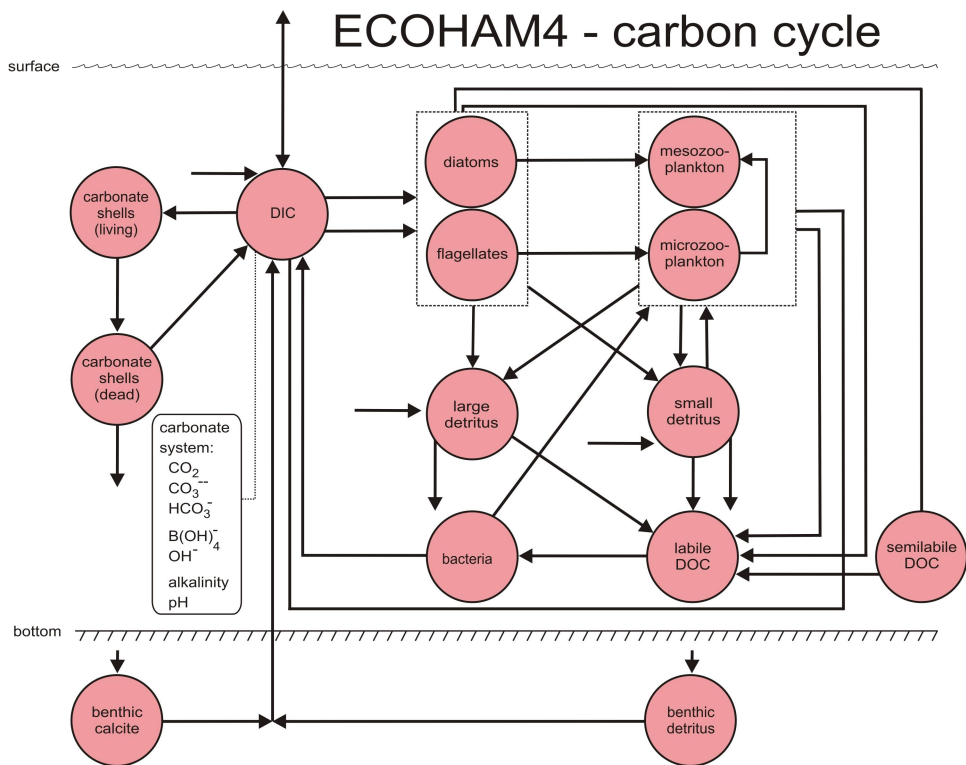


Figure 8.1: The carbon cycle as implemented in ECOHAM4. Figures modified after Pätsch *et al.* (2009). a) without coccolithophores b) with coccolithophores.

---

itself again influences calcification. Despite calcification, other biological processes, as e.g. the uptake of nitrate, influence the TA (Wolf-Gladrow *et al.* , 2007). To calculate the prognostic TA correctly, the freshwater fluxes from the rivers need to be included as well.



## 9 A1: The model equations

A flux from variable var1 to variable var2 is denoted by the acronym var1\_var2. The terms tra(var1) denote the transport and include advection and vertical mixing.

state variable	conservation equation
Diatoms carbon	$\frac{\partial p1c}{\partial t} = dic.p1c - p1c.zec - p1c.d1c - p1c.d2c - p1c.doc - p1c.soc + tra(p1c)$
Non-diatoms carbon	$\frac{\partial p2c}{\partial t} = dic.p2c - p2c.zic - p2c.d1c - p2c.d2c - p2c.doc - p2c.soc + tra(p2c)$
Diatoms nitrogen	$\frac{\partial p1n}{\partial t} = n3n.p1n + n4n.p1n - p1n.zen - p1n.d1n - p1n.d2n - p1n.don + tra(p1n)$
Non-diatoms nitrogen	$\frac{\partial p2n}{\partial t} = n3n.p2n + n4n.p2n - p2n.zin - p2n.d1n - p2n.d2n - p2n.don + tra(p2n)$
Diatoms phosphor	$\frac{\partial p1p}{\partial t} = n1p.p1p - p1p.zep - p1p.d1p - p1p.d2p - p1p.dop + tra(p1p)$
Non-diatoms phosphor	$\frac{\partial p2p}{\partial t} = n1p.p2p - p2p.zip - p2p.d1p - p2p.d2p - p2p.dop + tra(p2p)$
Diatoms silicate	$\frac{\partial p1s}{\partial t} = n5s.p1s - p1s.d2s + tra(p1s)$
Phytoplankton calcite shells	$\frac{\partial psc}{\partial t} = dic.psc - psc.dsc + tra(psc)$

state variable	conservation equation
Mesozooplankton carbon	$\frac{\partial zec}{\partial t} = p1c.zec + d1c.zec + zic.zec - zec.d1c - zec.d2c - zec.doc - zec.dic + tra(zec)$
Microzooplankton carbon	$\frac{\partial zic}{\partial t} = p2c.zic + bac.zic + d1c.zic - zic.zec - zic.d1c - zic.d2c - zic.doc - zic.dic + tra(zic)$
Mesozooplankton nitrogen	$\frac{\partial zen}{\partial t} = p1n.zen + d1n.zen + zin.zen - zen.d1n - zen.d2n - zen.doc - zen.n4n + tra(zen)$
Microzooplankton nitrogen	$\frac{\partial zin}{\partial t} = p2n.zin + ban.zin + d1n.zin - zin.zen - zin.d1n - zin.d2n - zin.doc - zin.n4n + tra(zin)$
Mesozooplankton phosphor	$\frac{\partial zep}{\partial t} = p1p.zep + d1p.zep + zip.zep - zep.d1p - zep.d2p - zep.doc - zep.n1p + tra(zep)$
Microzooplankton phosphor	$\frac{\partial zip}{\partial t} = p2p.zip + bap.zip + d1p.zip - zip.zep - zip.d1p - zip.d2p - zip.doc - zip.n1p + tra(zip)$
Detritus carbon, slowly sinking	$\frac{\partial d1c}{\partial t} = p1c.d1c + p2c.d1c + zec.d1c + zic.d1c - d1c.zec - d1c.zic - d1c.doc - snk(d1c, w_{d1}) + tra(d1c)$
Detritus nitrogen, slowly sinking	$\frac{\partial d1n}{\partial t} = p1n.d1n + p2n.d1n + zen.d1n + zin.d1n - d1n.zen - d1n.zin - d1n.doc - snk(d1n, w_{d1}) + tra(d1n)$
Detritus phosphor, slowly sinking	$\frac{\partial d1p}{\partial t} = p1p.d1p + p2p.d1p + zep.d1p + zip.d1p - d1p.zep - d1p.zip - d1p.doc - snk(d1p, w_{d1}) + tra(d1p)$
Detritus carbon, fast sinking	$\frac{\partial d2c}{\partial t} = p1c.d2c + p2c.d2c + zec.d2c + zic.d2c - d2c.doc - snk(d2c, w_{d2}) + tra(d2c)$
Detritus nitrogen, fast sinking	$\frac{\partial d2n}{\partial t} = p1n.d2n + p2n.d2n + zen.d2n + zin.d2n - d2n.doc - snk(d2n, w_{d2}) + tra(d2n)$

state variable	conservation equation
Detritus phosphor, fast sinking	$\frac{\partial d2p}{\partial t} = p1p\_d2p + p2p\_d2p + zep\_d2p + zip\_d2p - d2p\_dop - snk(d2p, w_{d2}) + tra(d2p)$
Detritus silicate, fast sinking	$\frac{\partial d2s}{\partial t} = p1s\_d2s - d2s\_n5s - snk(d2s, w_{d2}) + tra(d2s)$
Detritus calcite, fast sinking	$\frac{\partial dsc}{\partial t} = psc\_dsc - dsc\_dic - snk(dsc, w_{d2}) + tra(dsc)$
Dissolved organic carbon	$\frac{\partial doc}{\partial t} = p1c\_doc + p2c\_doc + zec\_doc + zic\_doc + d1c\_doc + d2c\_doc - doc\_bac + soc\_doc + tra(doc)$
Dissolved organic carbon, semi labile	$\frac{\partial soc}{\partial t} = p1c\_soc + p2c\_soc - soc\_doc + tra(soc)$
Dissolved organic nitrogen	$\frac{\partial don}{\partial t} = p1n\_don + p2n\_don + zen\_don + zin\_don + d1n\_don + d2n\_don - don\_ban + tra(don)$
Dissolved organic phosphor	$\frac{\partial dop}{\partial t} = p1p\_dop + p2p\_dop + zep\_dop + zip\_dop + d1p\_dop + d2p\_dop - dop\_bap + tra(dop)$
Bacteria carbon	$\frac{\partial bac}{\partial t} = doc\_bac - bac\_zic - bac\_dic + tra(bac)$
Bacteria nitrogen	$\frac{\partial ban}{\partial t} = don\_ban + n4n\_ban - ban\_zin - ban\_n4n + tra(ban)$
Bacteria phosphor	$\frac{\partial bap}{\partial t} = dop\_bap + n1p\_bap - bap\_zip - bap\_n1p + tra(bap)$

state variable	conservation equation
Ammonium	$\frac{\partial n_{4n}}{\partial t} = ban\_n4n + zen\_n4n + zin\_n4n - n_{4n\_p1n} - n_{4n\_p2n} - n_{4n\_ban}$ $- n_{4n\_n3n} + ban\_n4n + riv\_n4n + tra(n_{4n})$
Nitrate	$\frac{\partial n_{3n}}{\partial t} = n_{4n\_n3n} - n_{3n\_nn2} - n_{3n\_p1n} - n_{3n\_p2n} + riv\_n3n + tra(n_{3n})$
Phosphate	$\frac{\partial n_{1p}}{\partial t} = -n_{1p\_p1p} - n_{1p\_p2p} + zep\_n1p + zip\_n1p + bap\_n1p - bap\_n1p$ $+ riv\_n1p + tra(n_{1p})$
Silicate	$\frac{\partial n_{5s}}{\partial t} = -n_{5s\_p1s} + d_{2s\_n5s} + bos\_n5s + riv\_n5s + tra(n_{5s})$
Dissolved inorganic carbon	$\frac{\partial dic}{\partial t} = -dic\_p1c - dic\_p2c - dic\_psc + air\_o2c + dsc\_dic + zec\_dic + zic\_dic$ $+ bac\_dic + bsc\_dic + boc\_dic + riv\_dic + tra(dic)$
Oxygen	$\frac{\partial o_{2o}}{\partial t} = p_{1c\_o2o} + p_{2c\_o2o} - o_{2o\_zec} - o_{2o\_zic} - o_{2o\_bac} - o_{2o\_n4n} - o_{2o\_sed}$ $+ air\_o2o + tra(o_{2o})$
Benthic organic carbon	$\frac{\partial boc}{\partial t} = dz(k0) \cdot snk(d_{1c}, w_{d1}) _{z=H} + dz(k0) \cdot snk(d_{2c}, w_{d2}) _{z=H} - boc\_dic$
Benthic organic nitrogen	$\frac{\partial bon}{\partial t} = dz(k0) \cdot snk(d_{1n}, w_{d1}) _{z=H} + dz(k0) \cdot snk(d_{2n}, w_{d2}) _{z=H} - bon\_n4n$ $- bon\_n2n$
Benthic organic phosphor	$\frac{\partial bop}{\partial t} = dz(k0) \cdot snk(d_{1p}, w_{d1}) _{z=H} + dz(k0) \cdot snk(d_{2p}, w_{d2}) _{z=H} - bop\_n1p$
Benthic opal	$\frac{\partial bos}{\partial t} = dz(k0) \cdot snk(d_{2s}, w_{d2}) _{z=H} - bos\_n5s$
Benthic calcite	$\frac{\partial bsc}{\partial t} = dz(k0) \cdot snk(d_{sc}, w_{dsc}) _{z=H} - bsc\_dic$

## 10 A2: Processes and their parameterisation

phytoplankton	
Redfield carbon fixation, diatoms	$dic-p1c-red = T_{fac1} \cdot p1c \cdot F(I, v_{p1}, p1c) \cdot limd_nps$
effective carbon fixation, diatoms	$dic-p1c = dic-p1c-red + excess \cdot (h\_dic-p1c - dic-p1c-red)$
gross carbon fixation, diatoms	$h\_dic-p1c = T_{fac1} \cdot p1c \cdot F(I, v_{p1}, p1c)$
Redfield carbon fixation, non-diatoms	$dic-p2c-red = T_{fac2} \cdot p2c \cdot F(I, v_{p2}, p2c) \cdot limf_np$
effective carbon fixation, non-diatoms	$dic-p2c = dic-p2c-red + excess \cdot (h\_dic-p2c - dic-p2c-red)$
gross carbon fixation, non-diatoms	$h\_dic-p2c = T_{fac2} \cdot p2c \cdot F(I, v_{p2}, p2c)$
nitrate uptake, diatoms	$n3n-p1n = T_{fac1} \cdot p1n \cdot F(I, v_{p1}, p1c) \cdot Q_{11}$
nitrate uptake, non-diatoms	$n3n-p2n = T_{fac2} \cdot p2n \cdot F(I, v_{p2}, p2c) \cdot Q_{21}$
ammonium uptake, diatoms	$n4n-p1n = T_{fac1} \cdot p1n \cdot F(I, v_{p1}, p1c) \cdot Q_{12}$
ammonium uptake, non-diatoms	$n4n-p2n = T_{fac2} \cdot p2n \cdot F(I, v_{p2}, p2c) \cdot Q_{22}$

<b>phytoplankton</b>	
phosphate uptake, diatoms	$n1p\_p1p = \frac{dic\_p1c\_red}{r_{pcp}}$
phosphate uptake, non-diatoms	$n1p\_p2p = \frac{dic\_p2c\_red}{r_{pcp}}$
silicate uptake, diatoms	$n5s\_p1s = \frac{dic\_p1c\_red}{r_{cs}}$
exudation of DOC, diatoms	$p1c\_doc = \gamma_1 \cdot dic\_p1c$
exudation of DOC, non-diatoms	$p2c\_doc = \gamma_2 \cdot dic\_p2c$
exudation of DON, diatoms	$p1n\_don = \frac{p1c\_doc}{r_{pen}}$
exudation of DON, non-diatoms	$p2n\_don = \frac{p2c\_doc}{r_{pen}}$
exudation of DOP, diatoms	$p1p\_dop = \frac{p1c\_doc}{r_{pcp}}$
exudation of DOP, non-diatoms	$p2p\_dop = \frac{p2c\_doc}{r_{pcp}}$
exudation of semi-labile organic carbon, diatoms	$p1c\_soc = dic\_p1c - dic\_p1c\_red$
exudation of semi-labile organic carbon, non-diatoms	$p2c\_soc = dic\_p2c - dic\_p2c\_red$
loss of diatoms to d1c	$p1c\_d1c = T_{fac} \cdot (1 - f_{d2}) \cdot (\mu_{11} \cdot p1c + \mu_6 \cdot p1c \cdot p1c)$
loss of non-diatoms to d1c	$p2c\_d1c = T_{fac} \cdot (1 - f_{d2}) \cdot (\mu_{12} \cdot p2c + \mu_6 \cdot p2c \cdot p2c)$
loss of diatoms to d2c	$p1c\_d2c = T_{fac} \cdot f_{d2} \cdot (\mu_{11} \cdot p1c + \mu_6 \cdot p1c \cdot p1c)$

---

## phytoplankton

---

loss of non-diatoms to d2c	$p2c\_d2c = T_{fac} \cdot f_{d2} \cdot (\mu_{12} \cdot p2c + \mu_6 \cdot p2c \cdot p2c)$
loss of diatoms to d1n	$p1n\_d1n = \frac{p1c\_d1c}{r_{pcn}}$
loss of non-diatoms to d1n	$p1n\_d1n = \frac{p1c\_d1c}{r_{pcn}}$
loss of diatoms to d2n	$p1n\_d2n = \frac{p1c\_d2c}{r_{pcn}}$
loss of non-diatoms to d2n	$p2n\_d2n = \frac{p2c\_d2c}{r_{pcn}}$
loss of diatoms to d1p	$p1p\_d1p = \frac{p1c\_d1c}{r_{pcp}}$
loss of non-diatoms to d1p	$p1p\_d1p = \frac{p1p\_d1p}{r_{pcp}}$
loss of diatoms to d2p	$p1p\_d2p = \frac{p1c\_d2c}{r_{pcp}}$
loss of non-diatoms to d2p	$p2p\_d2p = \frac{p2c\_d2c}{r_{pcp}}$
loss of diatoms to d2s	$p1s\_d2s = \frac{p1c\_d2c+p1c\_d1c}{r_{pcs}} + \max(0, \frac{(p1c\_doc+p1c\_zec)}{r_{cps}}) - n5s\_p1s$
calcification	$dic\_psc = \frac{dic\_p2c}{q_{cal}}$
formation of detritus calcite	$psc\_dsc = \frac{p2c\_zic+p2c\_d1c+p2c\_d2c+p2c\_doc}{q_{cal}}$

zooplankton		
grazing of diatoms by mesozooplankton, carbon	$p1c\_zec = G_{11}$	
grazing of microzooplankton by mesozooplankton, carbon	$zic\_zec = G_{12}$	
grazing of detritus by mesozooplankton, carbon	$d1c\_zec = G_{13}$	
grazing of non-diatoms by microzooplankton, carbon	$p2c\_zic = G_{21}$	
grazing of detritus by microzooplankton, carbon	$d1c\_zic = G_{23}$	
grazing of bacteria by microzooplankton, carbon	$bac\_zic = G_{24}$	
grazing of diatoms by mesozooplankton, nitrogen	$p1n\_zen = \frac{G_{11}}{r_{pen}}$	
grazing of microzooplankton by mesozooplankton, nitrogen	$zin\_zen = \frac{G_{12}}{r_{zen}}$	
grazing of detritus by mesozooplankton, nitrogen	$d1n\_zen = \frac{G_{13}}{d1c} \cdot d1n$	
grazing of non-diatoms by microzooplankton, nitrogen	$p2n\_zin = \frac{G_{21}}{r_{pen}}$	
grazing of detritus by microzooplankton, nitrogen	$d1n\_zin = \frac{G_{23}}{d1c} \cdot d1n$	
grazing of bacteria by microzooplankton, nitrogen	$ban\_zin = \frac{G_{24}}{r_{bcn}}$	
grazing of diatoms by mesozooplankton, phosphor	$p1p\_zep = \frac{G_{11}}{r_{pep}}$	
grazing of microzooplankton by mesozooplankton, phosphor	$zip\_zep = \frac{G_{12}}{r_{zep}}$	
grazing of detritus by mesozooplankton, phosphor	$d1p\_zep = \frac{G_{13}}{d1c} \cdot d1p$	
grazing of non-diatoms by microzooplankton, phosphor	$p2p\_zip = \frac{G_{21}}{r_{pep}}$	
grazing of detritus by microzooplankton, phosphor	$d1p\_zip = \frac{G_{23}}{d1c} \cdot d1p$	

zooplankton		
grazing of bacteria by microzooplankton, phosphor	$bap\_zip = \frac{G_{24}}{r_{bcp}}$	
fecal pellets into d1c by mesozooplankton	$zec\_d1c = r_{zcn} \cdot zen\_d1n$	
fecal pellets into d1c by microzooplankton	$zic\_d1c = r_{zcn} \cdot zin\_d1n$	
fecal pellets into d2c by mesozooplankton	$zec\_d2c = r_{zcn} \cdot zen\_d2n$	
fecal pellets into d2c by microzooplankton	$zic\_d2c = r_{zcn} \cdot zin\_d2n$	
fecal pellets into d1n by mesozooplankton	$zen\_d1n = (1 - f_{d2}) \cdot (1 - \delta - \epsilon) \cdot \mu_2 \frac{zen}{zen+K_6} zen$ $+ (1 - \beta) \cdot \frac{G_{11}+G_{12}+G_{13}}{r_{zcn}}$	
fecal pellets into d1n by microzooplankton	$zin\_d1n = (1 - f_{d2}) \cdot (1 - \delta - \epsilon) \cdot \mu_2 \frac{zin}{zin+K_6} zin$ $+ (1 - \beta) \cdot \frac{G_{21}+G_{23}+G_{24}}{r_{zcn}}$	
fecal pellets into d2n by mesoz.	$zen\_d2n = f_{d2} \cdot (1 - \delta - \epsilon) \cdot \mu_2 \frac{zen}{zen+K_6} zen$ $+ (1 - \beta) \cdot \frac{G_{11}+G_{12}+G_{13}}{r_{zcn}}$	
fecal pellets into d2n by microz.	$zin\_d2n = f_{d2} \cdot (1 - \delta - \epsilon) \cdot \mu_2 \frac{zin}{zin+K_6} zin$ $+ (1 - \beta) \cdot \frac{G_{21}+G_{23}+G_{24}}{r_{zcn}}$	
fecal pellets into d1p by mesoz.	$zep\_d1p = \frac{r_{zcn} \cdot zen\_d1n}{r_{zcp}}$	
fecal pellets into d1p by microz.	$zip\_d1p = \frac{r_{zcn} \cdot zin\_d1n}{r_{zcp}}$	
fecal pellets into d2p by mesoz.	$zep\_d2p = \frac{r_{zcn} \cdot zen\_d2n}{r_{zcp}}$	
fecal pellets into d2p by microz.	$zip\_d2p = \frac{r_{zcn} \cdot zin\_d2n}{r_{zcp}}$	

Zooplankton	
respiration by mesozooplankton	$ \begin{cases} f_{-zec} - rzcp \cdot f_{-zep} + h_{-zec\_dic} & \text{for } \frac{f_{-zec}}{f_{-zep}} \geq rzcp \wedge \frac{f_{-zen}}{f_{-zep}} \geq rznp \\ f_{-zec} - rz \cdot f_{-zen} + h_{-zec\_dic} & \text{for } \frac{f_{-zec}}{f_{-zen}} \geq rzcn \wedge \frac{f_{-zen}}{f_{-zep}} \leq rznp \\ h_{-zec\_dic} & \text{else} \end{cases} $
respiration by microzooplankton	$ \begin{cases} f_{-zic} - rzcp \cdot f_{-zip} + h_{-zic\_dic} & \text{for } \frac{f_{-zic}}{f_{-zip}} \geq rzcp \wedge \frac{f_{-zin}}{f_{-zip}} \geq rznp \\ f_{-zic} - rz \cdot f_{-zin} + h_{-zic\_dic} & \text{for } \frac{f_{-zic}}{f_{-zin}} \geq rzcn \wedge \frac{f_{-zin}}{f_{-zip}} \leq rznp \\ h_{-zic\_dic} & \text{else} \end{cases} $
excretion of DON by mesoz.	$ \begin{cases} \frac{f_{-zen} - rznp \cdot f_{-zep}}{2} + h_{-zen\_don} & \text{for } \frac{f_{-zec}}{f_{-zep}} \geq rzcp \wedge \frac{f_{-zen}}{f_{-zep}} \geq rznp \\ \frac{f_{-zen} - \frac{f_{-zec}}{rz}}{2} + h_{-zen\_don} & \text{for } \frac{f_{-zec}}{f_{-zen}} \leq rzcn \wedge \frac{f_{-zec}}{f_{-zep}} \geq rzcp \\ h_{-zen\_don} & \text{else} \end{cases} $
excretion of DON by microz.	$ \begin{cases} \frac{f_{-zin} - rznp \cdot f_{-zip}}{2} + h_{-zin\_don} & \text{for } \frac{f_{-zic}}{f_{-zip}} \geq rzcp \wedge \frac{f_{-zin}}{f_{-zip}} \geq rznp \\ \frac{f_{-zin} - \frac{f_{-zic}}{rz}}{2} + h_{-zin\_don} & \text{for } \frac{f_{-zic}}{f_{-zin}} \leq rzcn \wedge \frac{f_{-zic}}{f_{-zip}} \geq rzcp \\ h_{-zin\_don} & \text{else} \end{cases} $

Zooplankton

$$\begin{aligned}
 \text{excretion of ammonium by mesoz.} \quad \text{zen\_n4n} = & \left\{ \begin{array}{l} \frac{f_{\text{-zen-rznp}} \cdot f_{\text{-zep}}}{2} + h_{\text{-zen\_n4n}} \quad \text{for } \frac{f_{\text{-zec}}}{f_{\text{-zep}}} \geq \text{rzcp} \wedge \frac{f_{\text{-zen}}}{f_{\text{-zep}}} \geq \text{rznp} \\ \frac{f_{\text{-zen}} - f_{\text{-zec}}}{2} + h_{\text{-zen\_n4n}} \quad \text{for } \frac{f_{\text{-zec}}}{f_{\text{-zen}}} \leq \text{rzcn} \wedge \frac{f_{\text{-zec}}}{f_{\text{-zep}}} \leq \text{rzcp} \\ h_{\text{-zen\_n4n}} \quad \text{else} \end{array} \right. \\
 \text{excretion of ammonium by microz.} \quad \text{zin\_n4n} = & \left\{ \begin{array}{l} \frac{f_{\text{-zin-rznp}} \cdot f_{\text{-zip}}}{2} + h_{\text{-zin\_n4n}} \quad \text{for } \frac{f_{\text{-zic}}}{f_{\text{-zip}}} \geq \text{rzcp} \wedge \frac{f_{\text{-zin}}}{f_{\text{-zip}}} \geq \text{rznp} \\ \frac{f_{\text{-zin}} - f_{\text{-zic}}}{2} + h_{\text{-zin\_n4n}} \quad \text{for } \frac{f_{\text{-zic}}}{f_{\text{-zin}}} \leq \text{rzcn} \wedge \frac{f_{\text{-zic}}}{f_{\text{-zip}}} \leq \text{rzcp} \\ h_{\text{-zin\_n4n}} \quad \text{else} \end{array} \right. \\
 \text{excretion of phosphate by mesoz.} \quad \text{zep\_n1p} = & \left\{ \begin{array}{l} \frac{f_{\text{-zep}} \cdot f_{\text{-zen}}}{2} + h_{\text{-zep\_n1p}} \quad \text{for } \frac{f_{\text{-zec}}}{f_{\text{-zen}}} \geq \text{rzcn} \wedge \frac{f_{\text{-zen}}}{f_{\text{-zep}}} \leq \text{rznp} \\ \frac{f_{\text{-zep}} - f_{\text{-zec}}}{2} + h_{\text{-zep\_n1p}} \quad \text{for } \frac{f_{\text{-zec}}}{f_{\text{-zen}}} \leq \text{rzcn} \wedge \frac{f_{\text{-zec}}}{f_{\text{-zep}}} \leq \text{rzcp} \\ h_{\text{-zep\_n1p}} \quad \text{else} \end{array} \right. \\
 \text{excretion of phosphate by microz.} \quad \text{zip\_n1p} = & \left\{ \begin{array}{l} \frac{f_{\text{-zip}} \cdot f_{\text{-zin}}}{2} + h_{\text{-zip\_n1p}} \quad \text{for } \frac{f_{\text{-zic}}}{f_{\text{-zin}}} \geq \text{rzcn} \wedge \frac{f_{\text{-zin}}}{f_{\text{-zip}}} \leq \text{rznp} \\ \frac{f_{\text{-zip}} - f_{\text{-zic}}}{2} + h_{\text{-zip\_n1p}} \quad \text{for } \frac{f_{\text{-zic}}}{f_{\text{-zin}}} \leq \text{rzcn} \wedge \frac{f_{\text{-zic}}}{f_{\text{-zip}}} \leq \text{rzcp} \\ h_{\text{-zip\_n1p}} \quad \text{else} \end{array} \right.
 \end{aligned}$$

Zooplankton	
excretion of DOC by mesoz.	$z_{ec\_doc} = h_{zen\_don} \cdot r_{zcn}$
excretion of DOC by microz.	$z_{ic\_doc} = h_{zin\_don} \cdot r_{zcn}$
uncorrected excretion of DON, mesoz.	$h_{zen\_don} = \mu_2 \cdot \delta \cdot zen \cdot \frac{zen}{K_6 + zen}$
uncorrected excretion of DON by microz.	$h_{zin\_don} = \mu_2 \cdot \delta \cdot zin \cdot \frac{zin}{K_6 + zin}$
uncorrected respiration of mesoz.	$h_{z_{ec\_dic}} = h_{zen\_n4n} \cdot r_{zcn}$
uncorrected respiration of microz.	$h_{z_{ic\_dic}} = h_{zin\_n4n} \cdot r_{zcn}$
uncorrected excretion of ammonium, mesoz.	$h_{zen\_n4n} = \mu_2 \cdot \epsilon \cdot zen \cdot \frac{zen}{K_6 + zen}$
uncorrected excretion of ammonium, microz.	$h_{zin\_n4n} = \mu_2 \cdot \epsilon \cdot zin \cdot \frac{zin}{K_6 + zin}$
sum of unbalanced carbon fluxes, mesoz.	$f_{z_{ec}} = p1c_{z_{ec}} + d1c_{z_{ec}} - z_{ec\_d1c} - z_{ec\_d2c} - h_{z_{ec\_dic}} - z_{ec\_doc} + z_{ic\_z_{ec}}$
sum of unbalanced carbon fluxes, microz.	$f_{z_{ic}} = p2c_{z_{ic}} + bac_{z_{ic}} + d1c_{z_{ic}} - z_{ic\_d1c} - z_{ic\_d2c} - h_{z_{ic\_dic}} - z_{ic\_doc} - z_{ic\_z_{ec}}$
sum of unbalanced nitrogen fluxes, mesoz.	$f_{z_{en}} = p1n_{z_{en}} + d1n_{z_{en}} - zen\_d1n - zen\_d2n - h_{zen\_n4n} - h_{zen\_don} + zin_{z_{en}}$

Zooplankton	
sum of unbalanced nitrogen fluxes, microz.	$f\_zin = p2n\_zin + ban\_zin + d1n\_zin - zin\_d1n - zin\_d2n$ $-h\_zin\_n4n - h\_zin\_don - zin\_zen$
sum of unbalanced phosphorus fluxes, mesoz.	$f\_zep = p1p\_zep + d1p\_zep - zep\_d1p - zep\_d2p$ $-h\_zep\_n1p - h\_zep\_dop + zip\_zep$
sum of unbalanced phosphorus fluxes, microz.	$f\_zip = p2p\_zip + bap\_zip + d1p\_zip - zip\_d1p - zip\_d2p$ $-h\_zip\_n1p - h\_zip\_dop - zip\_zep$
decay of slowly sinking detritus into DOC	$d1c\_doc = \mu_4 \cdot d1c$
decay of slowly sinking detritus into DON	$d1n\_don = \mu_4 \cdot d1n$
decay of slowly sinking detritus into DOP	$d1p\_dop = \mu_4 \cdot d1p$
decay of fast sinking detritus into DOC	$d2c\_doc = \mu_5 \cdot d2c$
decay of fast sinking detritus into DON	$d2n\_don = \mu_5 \cdot d2n$
decay of fast sinking detritus into DOP	$d2p\_dop = \mu_5 \cdot d2p$
decay of fast sinking detritus into dissolved silicate	$d2s\_n5s = \mu_5 \cdot d2s$
dissolution rate of calcite	$dsc\_dic = \mu_7 \cdot dsc \left( 1 - \frac{\delta CO_3^-}{\delta CO_3^- + 100} \right)$
oversaturation of calcium carbonate	$\delta CO_3^{2-} = \max \left( 0, [CO_3^{2-}] - \frac{K_{sp}}{[Ca^{2+}]} \right)$

bacteria	
uptake of DOC by bacteria	$doc\_bac = U_1 \cdot \frac{doc}{don}$
uptake of DON by bacteria	$don\_ban = U_1$
uptake of DOP by bacteria	$dop\_bap = \frac{dop}{x_{kpb} + dop} \cdot bap$ if $dop > 10^{-6} \text{ mmol } P \text{ m}^{-3}$
uncorrected respiration by bacteria	$h\_bac\_dic = \mu_3 \cdot bac$
sum of unbalanced carbon fluxes into bacteria	$f\_bac = doc\_bac - bac\_zic - h\_bac\_dic$
sum of unbalanced nitrogen fluxes into bacteria	$f\_ban = don\_ban - ban\_zin - ban\_n4n + n4n\_ban$
bacterial respiration	$bac\_dic = \begin{cases} h\_bac\_dic + fdc & \text{for } fdc > 0 \wedge n4n < tres\_n4n \\ \max(0, h\_bac\_dic + fdc) & \text{for } fdc \leq 0 \end{cases}$
	$fdc = f\_bac - f\_ban \cdot rbcn$
uptake of ammonium by bacteria	$n4n\_ban = \begin{cases} (\frac{r_{do}}{r_{bcn}} - 1) \cdot U_1' & \text{for } fdc > 0 \wedge n4n \geq tres\_n4n \\ 0 & \text{otherwise} \end{cases}$
excretion of ammonium by bacteria	$ban\_n4n = \begin{cases} h\_ban\_n4n - \min(0, h\_bac\_dic + \frac{fdc}{r_{bcn}}) & \text{for } fdc \leq 0 \\ h\_ban\_n4n & \text{for } fdc > 0 \end{cases}$
uncorrected excretion of ammonium by bacteria	$h\_ban\_n4n = \mu_3 \cdot \frac{bac}{r_{bcn}}$

bacteria	
max. possible uptake of phosphate by bacteria	$fbpmax = \frac{n4n\_ban}{n4n} \cdot n1p$
phosphate required by bacteria	$fbpreq = \frac{don\_ban+n4n\_ban-ban\_n4n}{rbmp} - dop\_bap$
phosphate uptake by bacteria	$n1p\_bap = \min(max(0, fbpreq), fbpmax)$
phosphate release by bacteria	$bap\_n1p = max(0, -fbpreq)$
further processes	
nitrification	$n4n\_n3n = r_n(I, z) \cdot oswitch \cdot n4n$
benthic carbon remineralisation	$boc\_dic = \frac{brc}{dz(k0)} \cdot boc\ k0 : pelagic\ bottom\ layer$
benthic denitrification	$bon\_n2n = bdnf\_basic - max[0, (bdnf\_basic - h\_bon\_n4n)]$
potential benthic denitrification	$bdnf\_basic = rbd \cdot o2o\_sed$
uncorrected benthic nitrogen remineralisation	$h\_bon\_n4n = \frac{brn}{dz(k0)} \cdot bon$
benthic nitrogen remineralisation	$bon\_n4n = max[0, (h\_bon\_n4n - bdnf\_basic)]$
benthic calcite dissolution	$bsc\_dic = \mu7 \cdot bsc \cdot \left(1 - \frac{\delta CO_3^2- k0}{\delta CO_3^2- k0+100}\right)$
oxygen consumption during benthic carbon remin.	$o2o\_sed = uco \cdot boc\_dic$
oxygen release during photosynthesis	$phc\_o2o = uno \cdot (rpen \cdot n4n\_phn + (rpen + 2) \cdot n3n\_phn) + dic\_phc$ $- dic\_phc\_red$

further processes	
oxygen consumption by mesozooplankton	$o2o\_zec = uco \cdot zec\_dic$
oxygen consumption by microzooplankton	$o2o\_zic = uco \cdot zic\_dic$
oxygen consumption by bacteria	$o2o\_bac = uco \cdot oswitch \cdot bac\_dic$
N <sub>2</sub> production due to denitrification	$n3n\_nn2 = 0.5 \cdot (1 - oswitch) \cdot nswitch \cdot \frac{bac\_dic}{rben}$
anoxic H <sub>2</sub> S production	$o2o\_bac = (1 - oswitch) \cdot (1 - nswitch) \cdot bac\_dic$
oxygen consumption by nitrification	$o2o\_n4n = 2 \cdot uno \cdot n4n\_n3n$
air-sea flux of oxygen	$air\_o2o = K_W \cdot K_H \cdot \frac{pO_2(air) - pO_2(sea)}{dz(1)}$
air-sea flux of CO <sub>2</sub>	$air\_o2c = K_W \cdot K_H \cdot \frac{pCO_2(air) - pCO_2(sea)}{dz(1)}$
sinking of matter X	$snk(X, w) = w \cdot \frac{\partial X}{\partial z}$
vertical mixing of matter X	$mix_v(X) = \frac{\partial}{\partial z} (A_v \cdot \frac{\partial X}{\partial z})$
horizontal mixing of matter X	$mix_h = \frac{\partial}{\partial x} (A_h \cdot \frac{\partial X}{\partial x}) + \frac{\partial}{\partial y} (A_h \cdot \frac{\partial X}{\partial y})$
advection of matter X	$adv(X) = u \cdot \frac{\partial X}{\partial x} + v \cdot \frac{\partial X}{\partial y} + w \cdot \frac{\partial X}{\partial z}$
transport of matter X	$tra(X) = adv(X) + mix_v(X) + mix_h(X)$

## 11 A3: Special functions used for process parameterisations

name	function
light-dependent growth rate	$F(I, v_p, phc) = v_p \cdot \frac{I^{par}(z)}{I_{opt}} \cdot \exp(1 - \frac{I^{par}}{I_{opt}})$ $z$ : depth
depth-dependent PAR	$I_{par}(z) = k_{par} \cdot I_0 \cdot \exp(\epsilon(z))$ $\epsilon(z) = (k_w + k_c \cdot phc + k_s \cdot silt) \cdot z$
light limitation diatoms	$lip1\_ir = F(I, v_{p1}, phc)$
light limitation non-diatoms	$lip2\_ir = F(I, v_{p2}, phc)$
light adaption	$\frac{\partial I_{opt}}{\partial t} = r_{upli} \cdot (actual\_light - I_{opt})$ $r_{upli} = 0.25d^{-1}$ $actual\_light = k_{par} \cdot \bar{I}_0 \cdot \exp(\epsilon(z_a))$ $z_a = \min(z, z_{max})$ $z_{max} = 4$ m $\bar{I}_0$ : daily mean irradiance

<b>name</b>	<b>function</b>
nitrate limitation diatoms	$lip1\_n3 = \frac{n3n/K_1}{1+n3n/K_1+n4n/K_{21}} = Q_{11}$
nitrate limitation non-diatoms	$lip2\_n3 = \frac{n3n/K_1}{1+n3n/K_1+n4n/K_{22}} = Q_{12}$
ammonium limitation diatoms	$lip1\_n4 = \frac{n4n/K_{21}}{1+n3n/K_1+n4n/K_{21}} = Q_{21}$
ammonium limitation non-diatoms	$lip2\_n4 = \frac{n4n/K_{22}}{1+n3n/K_1+n4n/K_{22}} = Q_{22}$
total nitrogen limitation diatoms	$lip1\_hn = lip1\_3n + lip1\_4n$
total nitrogen limitation non-diatoms	$lip2\_hn = lip2\_3n + lip2\_4n$
phosphate limitation diatoms	$lip1\_1p = \frac{n1p}{K_P+n1p}$
silicate limitation diatoms	$lip1\_5s = \frac{n5s}{K_S+n5s}$
phosphate limitation non-diatoms	$lip2\_1p = \frac{n1p}{K_P+n1p}$
mesozooplankton grazing rates	$G_{1i} = g_1 \cdot \frac{p_{1i} \cdot X_{1i}}{K_3 + \sum_j p_{1j} \cdot X_{1j}}$
	$X_{11} = p1c, X_{12} = zic, X_{13} = d1c$
microzooplankton grazing rates	$G_{2i} = g_2 \cdot \frac{p_{2i} \cdot X_{2i}}{K_3 + \sum_j p_{2j} \cdot X_{2j}}$
	$X_{21} = p2c, X_{22} = bac, X_{23} = d1c$

name	function
concentration dependent grazing preferences	$p_{ki} = \frac{\pi_{ki} \cdot X_{ki}}{\sum_j \pi_{kj} \cdot X_{kj}}$ with $\sum \pi_{kj} = 1$
DON uptake by bacteria	$U_1 = vb \cdot \frac{don}{K_d + don} \cdot ban$
light-dependent nitrification rate	$r_n(I, z) = \begin{cases} r_0 & \text{for } z \geq d_{eu}; d_{eu} : \text{depth of 1\% light level} \\ 0.01 \cdot r_0 \cdot \frac{I_{par}(0)}{I_{par}(z)} & \text{for } z < d_{eu} \end{cases}$
temperature factor	$T_{fac}(T) = 1.5^{\frac{T-10^{\circ}C}{10^{\circ}C}}$
switch for oxygen variability	$oswitch = \begin{cases} 0 & \text{for } o2o \leq 0 \\ 1 & \text{for } o2o > 0 \end{cases}$
switch for nitrate variability	$nswitch = \begin{cases} 0 & \text{for } n3n \leq 0.1 \\ 1 & \text{for } n3n > 0.1 \end{cases}$



## 12 A4: Parameters of the biogeochemical model

**Note:** All rates are valid for 10° C.

parameter	unit	value
assimilation efficiency of zooplankton		$\beta = 0.75$
remineralsation rate of benthic carbon	$d^{-1}$	$brc = 0.028$
remineralsation rate of benthic nitrogen and phosphate	$d^{-1}$	$brn = 0.033$
remineralsation rate of benthic silicate	$d^{-1}$	$brs = 0.013$
DON fraction of losses from zooplankton		$\delta = 0.4$
ammonium fraction of losses from zooplankton		$\epsilon = 0.4$
ratio of breakdown rate C to breakdown rate N	$\frac{mol\ C}{mol\ N}$	$\phi = 0.85$
fraction of fast sinking detritus		$f_{d2} = 0.15$

parameter	unit	value
maximum ingestion rate of mesozooplankton	$d^{-1}$	$g_1 = 0.4$
maximum ingestion rate of microzooplankton	$d^{-1}$	$g_2 = 0.5$
exudation fraction of phytoplankton		$\gamma = 0.05$
half-saturation constant of nitrate uptake by phytoplankton	$mmol\ N\ m^{-3}$	$K_1 = 0.5$
half-saturation constant of ammonium uptake by diatoms	$mmol\ N\ m^{-3}$	$K_{21} = 0.5$
half-saturation constant of ammonium uptake by non-diatoms	$mmol\ N\ m^{-3}$	$K_{22} = 0.05$
half-saturation constant of phosphate uptake by phytoplankton	$mmol\ P\ m^{-3}$	$K_P = 0.05$
half-saturation constant of silicate uptake by diatoms	$mmol\ Si\ m^{-3}$	$K_S = 0.5$
half-saturation constant of zooplankton ingestion	$mmol\ N\ m^{-3}$	$K_3 = 1.0$
half-saturation constant of bacteria uptake	$mmol\ N\ m^{-3}$	$K_4 = 0.1$
half-saturation constant of zooplankton loss	$mmol\ N\ m^{-3}$	$K_6 = 0.2$
extinction coefficient for phytoplankton	$\frac{m^2}{mmol\ C}$	$k_c = 4.53 \cdot 10^{-3}$
extinction coefficient silt	$\frac{m^2}{mg}$	$k_s = 0.06 \cdot 10^{-3}$
conversion factor for PAR		$k_{par} = 0.43$
locally varying extinction coefficient for water	$m^{-1}$	$0.09 \leq k_W \leq 0.1$

parameter	unit	value
phytoplankton mortality rate	$d^{-1}$	$\mu_1 = 0.035$
maximum loss rate of zooplankton	$d^{-1}$	$\mu_2 = 0.2$
excretion rate of bacteria	$d^{-1}$	$\mu_3 = 0.1$
breakdown rate of slowly sinking detritus-N	$d^{-1}$	$\mu_4 = 0.12$
breakdown rate of fast sinking detritus-N	$d^{-1}$	$\mu_5 = 0.1$
phytoplankton quadratic mortality factor	$m^3 mmol C^{-1} d^{-1}$	$\mu_6 = 0.01$
maximum dissolution rate of calcite	$d^{-1}$	$\mu_7 = 0.0333$
grazing preference of microzooplankton for non-diatoms		$\pi_{21} = 0.33$
grazing preference of microzooplankton for bacteria		$\pi_{22} = 0.33$
grazing preference of microzooplankton for detritus		$\pi_{23} = 0.34$
grazing preference of mesozooplankton for diatoms		$\pi_{11} = 0.33$
grazing preference of mesozooplankton for detritus		$\pi_{12} = 0.33$
grazing preference of mesozooplankton for microzooplankton		$\pi_{13} = 0.34$
ratio of phytoplankton carbon to calcite shells	$\frac{mol C}{mol CaCO_3}$	$q_{cal} = 70$
maximum nitrification rate	$d^{-1}$	$r_0 = 0.02$
C:N of bacteria	$\frac{mol C}{mol N}$	$r_{bcn} = 4$
ratio of oxygen consumption by benthic denitrification		$r_{bd} = 0.116$

parameter	unit	value
C:N ratio of dissolved organic matter	$\frac{mol\ C}{mol\ N}$	$r_{do} = \frac{doc}{don}$
C:N ratio of zooplankton	$\frac{mol\ C}{mol\ N}$	$r_{zcn} = 5.5$
C:P ratio of zooplankton	$\frac{mol\ C}{mol\ P}$	$r_{zcp} = 110$
N:P ratio of phyto-and zooplankton	$\frac{mol\ N}{mol\ P}$	$r_{znp} = 20$
N:P ratio of bacteria	$\frac{mol\ N}{mol\ P}$	$r_{bnp} = 10$
C:P ratio of bacteria	$\frac{mol\ C}{mol\ P}$	$r_{bcp} = 40$
C:N ratio of phytoplankton	$\frac{mol\ C}{mol\ N}$	$r_{pcn} = 6.625$
C:Si ratio of diatoms	$\frac{mol\ C}{mol\ Si}$	$r_{pcs} = 5.76$
locally varying silt concentration	$mg\ l^{-1}$	$0.0 \leq silt \leq 35.7$
decay rate of SOC	$d^{-1}$	$soc\_rate = 0.00274$
threshold for ammonium uptake by bacteria	$mmol\ N\ m^{-3}$	$tres\_n4n = 0.001$
oxygen to carbon ratio	$\frac{mol\ O}{mol\ C}$	$uco = 1$
oxygen to nitrogen ratio	$\frac{mol\ O}{mol\ N}$	$uno = 1$
maximum uptake rate bacteria	$d^{-1}$	$v_b = 1.4$
maximum growth rate diatoms	$d^{-1}$	$v_{p1} = 1.1$
maximum growth rate non-diatoms	$d^{-1}$	$v_{p2} = 0.9$
velocity of slowly sinking detritus	$md^{-1}$	$w_{d1} = 0.4$
velocity of fast sinking detritus	$md^{-1}$	$w_{d2} = 10.0$

## 13 A5: Equations for the implementation of coccolithophores

The conservation equations for the coccolithophores are:

$$\frac{\partial p3c}{\partial t} = dic\_p3c - p3c\_doc - p3c\_soc - p3c\_d1c - p3c\_d2c - p3c\_zic + tra\_p3c \quad (13.1)$$

$$\frac{\partial p3n}{\partial t} = -p3n\_don - p3n\_d1n - p3n\_d2n - p3n\_zin + n4n\_p3n + n3n\_p3n + tra\_p3n \quad (13.2)$$

$$\frac{\partial p3p}{\partial t} = n1p\_p3p - p3p\_dop - p3p\_d1p - p3p\_d2p - p3p\_zip + dop\_p3p + tra\_p3p \quad (13.3)$$

$$\frac{\partial p3k}{\partial t} = dic\_p3k - p3k\_zik - p3k\_dsc + tra\_p3k, \quad (13.4)$$

where  $p3X$  denotes the different components of the coccolithophores, namely  $c$  for carbon,  $n$  for nitrogen,  $p$  for phosphor and  $k$  for calcite. The fluxes are always denoted as  $var1\_var2$ , indicating a flux from  $var1$  to  $var2$  and  $tra\_p3X$  is a placeholder for the hydrodynamic transport equations and the flux into the sediment.

The variables are:

dic: dissolved inorganic carbon

doX: dissolved organic matter

soc: semi-labile organic carbon

d1X: slowly sinking detritus

d2X: fast sinking detritus

ziX: microzooplankton

n4n: ammonium

n3n: nitrate

n1p: phosphate

dsc: calcite detritus

The growth of coccolithophores is implemented as follows:

$$dic_{p3c\_ex} = p3c \cdot tfac3 \cdot vp3 \cdot fp3c \cdot lim\_dep \cdot lim\_calc \quad (13.5)$$

$$dic_{p3c\_red} = p3c \cdot tfac3 \cdot vp3 \cdot fp3c \cdot limc\_npc \cdot lim\_dep \quad (13.6)$$

$$dic_{p3c} = dic_{p3c\_red} + excess \cdot (dic_{p3c\_ex} - dic_{p3c\_red}), \quad (13.7)$$

where  $dic_{p3c\_ex}$  is the overflow primary production (as described in Prowe *et al.* (2009); adapted to the coccolithophores),  $p3c$  is the carbon portion of coccolithophore biomass,  $tfac3$  is the temperature dependency of coccolithophore growth (Eq. 13.8),  $vp3$  is the maximum growth rate,  $fp3c$  is the light dependency factor (Eq. 13.9,  $lim\_dep$  is an artificial restricting factor to limit coccolithophore growth in too shallow, turbulent water, which will be discussed later, and  $lim\_calc$  is the dependency on the calcite saturation state after Gehlen *et al.* (2007)(Eq.13.12).

$$tfac3 = 1.5^{\frac{T-10}{10}} \quad (13.8)$$

The nutrient limited Redfield production  $dic_{p3c\_red}$  additionally contains the limitation factor  $limc\_npc$  (Eq. 13.13). The net production  $dic_{p3c}$  is then described as the sum of the Redfield production and the difference between Redfield and excess production multiplied by a tuning factor  $excess$  (see Prowe *et al.* (2009)).

$$fp3c = I/(I + xkc\_ir) \quad (13.9)$$

$$fp3k = I/(I + xkk\_ir), \quad (13.10)$$

$xkc\_ir$  and  $xkk\_ir$  are the different half saturation constants for primary production and calcification (Tab. 4.2 ).

The calcification  $dic_{p3k}$ , where  $p3k$  describes the amount of calcite attributed to the living coccolithophores, is described by :

$$dic_{p3k} = p3c \cdot tfac3 \cdot fp3k \cdot c\_max \cdot lim\_calc \cdot lim\_dep, \quad (13.11)$$

where  $fp3k$  is the light dependency of calcification (Eq.13.10) and  $c\_max$  is the maximum calcification rate (Tab. 4.2). The coccolithophores are not light inhibited (Merico *et al.* , 2006) and thus the light dependency is described as a simple Michaelis-Menten function with different half saturation constants for calcification and production (Tab. 4.2). The dependency on the calcite saturation state is described after Gehlen *et al.* (2007) as

$$lim\_calc = ((\Omega - 1.0)/((\Omega - 1.0) + xkk)), \quad (13.12)$$

where  $\Omega$  is the calcite saturation state of the water and  $xkk$  is a half saturation constant (Tab. 4.2). The limitation factor  $limc\_npc$  is defined as the minimum of the potentially limiting factors nitrate+ammonium, phosphate and calcite saturation

---


$$limc\_npc = \min(limc\_np, lim\_calc) \quad (13.13)$$

$$limc\_n = q1c + q2c \quad (13.14)$$

$$limc\_p = q3c \quad (13.15)$$

$$limc\_np = \min(limc\_n, limc\_p) \quad (13.16)$$

$$x13 = n3n/xk13 \quad (13.17)$$

$$x23 = n4n/xk23 \quad (13.18)$$

$$q1c = x13/(1. + x13 + x23) \quad (13.19)$$

$$q2c = x23/(1. + x13 + x23) \quad (13.20)$$

$$q3c = n1p/(xkp3 + n1p). \quad (13.21)$$

The limitation factor for nitrate+ammonium is  $limc\_n$  and the limitation factor for phosphate  $limc\_p$ .  $xk13$  is the half saturation constant for nitrate and  $xk23$  the half saturation for ammonium (Tab. 4.2), while  $n3n$  describes the nitrate concentration and  $n4n$  the ammonium concentration.  $n1p$  is the phosphate concentration and  $xkp3$  is the half saturation constant for the uptake of phosphate. One speciality of coccolithophores is that they are able to use dissolved organic phosphorus (DOP) as a nutrient source (Benner & Passow, 2010). Therefore, if the phosphate limitation factor falls below a certain threshold (0.7), and the DOP limitation is above this threshold, they take up DOP ( $dop$ ) instead and  $q3c$  changes to

$$q3cdop = dop/(xkp3 + dop). \quad (13.22)$$

The uptake of nitrate ( $n3n\_p3n$ ), ammonium ( $n4n\_p3n$ ) and phosphate ( $n1p\_p3p$ ) is proportional to the uptake of carbon due to a constant C:N:P ratio (Tab. 4.2). The grazing of coccolithophores by microzooplankton ( $p3c\_zic$ ) follows the same mechanism as for the other food sources already described Lorkowski *et al.* (2012). The proportion of nitrogen ( $p3n\_zin$ ), phosphate ( $p3p\_zep$ ) and calcite ( $p3k\_zik$ ) ingested by microzooplankton is calculated by dividing the carbon part by the respective ratios. Decay of coccolithophore biomass is described as a combination of a linear and a quadratic loss term. 15% is entering the fast sinking detritus ( $p3c\_d2c$ ) and 85 % is entering the slowly sinking detritus ( $p3c\_d1c$ ). The release of coccoliths consists of two parts. One part is proportional to the loss into the two detritus fractions:

$$ploss3k = (p3c\_d1c + p3c\_d2c)/rccalc, \quad (13.23)$$

where  $rccalc$  is the instantaneous ratio of organic carbon to calcite carbon in the coccolithophores before the fluxes are calculated at the beginning of each time step. We then calculate the new organic carbon to calcite ratio:

$$rccalc\_new = \frac{p3c + dic\_p3c - p3c\_doc - p3c\_soc - p3c\_d1c - p3c\_d2c - p3c\_zic}{p3k + dic\_p3k - ploss3k - p3k\_zik}, \quad (13.24)$$

and if this ratio is not below a certain threshold ( $rccalc\_min$  Tab. 4.2), the second part ( $plossk$ ) is described by a constant loss of 10 % of coccoliths because the maximum calcite cover is not reached (Tyrrell & Taylor, 1996):

$$plossk = 0.1 \cdot p3k. \quad (13.25)$$

Otherwise, all additional calcite is released to the water column (Tyrrell & Taylor, 1996)

$$plossk = (p3k + dic\_p3k - p3k\_zik) \frac{p3c + dic\_p3c - p3c\_doc - p3c\_soc - p3c\_d1c - p3c\_d2c - p3c\_zic}{rccalc\_min} \quad (13.26)$$

and the total flux of coccoliths into detritus is given by:

$$p3k\_dsc = plossk + ploss3k. \quad (13.27)$$

The overflow production of coccolithophores is channelled directly into the semi-labile carbon pool ( $p3c\_soc$ ). The exudation of dissolved organic carbon ( $p3c\_doc$ ) is a constant portion ( $gam3$  Tab. 4.2) of the Redfield production ( $dic\_p3c\_red$ ) and the exudation of dissolved organic nitrogen and dissolved organic phosphorous is calculated by applying the C:N:P ratio.

## 14 A6: Sinking and mineral ballast

$$\frac{\partial d3c}{\partial t} = zic\_d3c - d3c\_doc + tra\_d3c \quad (14.1)$$

$$\frac{\partial d3n}{\partial t} = zin\_d3n - d3n\_don + tra\_d3n \quad (14.2)$$

$$\frac{\partial d3p}{\partial t} = zip\_d3p - d3p\_dop + tra\_d3p \quad (14.3)$$

$$\frac{\partial d3k}{\partial t} = zik\_d3k - d3k\_dic + tra\_d3k. \quad (14.4)$$

$$faec2\_ratio = \frac{p3k\_zik}{0.25 \cdot (d1c\_zic + p2c\_zic + bac\_zic + p3c\_zic)}, \quad (14.5)$$

where  $d1c\_zic$  denotes the grazing on detritus,  $p2c\_zic$  the grazing on flagellates and  $bac\_zic$  the grazing on bacteria. This ratio determines, how much material is entering the heavy detritus (with the constraint that it can be at maximum equal to one):

$$zic\_d3c = faec2\_ratio \cdot 0.25 \cdot (d1c\_zic + p2c\_zic + bac\_zic + p3c\_zic). \quad (14.6)$$

The rest of the excreted carbon is divided into slowly ( $d1c$ ) and fast ( $d2c$ ) sinking detritus as before. The nitrogen and phosphorus components are calculated by dividing by the respective stoichiometric ratios of zooplankton.



## 15 A7: List of resulting publications

*Lorkowski, I., Pätsch, J., Moll, A. & Kühn, W. 2012. Interannual variability of carbon fluxes in the North Sea (1970-2006) - Abiotic and biotic drivers of the gas-exchange of CO<sub>2</sub>. Estuarine Coastal and Shelf Science, 100, 38-57.*

*Pätsch, J. & Lorkowski, I. Comparison of two techniques to separate physical and biological mediated pCO<sub>2</sub> in seawater. Limnol. Oceanogr. Methods. Obtained a conditional accept up to now (Oct 2012) with minor revisions to be done.*

*Lorkowski, I., Pätsch, J. & Schwichtenberg, F. The impact of coccolithophores on the carbon budget of the North Sea. Will be submitted soon.*



# Bibliography

- Archer, S. D., Widdicombe, C. E., Tarran, G. A., Rees, A. P. & Burkill, P. H. 2001. Production and turnover of particulate dimethylsulphoniopropionate during a coccolithophore bloom in the northern North Sea. *Aquatic Microbial Ecology*, **24**(3), 225–241.
- Armstrong, R. A., Lee, C., Hedges, J. I., Honjo, S. & Wakeham, S. G. 2002. A new, mechanistic model for organic carbon fluxes in the ocean based on the quantitative association of POC with ballast minerals. *Deep-Sea Research Part II-Topical Studies in Oceanography*, **49**(1-3), 219–236.
- Backhaus, J. O. 1985. A three-dimensional model for the simulation of shelf sea dynamics. *Deutsche Hydrographische Zeitschrift*, **38**(4), 165–187.
- Backhaus, J. O. & Hainbucher, D. 1987. A finite difference general circulation model for shelf seas and its application to low frequency variability on the north European Shelf. *Pages 221–244 of: Nihoul, J. C. J. & Jamart, B. M. (eds), Three-dimensional models of marine and estuarine dynamics*. Amsterdam: Elsevier Science Publishers B. V.
- Balch, W.M., Fritz, J.J & Fernandez, E. 1996. Decoupling of calcification and photosynthesis in the coccolithophore *Emilinia huxleyi* under steady-state light-limited growth. *Marine Ecology Progress Series*, **142**, 87–97.
- Ballantyne, A.P., Alden, C.B., Miller, J.B, Tans, P.P & White, J.W.C. 2012. Increase in observed net carbon dioxide uptake by land and oceans during the past 50 years. *Nature*, **488**, 70–72.
- Bates, N. 2006. Air-sea CO<sub>2</sub> fluxes and the continental shelf pump of carbon in the Chukchi Sea adjacent to the Arctic Ocean. *Journal of Geophysical Research*, **111**.
- Benner, I. & Passow, U. 2010. Utilization of organic nutrients by coccolithophores. *Marine Ecology-Progress Series*, **404**, 21–29.
- Berliand, T.G. 1960. Methods of climatological computation of total incoming solar radiation. *Meteorol. Gidrol.*, **6**, 9–12.
- Blackford, J. C., Jones, N., Proctor, R. & Holt, J. 2008. Regional scale impacts of distinct CO<sub>2</sub> additions in the North Sea. *Marine Pollution Bulletin*, **56**, 1461–1468.
- Borges, A. 2005. Do we have enough pieces of the jigsaw to integrate CO<sub>2</sub> fluxes in the coastal Ocean? *Estuaries*, **28**, 3–27.
- Borges, A. V. & Gypens, N. 2010. Carbonate chemistry in the coastal zone responds more strongly to eutrophication than to ocean acidification. *Limnology and Oceanography*, **55**(1), 346–353.

- Bozec, Y., Thomas, H., Elkalay, K. & de Baar, H. J. W. 2005. The continental shelf pump for CO<sub>2</sub> in the North Sea - evidence from summer observation. *Marine Chemistry*, **93**(2-4), 131–147.
- Bozec, Y., Thomas, H., Schiettecatte, L., Borges, A.V., Elkalay, K. & De Baar, H.J.W. 2006. Assessment of the processes controlling seasonal variations of dissolved inorganic carbon in the North Sea. *Limnology and Oceanography*, **51**(6), 2746–2762.
- Budyko, M. I. 1974. *Climate and Life*. International Geophysics, vol. 18. Elsevier.
- Buitenhuis, E., Van Bleijswijk, J., Bakker, D. & Veldhuis, M. 1996. Trends in inorganic and organic carbon in a bloom of *Emiliana huxleyi* in the North Sea. *Marine Ecology Progress Series*, **146**(1-3), 271–282.
- Buitenhuis, E. T., van der Wal, P. & de Baar, H. J. W. 2001. Blooms of *Emiliana huxleyi* are sinks of atmospheric carbon dioxide: A field and mesocosm study derived simulation. *Global Biogeochemical Cycles*, **15**(3), 577–587.
- Burkill, P.H., Archer, S.D., Robinson, C., Nightingale, P. D., Groom, S.B., Tarran, G.A. & Zubkov, M.V. 2002. Dimethyl sulphide biogeochemistry within a coccolithophore bloom (DISCO): an overview. *Deep-Sea Research II*, **49**, 2863–2885.
- Cai, W.-J., Dai, M. & Wang, Y. 2006. Air-sea exchange of carbon dioxide in ocean margins: A province-based synthesis. *Geophysical Research Letters*, **33**.
- Chung, S.-N., Lee, K., Feely, R. A., Sabine, C. L., Millero, F. J., Wanninkhof, R., Bullister, J. L., Key, R. M. & Peng, T.-H. 2003. Calcium carbonate budget in the Atlantic Ocean based on water column inorganic carbon chemistry. *Global Biogeochemical Cycles*, **17**(4), 1–16.
- Conkright, M. E., Locarnini, R. A., Garcia, H. E., O'Brien, T. D., Boyer, T. P., Stephens, C. & Antonov, J. I. 2002. World Ocean Atlas 2001: Objective analyses, data statistics, and figures CD-ROM documentation. *National Oceanographic Data Center Internal Report (NOAA Atlas NESDIS)*, **17**, 17.
- Conway, T. J., P.M., Lang & Masarie, K.A. 2011. Atmospheric Carbon Dioxide Dry Air Mole Fractions from the NOAA ESRL Carbon Cycle Cooperative Global Air Sampling Network, 1968-2010. *Version: 2011-10-14*, Path: <ftp://ftp.cmdl.noaa.gov/ccg/co2/flask/month/>.
- de Haas, H., van Weering, T. C. E. & de Stieger, H. 2002. Organic carbon in shelf seas: sinks or sources, processes and products. *Continental Shelf Research*, **22**(5), 691–717.
- De La Rocha, C. L. & Passow, U. 2007. Factors influencing the sinking of POC and the efficiency of the biological carbon pump. *Deep-Sea Research Part II-Topical Studies in Oceanography*, **54**(5-7), 639–658.
- Delille, B., Harlay, J., Zondervan, I., Jacquet, S, Chou, L, Wollast, R, Bellerby, RGJ, Frankignoulle, M, Borges, AV, Riebesell, U & Gattuso, JP. 2005. Response of primary production and calcification to changes of pCO<sub>2</sub> during experimental blooms of the coccolithophorid *Emiliana huxleyi*. *Global Biogeochemical Cycles*, **19**(2).
- deYoung, B., Heath, M., Werner, F., Chai, F., Megrey, B. & Monfray, P. 2004. Challenges of Modeling ocean basin ecosystems. *Science*, **304**(5676), 1463–1466.

- Dickson, A. G. 1990. Thermodynamics of the dissociation of boric acid in synthetic seawater from 273.15 to 318 K. *Deep Sea Research*, **37**, 755–766.
- Dickson, A. G. & Millero, F. J. 1987. A comparison of the equilibrium-constants for the dissociation of carbonic-acid in seawater media. *Deep-Sea Research Part a-Oceanographic Research Papers*, **34**(10), 1733–1743.
- DOE. 1994. Handbook of methods for the analysis of the various parameters of the carbon dioxide system in seawater, version 2. *Dickson, A.G. and Goyet, C. editors, ORNL/CDIAC-74*.
- Doney, S. C., Balch, W. M., Fabry, V. J. & Feely, R. A. 2009. Ocean acidification: A critical emerging problem for the ocean sciences. *Oceanography*, **22**(4), 16–25.
- Eden, C. & Willebrand, J. 2000. Mechanism of Interannual to Decadal Variability of the North Atlantic Circulation. *Journal of Climate*, **14**, 2266–2280.
- Engel, A. 2002. Direct relationship between CO<sub>2</sub> uptake and transparent exopolymer particles production in natural phytoplankton. *Journal of Plankton Research*, **24**(1), 49–53.
- Engel, A, Zondervan, I, Aerts, K, Beaufort, L, Benthien, A, Chou, L, Delille, B, Gattuso, JP, Harlay, J, Heemann, C, Hoffmann, L, Jacquet, S, Nejstgaard, J, Pizay, MD, Rochelle-Newall, E, Schneider, U, Terbrueggen, A & Riebesell, U. 2005. Testing the direct effect of CO<sub>2</sub> concentration on a bloom of the coccolithophorid *Emiliana huxleyi* in mesocosm experiments. *Limnology and Oceanography*, **50**(2), 493–507.
- Fabry, V.J., Seibel, B.A., Feely, R.A. & Orr, J.C. 2008. Impacts of acidification on marine fauna and ecosystem processes. *ICES Journal of Marine Science*, **65**, 414–432.
- Feely, R., Sabine, C., Takahashi, T. & Wanninkhof, R. 2001. Uptake and Storage of Carbon Dioxide in the Ocean: The Global CO<sub>2</sub> Survey. *Oceanography*, **4**, 18–32.
- Fennel, K., Wilkin, J., Levin, J., Moisan, J., O'Reilly, J. & Haidvogel, D. 2006. Nitrogen cycling in the Middle Atlantic Bight: Results from a three-dimensional model and implications for the North Atlantic nitrogen budget. *Global Biogeochemical Cycles*, **20**, 1–14.
- Fogg, G.E. 1983. The ecological significance of extracellular products of phytoplankton photosynthesis. *Botanica Marina*, **26**, 3–14.
- Francois, R., Honjo, S., Krishfield, R. & Manganini, S. 2002. Factors controlling the flux of organic carbon to the bathypelagic zone of the ocean. *Global Biogeochemical Cycles*, **16**(4), 20.
- Gehlen, M., Gangsto, R., Schneider, B., Bopp, L., Aumont, O. & Etche, C. 2007. The fate of pelagic CaCO<sub>3</sub> production in a high CO<sub>2</sub> ocean: a model study. *Biogeosciences*, **4**, 505–519.
- Gregg, W.W. & Casey, N.W. 2007. Modeling coccolithophores in the global oceans. *Deep-Sea Research II*, **54**, 447–477.
- Gypens, N., Lancelot, C. & Borges, A.V. 2004. Carbon dynamics and CO<sub>2</sub> air-sea exchanges in the eutrophied coastal waters of the Southern Bight of the North Sea: a modelling study. *Biogeosciences*, **1**, 147–157.

- Gypens, N., Borges, A.V. & Lancelot, C. 2009. Effect of eutrophication on air-sea CO<sub>2</sub> fluxes in the coastal Southern North Sea: a model study of the past 50 years. *Global Change Biology*, **15**, 1040–1056.
- Gypens, N., Lacroix, G., Lancelot, C. & Borges, A. V. 2011. Seasonal and inter-annual variability of air-sea CO<sub>2</sub> fluxes and seawater carbonate chemistry in the Southern North Sea. *Progress in Oceanography*, **88**(1-4), 59–77.
- Haarich, M., Kienz, W., Krause, M., Zauke, G.-P. & Schmidt, D. 1992. Heavy metal distribution in different compartments of the northern North Sea and adjacent areas. *ICES CM*, **1992/E:45**.
- Harlay, J., De Bodt, C., Engel, A., Jansen, S., d’Hoop, Q., Piontek, J., Van Oostende, N., Groom, S., Sabbe, K. & Chou, L. 2009. Abundance and size distribution of transparent exopolymer particles (TEP) in a coccolithophorid bloom in the northern Bay of Biscay. *Deep-Sea Research Part I-Oceanographic Research Papers*, **56**(8), 1251–1265.
- Harlay, J., Borges, A. V., Van der Zee, C., Delille, B., Godoi, R. H. M., Schiettecatte, L. S., Røevros, N., Aerts, K., Lapernat, P. E., Rebreanu, L., Groom, S., Daro, M. H., Van Grieken, R. & Chou, L. 2010. Biogeochemical study of a coccolithophore bloom in the northern Bay of Biscay (NE Atlantic Ocean) in June 2004. *Progress in Oceanography*, **86**(3-4), 317–336.
- Harris, R.P. 1994. Zooplankton grazing on the coccolithophore *Emiliana huxleyi* and its role in inorganic carbon flux. *Marine Biology*, **119**, 431–439.
- Heath, M. R., Edwards, A. C., Pätsch, J. & Turrell, W. R. 2002. Modelling the behaviour of nutrient in the coastal waters of Scotland. *Report of the Fisheries Research Services*, **10**, 1–106.
- Hense, I. 2010. Approaches to model the life cycle of harmful algae. *Journal of Marine Systems*, **83**, 108–114.
- Hernandez-Ayon, J.M., Zirino, A., Dickson, A. G., Camiro-Vargas, T. & Valenzuela-Espinoza, E. 2007. Estimating the contribution of organic bases from microalgae to the titration alkalinity in coastal seawater. *Limnol. Oceanogr. Methods*, **5**, 225–232.
- Hofmann, M. & Schellnhuber, H.-J. 2009. Oceanic acidification affects marine carbon pump and triggers extended marine oxygen holes. *PNAS Early edition*.
- Holligan, P. M., Aarup, T. & Groom, S. B. 1989. The North Sea: Satellite colour atlas. *Continental Shelf Research*, **9**(8), 667–765. doi: DOI: 10.1016/0278-4343(89)90096-4.
- Holligan, P.M., Fernandez, E., Aiken, J., Balch, W.M., Boyd, P., Burkill, P.H., Finch, M., Groom, S.B., Malin, G., Muller, K., Puride, D.A., Robinson, C., Trees, C.C., Turner, S.M. & van der Wal, P. 1993a. A biogeochemical study of the coccolithophore, *Emiliana huxleyi*, in the North Atlantic. *Global Biogeochemical Cycles*, **7**(4), 879–900.
- Holligan, P.M., Groom, S.B. & Harbour, D.S. 1993b. What controls the distribution of the coccolithophore *Emiliana huxleyi* in the North Sea? *Fisheries Oceanography*, **2**, 175–183.

- Honjo, S. 1976. Coccoliths: production, transportation, sedimentation. *Marine Micropaleontology*, **1**, 65–79.
- Huthnance, J. M., Holt, J. T. & Wakelin, S. L. 2009. Deep ocean exchange with west-European shelf seas. *Ocean Science*, **5**(4), 621–634.
- ICES. 1983. Flushing times of the North Sea. *ICES Cooperative Research Report*, **123**, 125. 21.8.92:PO4NS-Review.
- Iglesias-Rodriguez, M. Debora, Halloran, Paul R., Rickaby, Rosalind E. M., Hall, Ian R., Colmenero-Hidalgo, Elena, Gittins, John R., Green, Darryl R. H., Tyrrell, Toby, Gibbs, Samantha J., von Dassow, Peter, Rehm, Eric, Armbrust, E. Virginia & Boessenkool, Karin P. 2008. Phytoplankton calcification in a high-CO<sub>2</sub> world. *SCIENCE*, **320**(5874), 336–340.
- Iida, T., Saitoh, S. I., Miyamura, T., Toratani, M., Fukushima, H. & Shiga, N. 2002. Temporal and spatial variability of coccolithophore blooms in the eastern Bering Sea, 1998–2001. *Progress in Oceanography*, **55**(1-2), 165–175.
- Ilyina, T., Zeebe, R. & Brewer, P.G. 2010. Future ocean increasingly transparent to low-frequency sound owing to carbon dioxide emissions. *Nature Geoscience*, **3**, 18–22.
- IPCC. 2001. *Climate Change 2001: Synthesis Report. A contribution of working groups I, II, and III to the Third Assessment Report of the IPCC*. Tech. rept. Cambridge.
- Jickells, Timothy. 2005. External inputs as a contributor to eutrophication problems. *Journal of Sea Research*, **54**, 58–69.
- Joassin, P., Delille, B., Soetaert, K., Harlay, J., Borges, A.V., L., Chou, Riebesell, U., Suykens, K. & Gregoire, M. 2011. Carbon and nitrogen fluxes during a bloom of the coccolithophore *Emiliana huxleyi*: Modelling a mesocosm experiment. *Journal of Marine Systems*, **85**, 71–85.
- Kalnay, E., Kanamitsu, M., Kistler, R., Collins, W., Deaven, D., Gandin, L., Iredell, M., Saha, S., White, G., Woollen, J., Zhu, Y., Chelliah, M., Ebisuzaki, W., Higgins, W., Janowiak, J., Mo, K. C., Ropelewski, C., Wang, J., Leetmaa, A., Reynolds, R., Jenne, R. & Joseph, D. 1996. The NCEP/NCAR 40-year reanalysis project. *Bulletin of the American Meteorological Society*, **77**(3), 437–471.
- Kaul, L.W. & Froelicher, N. Jr. 1984. Modeling estuarine nutrient geochemistry in a simple system. *Geochimica et Cosmochimica Acta*, **48**, 1417–1433.
- Klaas, C. & Archer, D. E. 2002. Association of sinking organic matter with various types of mineral ballast in the deep sea: Implications for the rain ratio. *Global Biogeochemical Cycles*, **16**(4), 14.
- Kleypas, J., Feely, R.A., Fabry, V., Langdon, C., Sabine, C.L. & Robbins, L.L. 2006. Impacts of Ocean Acidification on Coral Reefs and Other Marine Calcifiers: A Guide for Future Research, report of a workshop held 1820 April 2005, St. Petersburg, FL. sponsored by NSF, NOAA, and the U.S. Geological Survey, 88 pp.
- Koeve, W., Kim, H.-C., Lee, K. & Oschlies, A. 2010. Potential impact of DOC accumulation on fCO<sub>2</sub> and CO<sub>3</sub><sup>2-</sup> computations in ocean acidification experiments. *Biogeosciences Discussion*, **8**, 3797–3827.

- Kriest, I. 2002. Different parameterizations of marine snow in a 1D-model and their influence on representation of marine snow, nitrogen budget and sedimentation. *Deep Sea Research Part I: Oceanographic Research Papers*, **49**(12), 2133–2162.
- Kroeker, K.J., Kordas, R.L., Crim, R.N & Singh, G.G. 2010. Meta-analysis reveals negative yet variable effects of ocean acidification on marine organisms. *Ecology Letters*, **13**, 1419–1434.
- Kühn, W., Pätsch, J., Thomas, H., Borges, A. V., Schiettecatte, L., Bozec, Y. & Prowe, A.E.F. 2010. Nitrogen and carbon cycling in the North Sea and exchange with the North Atlantic - A model study, Part II: Carbon budget and fluxes. *Continental Shelf Research*, **30**(16), 1701–1716.
- Langer, G., Geisen, M., Baumann, K., Klaes, J., Riebesell, U., Thoms, S. & Young, J. R. 2006. Species-specific responses of calcifying algae to changing seawater carbonate chemistry. *Geochemistry Geophysics Geosystems*, **7**(SEP 20).
- Langer, M. R. 2008. Assessing the contribution of foraminiferan protists to global ocean carbonate production. *Journal of Eukaryotic Microbiology*, **55**(3), 163–169.
- Laruelle, G., Dürr, H., Slomp, C.P. & Borges, A.V. 2001. Evaluation of sinks and sources of CO<sub>2</sub> in the global coastal ocean using a spatially-explicit typology of estuaries and continental shelves. *Geophysical Research Letters*, **37**.
- Le Quere, C., Roedenbeck, C., Buitenhuis, E., Conway, T. J., Langenfelds, R., Gomez, A., Labuschagne, C., Ramonet, M., T., Nakazawa., Metzl, N., Gillet, N. & Heimann, M. 2007. Saturation of the Southern Ocean CO<sub>2</sub> Sink Due to Recent Climate Change. *Science*, **316**, 1735–1738.
- Lenhart, Hermann-J., Mills, David K., Baretta-Bekker, Hanneke, van Leeuwen, Sonja M., van der Molen, Johan, Baretta, Job W., Blaas, Meinte, Desmit, Xavier, Kühn, Wilfried, Lacroix, Genevive, Los, Hans J., Menesguen, Alain, Neves, Ramiro, Proctor, Roger, Ruardij, Piet, Skogen, Morten D., Vanhoutte-Brunier, Alice, Villars, Monique T. & Wakelin, Sarah L. 2010. Predicting the consequences of nutrient reduction on the eutrophication status of the North Sea. *Journal of Marine Systems*, **81**, 148 – 170.
- Lewis, E.D., Wallace, L. & Allison, C.D.I.A.C. 1998. *Programm developed for CO<sub>2</sub> system calculations, Carbon Dioxide Information Analysis Center, managed by Lockheed Martin Energy Research Corp. for the US Dept. of Energy.* Tech. rept. Lockheed Martin Energy Research Corp. for the US Dept. of Energy.
- Lindenthal, A., Langmann, B., Pätsch, J., Lorkowski, I. & Hort, M. 2012. The ocean response to volcanic iron fertilisation after the eruption of Kasatochi volcano: a regional scale biogeochemical ocean model study. *Biogeosciences Discussion*, **9**.
- Liu, K.K., Atkinson, L., Quinones, R. & Talaue-McManus, L. 2010. *Carbon and Nutrient Fluxes in Continental Margins*. Springer.
- Loewe, P., Brockmann, U., Dick, S., Frohse, A., Herrmann, J., Klein, B., Klein, H., Loewe, P., Nies, H., Schmolke, S., Schrader, D., Schulz, A., Theobald, N. & Weigelt-Krenz, S. 2009. *System Nordsee - Zustand 2005 im Kontext langzeitlicher Entwicklungen.* Tech. rept. Report No. 44. Bundesamt für Seeschifffahrt und Hydrographie.

- Lorkowski, I., Pätsch, J., Moll, A. & Kühn, W. 2012. Interannual variability of carbon fluxes in the North Sea (1970-2006) - Abiotic and biotic drivers of the gas-exchange of CO<sub>2</sub>. *Estuarine Coastal and Shelf Science*, **100**, 38–57.
- Luff, R. & Moll, A. 2004. Seasonal dynamics of the North Sea sediments using a three-dimensional coupled water-sediment model system. *Continental Shelf Research*, **24**(10), 1099–1127.
- Mann, M.E., R.S., Bradley & Hughes, M.K. 1998. Global scale temperature patterns and climate forcing over the past six centuries. *Nature*, **392**, 779–787.
- Mehrbach, C., Culberso, Ch, Hawley, J. E. & Pytkowic, Rm. 1973. Measurement of apparent dissociation-constants of carbonic acid in seawater at atmospheric pressure. *Limnology and Oceanography*, **18**(6), 897–907.
- Merico, A., Tyrell, T., Lessard, E.B., Oguz, T., Stabeno, P.J., Zeeman, S.I. & Whitley, T.E. 2004. Modelling phytoplankton succession on the Bering Sea shelf: role of climate influences and trophic interactions in generating *Emiliana huxleyi* blooms 1997-2000. *Deep-Sea Research I*, **51**, 1803–1826.
- Merico, A., Tyrell, T. & Cokacar, T. 2006. Is there any relationship between phytoplankton seasonal dynamics and the carbonat system? *Journal of Marine Systems*, **59**, 120–142.
- Metzl, N., Corbiere, A., Reverdin, G., Lenton, A., Takahashi, T., Olsen, A., Johannessen, T., Pierrot, D., Wanninkhof, R., Olafsdottir, S. R., Olafsson, J. & Ramonet, M. 2010. Recent acceleration of the sea surface fCO<sub>2</sub> growth rate in the North Atlantic subpolar gyre (1993-2008) revealed by winter observations. *Global Biochemical Cycles*, **24**.
- Millero, F., Pierrot, D., Lee, K., Wanninkhof, R., Feely, R., Sabine, C., Key, R. M. & Takahashi, T. 2002. Dissociation constants for carbonic acid determined from field measurements. *Deep Sea Research I*, **49**, 1705–1723.
- Millero, F. J. 1995. Thermodynamics of the carbon-dioxide system in the oceans. *Geochimica et Cosmochimica Acta*, **59**(4), 661–677.
- Moll, A. 1998. Regional distribution of primary production in the North Sea simulated by a three-dimensional model. *Journal of Marine Systems*, **16**(1-2), 151–170.
- Moll, A. & Radach, G. 1991. Application of Dobson and Smith's solar radiation model to German Bight data (at Helgoland Reede). *Quarterly Journal of the Royal Meteorological Society*, **117**, 845–851.
- Moll, A. & Radach, G. 2003. Review of three-dimensional ecological modelling related to the North Sea shelf system - Part 1: models and their results. *Progress in Oceanography*, **57**, 175–217.
- Müller, M.N., Antia, A.N. & LaRoche, J. 2008. Influence of cell cycle phase on calcification in the coccolithophore *Emiliana huxleyi*. *Limnol. Oceanogr.*, **53**(2), 506–512.
- Murata, A. 2006. Increased surface seawater pCO<sub>2</sub> in the eastern Bering Sea shelf: An effect of blooms of coccolithophorid *Emiliana huxleyi*? *Global Biochemical Cycles*, **20**.

- Neal, C. 2002. Calcite Saturation in eastern UK rivers. *The Science of the Total Environment*, **282-283**, 311–326.
- Neumann, T. 2000. Towards a 3D-ecosystem model of the Baltic Sea. *Journal of Marine Systems*, **25**, 405–419.
- Nielsen, M. H. & St John, M. 2001. Modelling thermal stratification in the North Sea: Application of a 2-D potential energy model. *Estuarine Coastal and Shelf Science*, **53**(5), 607–617.
- Nightingale, P. D., Malin, G., Law, C.S., Watson, A.J., Liss, P.S., Liddicoat, M.I., Boutin, J. & Upstill-Goddard, R.C. 2000. In situ evaluation of air-sea gas exchange parameterizations using novel conservative and volatile tracers. *Global Biogeochemical Cycles*, **14**(1), 373–387.
- Nimer, N.A., Dixon, G.K. & Merrett, M.J. 1991. Utilization of Inorganic Carbon by the Coccolithophorid *Emiliana huxleyi* (Lohmann) Kamptner. *New Phytologist*, **120**(1), 153–158.
- Nunez-Riboni, I., Bersch, M., Haak, H. & Junglaus, J. H. 2011. A multi-decadal meridional displacement of the Subpolar Front in the Newfoundland Basin. *Ocean Science Discussion*, **8**, 453–482.
- O’Driscoll, K., Mayer, B., Ilyina, T. & Pohlmann, T. 2012. Modelling the cycling of persistent organic pollutants (POPs) in the North Sea system: fluxes, loading, seasonality, trends. *Journal of Marine Systems*, **in press**.
- Olafsson, J., Olafsdottir, S. R., Benoit-Cattin, A., Danielsen, M., Arnarson, T. S. & Takahashi, T. 2009. Rate of Iceland Sea acidification from time series measurements. *Biogeosciences*, **6**(11), 2661–2668.
- Omar, A. M., Olsen, A., Johannessen, T., Hoppema, M., Thomas, H. & Borges, A. V. 2010. Spatiotemporal variations of fCO<sub>2</sub> in the North Sea. *Ocean Science*, **6**(1), 77–89.
- OSPAR. 2000. *Quality Status Report 2000*. London: OSPAR Commission.
- OSPAR. 2005. Assessment of data collected under the OSPAR Comprehensive Study on riverine inputs and direct discharges for the period 1990-2002. *Assessment and Monitoring Series*, 1–41.
- Otto, L., Zimmerman, J. T. F., Furnes, G. K., Mork, M., Saetre, R. & Becker, G. A. 1990. Review of the physical oceanography of the North Sea. *Netherlands Journal of Sea Research*, **26**(2-4), 161–238.
- Pätsch, J. & Kühn, W. 2008. Nitrogen and carbon cycling in the North Sea and exchange with the North Atlantic - a model study, Part I. Nitrogen budget and fluxes. *Continental Shelf Research*, **28**(6), 767–787.
- Pätsch, J. & Lenhart, H.-J. 2008. Daily Loads of Nutrients, Total Alkalinity, Dissolved Inorganic carbon and Dissolved organic carbon of the European Continental Rivers of the Years 1977-2006. *Berichte aus dem Zentrum fr Meeres- und Klimaforschung*.
- Pätsch, J. & Radach, G. 1997. Long-term simulation of the eutrophication of the North Sea: temporal development of nutrients, chlorophyll and primary production in comparison to observations. *Journal of Sea Research*, **38**, 275–310.

- Pätsch, J., Kühn, W., Radach, G., Santana Casiano, J.M., Gonzalez Davila, M., Neuer, S., Freudenthal, T. & Llinas, O. 2002. Interannual variability of carbon fluxes at the North Atlantic Station ESTOC. *Deep-Sea Research II*, **49**, 253–288.
- Pätsch, J., Kühn, W., Moll, A. & Lenhart, H. J. 2009. *ECOHAM4 - User Guide*. Tech. rept. Institute of Oceanography, University of Hamburg.
- Peeters, J. C. H. & Peperzak, L. 1990. Nutrient limitation in the North Sea: a bioassay approach. *Netherlands Journal of Sea Research*, **26**(1), 61–73.
- Pohlmann, T. 1996. Predicting the thermocline in a circulation model of the North Sea - Part I: Model description, calibration and verification. *Continental Shelf Research*, **16**(2), 131–146.
- Pohlmann, T. 2006. A meso-scale model of the central and southern North Sea: Consequences of an improved resolution. *Continental Shelf Research*, **26**(19), 2367–2385.
- Previdi, M., Fennel, K., Wilkin, J. & Haidvogel, D. 2009. Interannual variability in atmospheric CO<sub>2</sub> uptake on the northeast U.S. continental shelf. *Journal of Geophysical Research*, **114**.
- Prowe, A.E.F., Thomas, H., Pätsch, J., Kühn, W., Bozec, Y., Schiettecatte, L., Borges, A.V. & de Baar, H.J.W. 2009. Mechanisms controlling the CO<sub>2</sub> air-sea flux in the North Sea. *Continental Shelf Research*, **29**(XX), 1801–1808.
- Quigg, A., Finkel, Z.V., Irwin, A. J., Rosenthal, Y., Ho, T., Reinfelder, J.R., Schofield, O., Morel, F.M.M. & Falkowski, P.G. 2003. The evolutionary inheritance of elemental stoichiometry in marine phytoplankton. *Nature*, **425**, 291–294.
- Radach, G. & Lenhart, H. J. 1995. Nutrient dynamics in the North Sea - Fluxes and budgets in the water column derived from ERSEM. *Netherlands Journal of Sea Research*, **33**(3-4), 301–335.
- Radach, G. & Pätsch, J. 2007. Variability of continental riverine freshwater and nutrient inputs into the North Sea for the years 1977-2000 and its consequences for the assessment of eutrophication. *Estuaries and Coasts*, **30**(1), 66–81.
- Redfield, A.C. 1934. On the proportion of organic derivatives in seawater and their relation to the composition of plankton. *James Johnstone Memorial Volume*.
- Rees, A. P., Malcolm, E., Woodward, S., Robinson, C., Cummings, D. G., Tarran, G. A. & Joint, I. 2002. Size-fractionated nitrogen uptake and carbon fixation during a developing coccolithophore bloom in the North Sea during June 1999. *Deep-Sea Research Part II-Topical Studies in Oceanography*, **49**(15), 2905–2927.
- Riebesell, U., Zondervan, I., Rost, B., Tortell, P.D., Zeebe, R.E. & Morel, F.M.M. 2000. Reduced calcification of marine plankton response to increased atmospheric CO<sub>2</sub>. *Nature*, **407**, 364–367.
- Robertson, J.E., Robinson, C., Turner, D.R., Holligan, P., Watson, A., Boyd, P., Fernandez, E. & Finch, M. 1994. The impact of a coccolithophore bloom on oceanic carbon uptake in the northeast Atlantic during summer 1991. *Deep Sea Research Part I: Oceanographic Research Papers*, **41**, 297–314.

- Schartau, M., Engel, A., Schröter, J., Thoms, S., Völker, C. & Wolf-Gladrow, D. 2007. Modelling carbon overconsumption and the formation of extracellular particulate organic carbon. *Biogeosciences*, **4**(433-454).
- Schiettecatte, L. S., Thomas, H., Bozec, Y. & Borges, A. V. 2007. High temporal coverage of carbon dioxide measurements in the Southern Bight of the North Sea. *Marine Chemistry*, **106**(1-2), 161–173.
- Schlünzen, K. Heinke & Meyer, Elke M.I. 2007. Impacts of meteorological situations and chemical reactions on daily deposition of nitrogen into the southern North Sea. *Atmospheric Environment*, **41**, 289–302.
- Schrum, C. 2001. Regionalization of climate change for the North Sea and the Baltic Sea. *Climate Research*, **18**, 31–37.
- Schuster, U. & Watson, A. 2007. A variable and decreasing sink for atmospheric CO<sub>2</sub> in the North Atlantic. *Journal of Geophysical Research*, **112**.
- Shadwick, E.H., Thomas, H., Azetsu-Scott, K., Greenan, B.J.W., Head, E. & Horne, E. 2011. Seasonal variability of dissolved inorganic carbon and surface water pCO<sub>2</sub> in the Scotian Shelf region of the Northwestern Atlantic. *Marine Chemistry*, **124**, 23–37.
- Sharples, J., Ross, O. N., Scott, B. E., Greenstreet, S. P.R. & Fraser, H. 2006. Inter-annual variability in the timing of stratification and the spring bloom in the North-western North Sea. *Continental Shelf Research*, **26**, 733–751.
- Skogen, M. D. & Moll, A. 2005. Importance of ocean circulation in ecological modelling: An example from the North Sea. *Journal of Marine Systems*, **57**(3-4), 289–300.
- Suykens, K., Delille, B., Chou, L., De Bodt, C., Harlay, J. & Borges, A. V. 2010. Dissolved inorganic carbon dynamics and air-sea carbon dioxide fluxes during coccolithophore blooms in the northwest European continental margin (northern Bay of Biscay). *Global Biogeochemical Cycles*, **24**, 14.
- Takahashi, T., Olafsson, J., Goddard, J. G., Chipman, D. W. & Sutherland, S. C. 1993. Seasonal-Variation on CO<sub>2</sub> and Nutrients in the High-Latitude Surface Oceans - A Comparative-Study. *Global Biogeochemical Cycles*, **7**(4), 843–878.
- Takahashi, T., Sutherland, S. C., Sweeney, C., Poisson, A., Metzl, N., Tilbrook, B., Bates, N., Wanninkhof, R., Feely, R. A., Sabine, C., Olafsson, J. & Nojiri, Y. 2002. Global sea-air CO<sub>2</sub> flux based on climatological surface ocean pCO<sub>2</sub>, and seasonal biological and temperature effects. *Deep-Sea Research Part II-Topical Studies in Oceanography*, **49**(9-10), 1601–1622.
- Thomas, H., Ittekkot, V., Osterroht, C. & Schneider, B. 1999. Preferential recycling of nutrients - the oceans' way to increase new production and to pass nutrient limitation? *Limnology and Oceanography*, **44**(8), 1999–2004.
- Thomas, H., England, M. H. & Ittekkot, V. 2001. An off-line 3D model of anthropogenic CO<sub>2</sub> uptake by the oceans. *Geophysical Research Letters*, **28**(3), 547–550.
- Thomas, H., Bozec, Y., Elkalay, K. & de Baar, H.J.W. 2004. Enhanced open ocean storage of CO<sub>2</sub> from shelf sea pumping. *Science*, **304**, 1005–1008.

- Thomas, H., Bozec, Y., de Baar, H. J. W., Elkalay, K., Frankignoulle, M., Schiettecatte, L. S., Kattner, G. & Borges, A. V. 2005a. The carbon budget of the North Sea. *Biogeosciences*, **2**(1), 87–96.
- Thomas, H., Bozec, Y., Elkalay, K., de Baar, H. J. W., Borges, A. V. & Schiettecatte, L. S. 2005b. Controls of the surface water partial pressure of CO<sub>2</sub> in the North Sea. *Biogeosciences*, **2**(4), 323–334.
- Thomas, H., Prowe, A.E.F., van Heuven, S., Bozec, Y., de Baar, H.J.W, Schiettecatte, L., Suykens, K., Kon, M., Borges, A.V., Lima, I.D. & Doney, S.C. 2007. Rapid decline of the CO<sub>2</sub> buffering capacity in the North Sea and implications for the North Atlantic Ocean. *Global Biogeochemical Cycles*, **21**.
- Toggweiler, J.R. 1993. Carbon overconsumption. *Nature*, **363**, 210–211.
- Tsunogai, S., Watanabe, S. & Sato, T. 1999. Is there a "continental shelf pump" for the absorption of atmospheric CO<sub>2</sub>? *Tellus*, **51B**, 701–712.
- Turrell, W. R. 1992. New hypotheses concerning the circulation of the northern North Sea and its relation to North Sea fish stock recruitment. *ICES Journal of Marine Science*, **49**, 107–123.
- Tyrrell, T. & Taylor, A. H. 1996. A modelling study of *Emiliana huxleyi* in the NE atlantic. *Journal of Marine Systems*, **9**(1-2), 83–112.
- van der Wal, P., Kempers, R.S. & Veldhuis, J.W. 1995. Production and downward flux of organic matter and calcite in a North Sea bloom of the coccolithophore *Emiliana huxleyi*. *Marine Ecology Progress Series*, **126**, 247–265.
- van der Zee, C. & Chou, L. 2005. Seasonal cycling of phosphorus in the Southern Bight of the North Sea. *Biogeosciences*, **2**, 27–42.
- van Haren, H. & Howarth, M. J. 2004. Enhanced stability during reduction of stratification in the North Sea. *Continental Shelf Research*, **24**(7-8), 805–819.
- Vermaat, J.E., McQuatters-Gollop, A., Eleveld, M.A. & Gilbert, A.J. 2008. Past, present and future nutrient loads of the North Sea: causes and consequences. *Estuarine Coastal and Shelf Science*, **80**, 53–59.
- Wanninkhof, R. 1992. Relationship between wind speed and gas exchange over the ocean. *Journal of Geophysical Research*, **97**(C5), 7373–7382.
- Wanninkhof, R. & McGillis, W. R. 1999. A cubic relationship between air-sea CO<sub>2</sub> exchange and wind speed. *Geophysical Research Letters*, **26**(13), 1889–1892.
- Warrach, K. 1998. Modelling the thermal stratification in the North Sea. *Journal of Marine Systems*, **14**(1-2), 151–165.
- Watson, A. J., Schuster, U., Bakker, D. C. E., Bates, N. R., Corbiere, A., Gonzalez-Davila, M., Friedrich, T., Hauck, J., Heinze, C., Johannessen, T., Kortzinger, A., Metzl, N., Olafsson, J., Olsen, A., Oschlies, A., Padin, X. A., Pfeil, B., Santana-Casiano, J. M., Steinhoff, T., Telszewski, M., Rios, A. F., Wallace, D. W. R. & Wanninkhof, R. 2009. Tracking the Variable North Atlantic Sink for Atmospheric CO<sub>2</sub>. *Science*, **326**(5958), 1391–1393.

- Weiss, R.F. 1974. Carbon Dioxide in Water and Seawater: The Solubility of non-ideal gas. *Marine Chemistry*, **2**, 203–215.
- Widdicombe, C.E., Archer, S.D., Burkill, P.H. & Widdicombe, S. 2002. Diversity and structure of the microplankton community during a coccolithophore bloom in the stratified Northern North Sea. *Deep-Sea Research II*, **49**, 2887–2903.
- Wilson, W. H., Tarran, G. & Zubkov, M. V. 2002. Virus dynamics in a coccolithophore-dominated bloom in the North Sea. *Deep-Sea Research Part II-Topical Studies in Oceanography*, **49**(15), 2951–2963.
- Wiltshire, K. 2008. Resilience of North Sea Phytoplankton spring bloom dynamics: An analysis of long-term data at Heloland Roads. *Limnol. Oceanogr.*, **53**(4), 1294–1302.
- Wiltshire, K., Kraberg, A., Bartsch, I., Boersma, M., Franke, H., Freund, J., Gebuehr, C., Gerdts, G., Stockmann, K. & Wichels, A. 2010. Helgoland Roads, North Sea: 45 Years of Change. *Estuaries and Coasts*, **33**(2, Sp. Iss. SI), 295–310.
- Wiltshire, K. H. & Manly, B. F. J. 2004. The warming trend at Helgoland Roads, North Sea: phytoplankton response. *Helgoland Marine Research*, **58**(4), 269–273.
- Wolf-Gladrow, D. A., Zeebe, R. E., Klaas, C., Koertzing, A. & Dickson, A. G. 2007. Total alkalinity: The explicit conservative expression and its application to biogeochemical processes. *Marine Chemistry*, **106**(1-2), 287–300.
- Yool, A. & Fasham, M. J. R. 2001. An examination of the "continental shelf pump" in an open ocean general circulation model. *Global Biogeochemical Cycles*, **15**(4), 831–844.
- Zeebe, R.E. & Wolf-Gladrow, D. 2001. *CO<sub>2</sub> in seawater: Equilibrium, Kinetics, Isotopes*. 1st edn. ELSEVIER.
- Zondervan, I. 2007. The effects of light, macronutrients, trace metals and CO<sub>2</sub> on the production of calcium carbonate and organic carbon in coccolithophores - A review. *Deep-Sea Research Part II-Topical Studies in Oceanography*, **54**(5-7), 521–537.
- Zondervan, I., Zeebe, R.E., Rost, B. & Riebesell, U. 2001. Decreasing marine biogenic calcification: A negative feedback on rising atmospheric pCO<sub>2</sub>. *Global Biogeochemical Cycles*, **15**(2), 507–516.

# Acknowledgements

During the work on my thesis project, I learned a lot from several people on a scientific level as well as related to soft skills.

I am grateful for the advise and support by Dr. Johannes Pätsch. He taught me a lot and I thank him for sharing his knowledge and experience with me and for having an open ear for all kinds of questions.

I would also like to thank Prof. Dr. Carsten Eden and Prof. Dr. Inga Hense for their guidance and helpful recommendations during the whole thesis process.

I would like to thank Dr. Andreas Moll, Dr. Hermann Lenhart and Dr. Wilfried Kühn for sharing their knowledge and experience, for helping me with all kinds of issues and for the nice atmosphere.

Thanks to Fabian and Fabian, you were great office mates, sources of inspiration and helpful discussion partners, when I needed somebody who would listen to my uncompleted thoughts.

Special thanks go to Prof.em. Dr. Wolfgang Ebenhöh, who was the first to introduce me to mathematical modelling, specifically ecosystem modelling and who fascinated me with his enthusiasm.

### **Eidesstattliche Versicherung**

Ich erkläre hiermit an Eides statt, dass ich die vorliegende Arbeit selbständig angefertigt habe. Die aus fremden Quellen direkt oder indirekt übernommenen Gedanken wurden als solche kenntlich gemacht. Diese Arbeit wurde weder in gleicher noch in ähnlicher Form einer anderen Prüfungsbehörde vorgelegt.

Hamburg, den

Ina Lorkowski